Modelling of Multi-Tubular Fixed-Bed Reactor for Fischer-Tropsch Synthesis to Produce Synthetic Crude Using Syngas Obtained from the Work's Arising Gases of an Integrated Steel Mill

Master's Thesis

Asvin Sajeev Kumar

Modelling of Multi-Tubular Fixed-Bed Reactor for Fischer-Tropsch Synthesis to Produce Synthetic Crude Using Syngas Obtained from the Work's Arising Gases of an Integrated Steel Mill

Master's Thesis

by

Asvin Sajeev Kumar

to obtain the degree of Master of Science
in Sustainable Energy Technology
at the Delft University of Technology,
to be defended publicly on Thursday, August 15, 2019 at 02:00 PM.

Student Number:	4714253	
Project Duration:	January 2, 2019 – August 15, 2019	
Thesis Supervisors:	Prof. dr. ir. W. de Jong,	TU Delft
	PDEng. F. Sauerhöfer Rodrigo,	Tata Steel
	Dr. S. Santos,	Tata Steel
Thesis Committee:	Prof. dr. ir. W. de Jong,	TU Delft
	Prof. dr. A. Urakawa,	TU Delft
	Ir. P. L. J. Swinkels,	TU Delft

This thesis is confidential and cannot be made public until August 15, 2024.

Abstract

Steelmaking process is a highly carbon-intensive process. This is mainly due to the use of coke as a reducing agent in the blast furnaces to produce carbon-rich pig iron, which in turn, is used for the production of low-carbon steel in the basic oxygen furnaces. The exhaust gases from the blast and basic oxygen furnaces, which mainly contain CO and CO_2, are utilised for electricity generation, and thus, these pollutants are released to the atmosphere. One of the possible ways to treat these work's arising gases (WAGs) is to convert them into syngas, which can then be further converted into syncrude via Fischer-Tropsch synthesis (FTS). The FTS syncrude can then be further refined and processed to produce liquid fuels such as gasoline, kerosene, diesel, etc. These synthetic fuels are sulphur-lean and are essentially capable of replacing the existing fossil-derived liquid fuels, thus contributing to curbing the carbon emissions.

The main objective of this thesis was to develop a detailed model of a multi-tubular fixed-bed reactor (MTFBR) to produce synthetic crude from syngas via Fischer-Tropsch synthesis (FTS). The model was then used to simulate a reactor that utilises the syngas obtained from the processing of work's arising gases of an integrated steel mill to produce synthetic crude. The FTS product distribution was modelled using the kinetic model based on CO-insertion mechanism, developed by Todic et al. A basic MTFBR model was initially developed using the equations and assumptions from the fixed-bed reactor model of Todic, and the basic MTFBR model was able to produce similar results as that of the Todic's model, with slight deviations in the temperature and pressures profiles. The basic MTFBR model was then further improved to render it comparable with the commercial FT reactors. The main improvements in the model include the dynamic extraction of thermodynamic and transport properties of the system components using Aspen Properties; calculation of dynamic vapour-liquid equilibrium, liquid holdup and catalyst effectiveness factor; and the use of improved heat transfer and pressure drop equations.

A sensitivity analysis was performed to determine the effect of design and process parameters on the performance of the MTFBR model. The most crucial design parameter was observed to be the tube diameter as it had a considerable effect on the heat management and the pressure drop in the reactor bed. The most important process parameters for the reactor were observed to be the inlet temperature and the feed flow rate. A simplified FTS gas loop process was also modelled in Aspen Plus in order to introduce a recycle stream into the MTFBR. The effect of tail gas recycle for the recovery of unreacted H_2 and CO was also studied, and it was observed that higher recycle ratios resulted in lower conversions per pass; however, overall CO conversions were observed to increase until a maximum, and then decrease thereafter. The optimum conditions for the simplified gas loop process were estimated to be with an inlet temperature of 484.5K and a total recycle of tail gas to the recovery section, for a inlet pressure of 30 bar. Optimised process conditions resulted in a CO conversion per pass of 46%, an overall CO conversion of 89%, a C_{5+} selectivity of 86.6%, a CH_4 selectivity of 6.2%, and a C_{5+} productivity of 252,540 tonnes/y. The optimised model results, in terms of C_{5+} selectivity and overall CO conversion, were also pretty much inline with the available data from the Shell SMDS plant in Bintulu.

Preface

Dear reader,

This thesis is a product of seven memorable months of work at the Research & Development (R&D) Department, Tata Steel Nederland Technology B.V., in collaboration with the Process & Energy (P&E) Department, Delft University of Technology, Netherlands. Tata Steel is one of the leading steel producers in Europe, with steelmaking facilities in both the United Kingdom and the Netherlands.

Before getting into the details of the multi-tubular fixed-bed reactor modelling and the interesting nuances of synthetic crude production via Fischer-Tropsch synthesis, it is only appropriate to remember and thank the people without whom this project would not have seen completion.

First and foremost, I would like to thank Jan van der Stel, Manager, Blast Furnace Development & Alternative Ironmaking group, for giving me an opportunity to work on this exciting project. I will always be grateful for your mentorship, and genuine interest in the professional and personal development of interns.

Second, to Frank Sauerhöfer Rodrigo and Stanley Santos, for their valuable guidance and supervision during my entire project duration at Tata Steel. My heartfelt gratitude to Prof. Wiebren de Jong, for readily agreeing to be my supervisor at TU Delft, for all the interesting discussions, and for taking a keen interest in the progress of the project.

I would also like to thank the members of my thesis committee: Prof. Atsushi Urakawa and Prof. Pieter Swinkels, for generously offering their time, support, guidance, and goodwill throughout the preparation and review of this thesis.

Further, I would like to thank all other employees at the Tata Steel R&D for being so welcoming and supportive, for always having suggestions to improve the work, and for the wonderful working environment.

Last but not the least, I would like to thank all my friends from TU Delft, my best friend Lakshmi Baiju, and my family, for being so understanding and supportive during these seven months.

Asvin Sajeev Kumar
Delft, August 2019

Contents

List of Figures

List of Tables

Nomenclature

Abbreviations

ASF	Anderson-Schulz-Flory
BF	Blast Furnace
BOF	Basic Oxygen Furnace
BTL	Biomass-to-Liquids
CAER	Center for Applied Energy Research
CFB	Circulating Fluidised Bed
CSTR	Continuous Stirred-Tank Reactor
CTL	Coal-to-Liquid
DCL	Direct Coal Liquefaction
FTS	Fischer-Tropsch Synthesis
GTL	Gas-to-Liquid
HC	Hydrocarbons
HTFT	High Temperature Fischer-Tropsch
ISO	International Organisation for Standardisation
LNG	Liquefied Natural Gas
LPG	Liquefied Petroleum Gas
LTFT	Low Temperature Fischer-Tropsch
MMTPA	Million Metric Tons Per Annum
MTFBR	Multi-Tubular Fixed-Bed Reactor
OAPEC	Organisation of Arab Petroleum Exporting Countries
OPR	Olefin-to-Paraffin Ratio
PFD	Process Flow Diagram
POX	Partial Oxidation
PSA	Pressure Swing Adsorption
RR	Tail gas recycle ratio
RWGS	Reverse Water Gas Shift
SBCR	Slurry Bubble Column Reactor
VLE	Vapour-Liquid Equilibrium
WAGs	Work's Arising Gases
WGS	Water Gas Shift

Greek Letters

α_n	Chain growth probability for carbon number n ($n \geq 1$)
η	Catalyst effectiveness factor
λ	Thermal conductivity (W/m/K)
λ_{er}	Effective radial thermal conductivity (W/m/K)
μ	Dynamic viscosity (Pa·s)
ϕ	Thiele modulus
ϕ_p	Particle sphericity
ϕ_{CO}	Thiele modulus for CO
ρ	Density of fluid (kg/m^3)
τ	Tortuosity factor
ε_b	Bed porosity
ε_c	Catalyst porosity
ε_l	Dynamic liquid holdup
ε_w	Adjusted bed porosity

Subscripts and Superscripts

$\circ$	reference state
b	bed
c	catalyst
g	gas
in	inlet
l	liquid
out	outlet

Symbols

ΔE	Change in 1-olefin desorption activation energy caused by weak force interactions (J/mol/CH$_2$ group)
ΔH_i	Enthalpy of elementary step i (J/mol)
ΔH_r	Reaction enthalpy (J/mol)
$\Delta H_{r,e}$	Reaction enthalpy per reactor element (J/mol)
$\dot{m}$	Mass flow rate (kg/s)
A_i	Pre-exponential factor of rate constant for elementary step i
A_{cs}	Reactor tube cross-section area (m^2)
c	Constant determining chain length dependence

C_n	Hydrocarbon with n carbon atoms
c_p	Specific heat capacity of fluid (J/kg/K)
C_{CO}	Concentration of CO (mol/m^3)
d_p	Catalyst particle diameter (m)
d_t	Reactor tube diameter (m)
d_w	Reactor tube wall thickness (m)
$D_{e,i}$	Effective diffusivity of species i in wax (m^2/s)
$D_{wax,i}$	Diffusivity of species i in wax (m^2/s)
dH_{tot}	Total heat released during reaction at reference state conditions (W)
E_i	Activation energy of elementary step i (J/mol)
f	Friction factor for fluid flow in a packed bed
F_i	Molar flow rate of species i (mol/s)
g	Acceleration due to gravity (m/s^2)
H	Enthalpy of stream (J/mol)
$h_{wall,g}$	Convective contribution to heat transfer coefficient at the wall (W/m^2/K)
$h_{wall,o}$	Stagnant contribution to heat transfer coefficient at the wall (W/m^2/K)
h_{wall}	heat transfer coefficient at the wall (W/m^2/K)
K_i	Equilibrium constant for elementary step i
k_i	Reaction rate constant for elementary step i
L	Reactor length (m)
L_c	Characteristic diffusion length (m)
M	Average molar mass (kg/mol)
P	Pressure (Pa)
P_i	Partial pressure of species i (Pa)
P_t	Total pressure (Pa)
Pr	Prantl number
R	Universal gas constant (J/mol/K)
R_i	Reaction rate of species i (mol/kg$_{\text{cat}}$/s)
Re	Reynolds number
S	Vacant active site
S_n	Selectivity to hydrocarbons with n carbon atoms
T	Temperature (K)
T_c	Coolant temperature (K)

T_w	Reactor wall temperature (K)
U	Overall heat transfer coefficient (W/m^2/K)
u_s	Superficial velocity of fluid (m/s)
X_{CO}	CO Conversion
Y	Vapour fraction
y_i	Vapour composition of species i
y_n	Molar fraction of hydrocarbon with n carbon atoms
z	Dimensionless reactor length

1. Introduction

The modern civilisation is facing a lot of challenges in the 21st century, the biggest among which is the constantly increasing demand for energy and the environmental impacts associated with the conversion of energy from conventional sources. The high cost of developing new technologies, such as for storage in the case of intermittent energy sources like solar and wind, and inefficiencies of these technologies are among the main reasons why the conventional energy sources could not be completely replaced by alternative and renewable energy sources [1]. It is expected that the future energy requirements will be completely met by renewable sources, but the transition would be gradual. Hence, the energy needs of the current population will have to be catered by the existing non-renewable energy sources. It is also predicted that the transportation sector will continue to use fossil-derived liquid fuels as the main energy source during the 21st century [2]. Thus, cleaner and alternative liquid fuels play a major role in replacing these fossil-derived fuels and curbing the carbon emissions.

Steelmaking process is a highly carbon-intensive process. This is mainly due to the use of coke as a reducing agent in the blast furnace (BF) to produce carbon-rich pig iron from iron oxide ores. The pig iron is then fed to the basic oxygen furnace (BOF), along with some basic fluxes, where a stream of high purity oxygen is blown over it, resulting in the production of steel with lower carbon content. The exhaust gases from both blast and basic oxygen furnaces, which mainly contain carbon monoxide (CO) and carbon dioxide (CO_2), are currently being used for electricity generation in gas turbines, releasing these pollutants to the atmosphere.

One of the possible options to treat the work's arising gases (WAGs) of an integrated steel mill is to clean and process them in a water gas shift reactor with steam, remove CO_2 in a carbon capture unit, and produce syngas (a mixture of CO and H_2). Syngas finds several applications in the industry, such as in the production of methanol, ammonia, diesel, and other synthetic fuels [3]. However, due to the constantly increasing demand for fossil-derived liquid fuels, the market for synthetic liquid fuels, which are capable of replacing the conventional liquid fuels, is only expected rise in the near future [4]. The syngas can be converted into synthetic crude (liquid hydrocarbons) in a Fischer-Tropsch reactor and refined further to produce liquid fuels such as gasoline, kerosene, diesel, etc. Fischer-Tropsch Synthesis (FTS) is an established process for the conversion of CO into synthetic crude and has been commercialised by major companies like Sasol and Shell. The main advantages of utilising WAGs for FT Synthesis include the valorisation of WAGs as well as the production of sulphur-lean fuels.

1.1 Developments in Fischer-Tropsch Technology

The history of Fischer-Tropsch synthesis is quite intriguing and dates back to the early 20th century. The prices and availability of natural crude in those times were among the main factors which steered research focus into making crude synthetically [5]. However, the development of FTS technology was considered to be one of the important discoveries in the history of chemistry and chemical engineering [1].

An initial discovery was made by Sabatier and Senderens [6] in 1902, when they realised that various metallic catalysts (such as Fe, Ni, Co etc.) could be used to hydrogenate CO to methane. But, it was only during the 1920s that Franz Fischer and Hans Tropsch [7] discovered the reaction between H_2 and CO under mild (250-300°C and 1 atm), and then later, pressurised (10-20 atm) conditions over cobalt-iron catalysts, which gave liquid hydrocarbons and even solid paraffins. These discoveries laid the basis for the process now called as Fischer-Tropsch synthesis. Later, during the period prior to and during the World War II, Germany invested heavily to commercially develop the FTS process in order to produce synthetic crude oil, as Germany had no reserves of natural crude oil of its own [8]. The process mainly focused on the production of synthetic crude from coal via Coal-to-Liquid (CTL) process. The construction of the first small-scale FTS pilot plant was completed in 1932 at Mulheim. Later in the following years, several larger CTL plants were commissioned to increase the production capacity of liquid fuels. By the end of 1944, Germany had a production capacity of about 12,000 barrels (bbl) per day, which accounted to roughly 10-15% of its overall liquid synthetic fuel production [9].

Germany and United States both continued their research into FTS with several pilot plants across their countries, and the first Gas-to-Liquid (GTL) plant was established in Brownsville, Texas by 1951, which had a capacity of 7000 bbl/day [10]. A CTL plant was also constructed in Sasolburg, South Africa by 1955 following these developments. But the production of synthetic crude oil and related research came to a sudden halt soon, due to the discovery of large untapped oilfields in the Middle East, rendering the FTS process relatively uneconomical due to cheap oil prices. But the Sasol plant in South Africa continued to run throughout the 1960s and 70s as they had abundant availability of coal and also partly due to the political situation in the country which made it difficult to import crude oil from other countries [1, 10].

Later in the 1970s and 80s, due to the oil embargo initiated by the OAPEC (Organisation of Arab Petroleum Exporting Countries), there was a considerable growth and expansion in the FTS technology as the western countries were forced to look for alternatives to the oil from the Middle East. With the help of the earlier discoveries, considerable enhancements were made in the FTS process during this period, especially in the fields of catalyst preparation and reactor design [9]. Soon, South Africa achieved a combined production capacity of 120,000 bbl/day with an expansion of the Sasolburg plant along with the addition of two more plants [5]. But again, during the mid-1980s, the unviability of the FTS process due to the declined crude oil price resulted in a reduction in the funding for FTS related research works. However, the industry worked on developing the FTS technology with small scale research works still happening in the background.

Despite the declining crude oil prices, the first two industrial scale plants, using natural gas as feedstock instead of coal, were commissioned in Bintulu, Malaysia and Mossel Bay, South Africa, respectively. These plants became economically more viable when the crude oil price increased past $30 per barrel in 1999. Since the price of crude oil never dropped below $30 per bbl thereafter, the GTL process gained considerable attention due to its economic viability. Additionally, due to the discovery of large gas fields in far flung areas with no immediate market (i.e. inaccessible to pipelines), the GTL technology became one of the options considered to monetise these assets. As such, two of the world's largest GTL plants (oryx GTL by Sasol and Pearl GTL by Shell) were commissioned in Qatar in collaboration with Qatar Petroleum, with 34,000 and 140,000 bbl/day capacities, respectively. Other large scale GTL plants (i.e. Escravos in Nigeria and Oltin Yo'l in Uzbekistan) were also later developed with the goal to monetise far flung natural gas oil fields. [1, 10].

Recently, there has been a significant increase in the interest towards small scale GTL plants. This can be attributed to the development of new generation micro-channel reactors and other compact processes which make even the small-scale GTL processes viable. Several companies have also come forward with technologies that promise economical small-scale GTL plants with sizes varying from 1000 to 15,000 bbl/day [11, 12]. This is opposed to the long term belief that only large scale GTL plants would be economically viable.

Large scale GTL will remain as one of the monetising options for far flung conventional and non-conventional gas fields. However, this will be in competition with other options (i.e. LNG plant or chemical production). The viability of the GTL plant is not only hinged on the price of natural gas, but also connected to the price of crude oil. As such, GTL plants tend to play a significant role in niche markets (i.e. such as the production of low-sulphur fuel as blending stock or high-profit margin lubricant components and waxes). Small scale GTL plants can also grow easily due to the availability of flaring natural gas during oil production and the presence of several unutilised small scale natural gas fields around the globe. Biomass-to-Liquids (BTL) has also been gaining a lot of importance in Europe recently [13], along with Coal-to-Liquid in China [14] and other countries. Thus, it can be concluded that FTS would definitely play a key role in the future energy market.

1.2 Research Questions

The main question to be answered by this thesis is:

What is the benchmark performance of the multi-tubular fixed-bed reactor for Fischer-Tropsch synthesis, which produces synthetic crude using syngas obtained from the processing of work's arising gases of an integrated steel mill?

Answering the above question demands a detailed model of the multi-tubular fixed-bed reactor (MTFBR) that is comparable with that of the commercial FTS MTFBRs. Hence, the main objective of this thesis is to develop a detailed model of an FTS MTFBR, which can then be used to simulate a reactor that utilises the syngas obtained from the processing of work's arising gases of an integrated steel mill to produce synthetic crude. The key parts in the development of the detailed MTFBR model are as explained below:

FTS Product Distribution

Fischer-Tropsch synthesis is considered to be a complicated process due to its wide product spectrum, ranging from C_1 to C_{60+}, and the deviations shown by its products from the classical ASF product distribution model (explained in Section 2.6). Several models have been proposed by researchers in an attempt to explain these deviations; however, only very few of them could actually justify their models. Selection of a kinetic model that is capable of reproducing experimental product distribution results, without much deviations, is very crucial in the development of a detailed reactor model.

MTFBR Model

The FTS MTFBR reactor model needs to meet several demands in order to render it comparable with the commercial reactors. The most important one is that the model should be capable of describing the complex interplay between the reaction kinetics and various physical phenomena that exist within these reactors. Thus, the selection of proper mass, heat and momentum balance equations, and the use of accurate thermodynamic and transport properties of the components play a crucial role in determining the accuracy of the model.

Design and Process Parameters

The performance of MTFBR is influenced by several parameters, such as the catalyst particle size, tube diameter, inlet temperature, inlet pressure, feed flow rate and the feed H_2/CO ratio. Hence, it is important to study the effect of each parameter individually and determine the most influencing parameters, which will further help in the optimisation of the reactor.

FTS Process Model

It is not possible to achieve higher conversions in FTS processes with just a single pass reactor. Commercial FTS processes generally include recycle streams in order to maximise the productivity of syncrude and make the process economically more viable. Hence, it is also important to study the effect of recycle on the overall performance of the FTS process with MTFBR.

Optimal Parameters

The process conditions play a key role in the performance of the MTFB reactors. Thus, optimising the process conditions can significantly improve the overall productivity of syncrude, which is very desirable for the sustainability and profitability of the FTS plant. Also, the optimised MTFBR model can then be validated with the commercial reactors to establish the benchmark performance of the MTFBRs.

1.3 Methodology

Developing the FTS process model requires the integration of several complex process steps which include mainly syngas generation, FT conversion in reactor, product separation and syncrude refining or upgrading. The scope of this project is limited only to the FT conversion unit, which starts with the syngas feed stream, includes the MTFB reactor and ends with the syncrude leaving the reactor. The product separation unit is not included in the battery limits of this project; however, since the effect of recycle on the reactor performance is also estimated, a simplified product separation unit is modelled in this project. The desired product from the multi-tubular fixed-bed reactor is syncrude with a selectivity of at least 85% towards C_{5+} hydrocarbons. The basis of design considered is explained in detail in Chapter 3, and the tasks performed during the course of this project are summarised below:

- Definition of basis of design
- Selection and validation of FTS kinetic model
- Development of basic MTFBR model
- Improvement of basic MTFBR model and integration with Aspen
- Development of a simplified FTS gas loop process model
- Sensitivity analysis on reactor design and process parameters
- Optimisation of process parameters for maximum syncrude productivity

1.4 Thesis Structure

Chapter 2 summarises the key aspects of Fischer-Tropsch technology, based on the literature review performed. This includes the basic process steps, types of catalysts and reactors, primary and secondary FTS reactions and the FTS product distribution. Chapter 3 explains the basis of design considered, which is mainly based on the information gathered from the literature. This include the battery limits, feed and product specifications, selection of FTS process, catalyst, reactor and utilities. In Chapter 4, the equations and assumptions considered in the kinetic model, basic reactor model and the detailed reactor model are discussed. The process of implementing all the model equations in MATLAB, and integrating MATLAB with Aspen Plus and Aspen Properties are also discussed in Chapter 4. Chapter 5 consists of the kinetic model validation results and the simulations results of the basic and detailed reactor models. This include the simulation results of detailed reactor model with pure and WAGs syngas, sensitivity analysis performed on the reactor design and process parameters, development of FTS gas loop process with MTFBR, and the optimisation of process parameters. The conclusions and recommendations are included in Chapter 6, where the results obtained are viewed in light of the research questions posed in the beginning.

2. Fischer-Tropsch Technology

As discussed in the previous chapter, the transportation of natural gas to final customers, from remote locations inaccessible by pipeline, is one of the major problems with natural gas utilisation. Converting the natural gas indirectly into high value synthetic liquid oil through a GTL process is one of the ways in which this challenge can be overcome. Figure 2.1 shows a schematic of the GTL process, where natural gas is first converted into a synthetic gas mainly consisting of carbon monoxide (CO) and hydrogen (H_2), which is then converted into a mixture of liquid hydrocarbons (n-paraffins and 1-olefins) via a heterogeneous chemical reaction called Fischer-Tropsch Synthesis (FTS). These liquid hydrocarbons can then be processed into a variety of high value products such as gasoline, kerosine, diesel, etc.

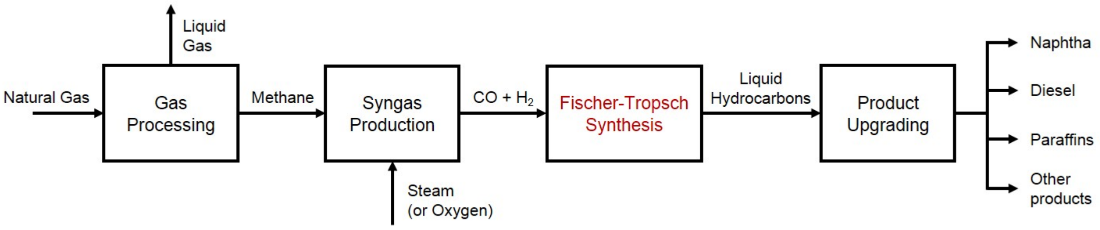

Figure 2.1: The schematic of a Gas-to-Liquid (GTL) process

Similarly, coal and biomass can also be converted into liquid fuels via the synthetic gas route, where the process is generally known as XTL (X-to-Liquid). Even though the GTL process is quite energy intensive, it can be justified by its economic viability which can be attributed to the higher prices of crude oil [15].

Modelling of an FTS reactor requires a proper understanding of what exactly happens inside the reactor and also how the selection of components affects the process. The following sections will explain in detail about the basic process steps and reactions involved, types of catalysts and reactors used, stoichiometry required, and the distribution of products in FTS.

2.1 Basic Process Steps

The application of FT technology requires an integration of several complex process steps. But the three main inevitable steps associated with FT technology include synthesis gas preparation, FT synthesis and product upgrading. These three basic steps are elaborated in the following sections.

2.1.1 Synthesis Gas Preparation

Synthesis gas (or syngas) can be prepared from any feedstock with carbon content (carbonaceous feedstock). The efficiency of hydrocarbon product formation can be improved if the feedstock also contains some amount of hydrogen in it. Hydrogen is mainly produced via the steam reforming of natural gas, or seldom, via an energy intensive water electrolysis process if the feedstock is deficient in hydrogen.

Coal is one of among the most used hydrogen-lean feedstocks for synthesis gas production, being the most abundantly available fossil fuel resource. Coal (or any other hydrogen-lean carbonaceous feedstock) is converted to synthesis gas using steam and oxygen, in a process called gasification. Several gasification technologies exist and the selection of a suitable technology depends on the characteristics of coal chosen as the feedstock. Due to the high heat value of coal, it produces a large amount of waste heat during the conversion process, which can be recovered and utilised for the production of electricity. At present, coal is being directly used to produce electrical power, which is quite an inefficient process. Co-production of hydrocarbons and electricity has been proven to be highly efficient compared to when these products are produced individually [16].

The production of synthesis gas from coal is considerably more expensive than producing it from natural gas. But as discussed before, most of the natural gas reserves explored recently are stranded in remote locations, making it difficult to transport the gas via pipelines [17]. Hence, the stranded gas can only be transported from these locations by converting them into shippable products such as ammonia, urea, methanol, LNG and FT hydrocarbons. All these products, except for LNG, can only be processed via a synthesis gas route which is generally classified as the GTL technology [8]. Since the markets of LNG and FT liquids are considerably large, they are economically more preferred over the other natural gas products. Liquid hydrocarbons can be made from methanol, but they can also be directly produced via FT synthesis, which is way cheaper than the double conversion (natural gas-methanol-hydrocarbons) pathway.

Natural gas comprises mainly methane, and the process of converting natural gas to synthesis gas is called methane reforming. The reforming of methane can be based on autothermal reforming, steam reforming or partial oxidation processes. During the autothermal reforming process, methane is made to react with oxygen and steam in order to produce a product mixture of hydrogen, carbon monoxide and carbon dioxide. Since the methane feed is sulphur-lean, it is also possible to use catalysts to improve the reforming reaction rate. The methane reforming process produces less carbon dioxide compared to the gasification process and can also take place in the absence of oxygen in the case of steam reforming. However, in such cases without partial internal combustion, an external supply of heat is necessary to keep the endothermic reforming reaction running. In the case of partial oxidation, a limited amount of oxygen is supplied in an exothermic process, resulting in the partial combustion of the substoichiometric fuel-air mixture, thus producing an H_2-rich syngas [18]. A complete conversion of methane to synthesis gas is not possible due to the equilibrium nature of these reactions, but oxygen is completely consumed in the reactions when used for reforming [8].

The unconverted methane can be recycled and the excess steam can be condensed out from the reformer outlet. Carbon dioxide may be either partially or totally recycled from the reformer outlet or fed to the FT synthesis step and then recycled back to the reformer depending on the process configuration selected. However, the selection of process configuration depends ultimately on the reforming technology and FT catalyst used [8].

2.1.2 FT Synthesis

The FT synthesis parameters basically depend on the type of feedstock and the desired products. Typically used FTS catalysts are based on iron or cobalt, depending on the type of process, syngas production method, and the desired products. Coal-derived syngas generally contains some amount of catalyst poisons and it is not possible to prevent all such catalyst poisons from reaching the FT catalyst. Hence, it is preferable to use iron catalysts, instead of cobalt catalysts, as they are less expensive and can be replaced more often. Iron catalysts are also preferred in the low temperature Fischer-Tropsch (LTFT) process, when the syngas is prepared via the high temperature coal gasification process resulting in a low H_2/CO ratio. This is because the reaction would mainly produce waxes and heavier carbon products in such conditions, and the need for an upstream shift reactor to increase the hydrogen content can be negated. In the case of high temperature Ficher-Tropsch (HTFT) process, higher fraction of light olefins are produced and require a higher H_2/CO ratio. Even though the HTFT process demands the need for an upstream shift reactor, it still can be competitive due to the increased income obtained from the higher valued light olefins. Also, achieving a higher conversion in HTFT process is easier with a higher H_2/CO ratio in the feed [8]. However, higher value products such as detergent feedstocks and lubrication oils can also be obtained from LTFT process with further processing of the products. With LTFT process, the tail gas can also be used to generate electricity and sold in the market, if required. Thus, the selection of the optimal FT route (LTFT or HTFT) mainly depends on the market value of the products produced from each route.

Since the tail gas from FT process using coal-derived syngas as feedstock can be used to generate electricity for export by directing it to a gas turbine (working in combined cycle with steam turbines), it is allowable to have lower conversions in the FT reactor. However, this is not the case with natural-gas-derived syngas as the FT tail gas typically cannot be used to generate electricity or for any other useful purposes [8]. Hence, it is desirable to achieve high levels of conversion to FT hydrocarbons if the syngas is derived from reforming of stranded natural gas.

The optimal syngas composition (H_2/CO ratio) required for LTFT using cobalt catalyst or HTFT using iron catalyst can be easily achieved in the case of natural gas reforming. This can be done just by cooling and condensing out water, without the need for any syngas processing step. Also, it is possible to remove potential FT catalyst poisons from natural gas with very less efforts compared to coal [8]. Cobalt is a more active catalyst compared to iron in the LTFT synthesis reaction. Hence, expensive recycles or multiple reactor stages are required in the case of LTFT iron catalyst owing to its low per pass conversion, which makes it even more expensive.

Similar to the application of coal in FT synthesis, natural gas feed also has a choice of selection between LTFT (using cobalt instead of iron) and HTFT processes. The product distribution obtained in the case of LTFT iron and cobalt catalysts are identical to a great extent. Among all types of FT reactors, the following four types are considered to have a higher chance of development and commercial application in the future [8]:

- HTFT two phase fluidised bed reactors using fused iron catalysts
- LTFT three phase slurry reactors using precipitated iron catalysts
- LTFT three phase slurry reactors using supported cobalt catalysts
- LTFT multi-tubular fixed-bed reactors using supported cobalt catalysts.

The types of catalysts and typical process conditions used in FT synthesis are discussed in detail in Sections 2.2 and 2.3, respectively.

2.1.3 Product Upgrading

The upgrading process mainly involves the separation and hydroprocessing of the FT products. Typically, removal of light hydrocarbons and dissolved gases are the starting steps in the product upgrading process. By doing so, the vapour pressure of liquid in the storage vessel is reduced, which facilitates atmospheric pressure storage of the hydrocarbons [8]. Fractionation or extractive distillation can be then used to separate olefins from the straight run liquid products to find use as chemical feedstocks.

Special final products, such as plastics and fibres, can be produced by the oligomerisation, hydroformylation or alkylation of olefins. It is desirable to not have any traces of oxygenated compounds in the stream prior to the olefin processing steps. To achieve this, processes such as liquid-liquid extraction can be used. The remaining parts of the straight run liquids can be hydrogenated into paraffins and further into products such as naphtha, diesel and optionally kerosene/jet fuel via fractionation. The fractions obtained in a conventional crude distillation column is also similar, as shown in Figure 2.2 [19]. Gasoline can then be produced by further upgrading naphtha via conventional refining techniques. While using cobalt catalysts in the LTFT process, it might not be justifiable to perform an olefin extraction or processing step due to the lower olefin contents

[8, 20]. Thus, in such cases, only hydroprocessing and separation would be performed to upgrade the products.

Hydrogenation of the products is performed mainly to extend its storage life without gum formation or discolouration. The diesel cut from fractionation process may even have sufficiently low olefin contents such that it can be directly used as a diesel blend material. But in such cases, the stability during storage, lubricity and other properties of the diesel cut can be enhanced by the addition of certain chemicals. Hydrogenation step is usually combined with several other processes that also use hydrogen, such as hydro-isomerisation and hydrocracking. The cold flow properties of the diesel cut can be improved by hydro-isomerisation where the straight chains are converted to branched chains [8, 20]. Collectively, all the processes that use hydrogen can be termed as hydroprocessing.

Wax from LTFT synthesis can be mixed with straight run material and processed in a hydrocracker to obtain valuable products such as naphtha, diesel or kerosene/jet fuel. The wax products can also be further processed into high quality lubricant base oils via special hydroprocessing technologies. Wax or heavy lubricant base oils can be separated using operations such as vacuum or short-path distillation, or supercritical solvent extraction to obtain desired product fractions or cuts. Hydrogenation, hydro-isomerisation or controlled oxidation processes can also be used to produce speciality products from wax [8]. The distillates from hydrocracking of wax have a larger market value compared to the lubricant base oils and speciality wax products.

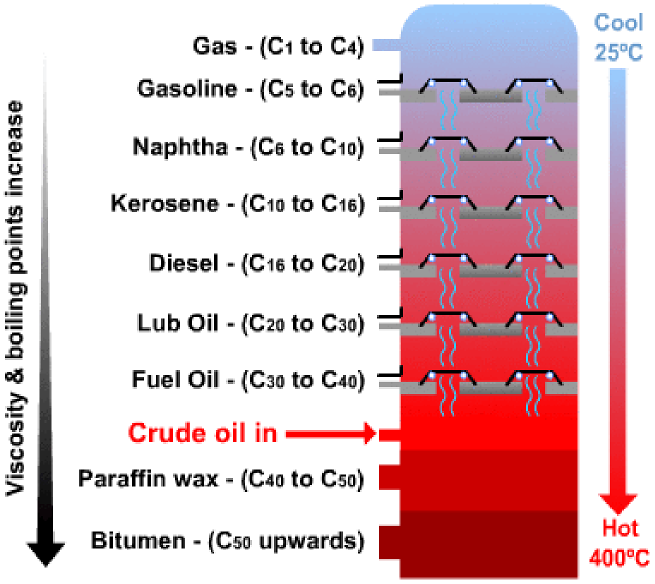

Figure 2.2: Fractions obtained in a conventional crude distillation column [19].

Ethylene (ethene), propylene (propene) and butylene (butene) can be recovered directly by cooling the FT reactor vapours below ambient temperatures. Ethene and propene find large applications in the plastic industry and even have significantly higher prices than fuels. Butene also finds applications as feedstock in the petrochemical industry. The paraffins in the range C2 to C4, associated with the FT reactor vapours, can be separated and cracked with steam to produce more olefins. LPG (liquefied petroleum gas), which is mainly used for domestic purposes, mainly consists of C3 and C4 paraffins (propane and butane) and can also be obtained from FT reactor [8, 20]. The small amounts of C3 and C4 paraffins recovered from natural gas prior to the syngas preparation step can also be mixed with the LPG obtained in the reactor.

The naphtha cut obtained by the fractionation of synthetic crude can be easily transported to existing refineries and further processed olefins in a naphtha cracker [8]. Since the naphtha produced from FT synthesis is highly paraffinic, the yield of olefins is much higher than that obtained from crude oil-derived naphtha.

Oxygenated products such as alcohols, acids, aldehydes and ketones are also produced in FT synthesis. Distillation of the water produced during the reaction can separate these dissolved compounds from the bulk of the water. The separated mixture of oxygenated products can have wide range of applications in the chemical industry and as fuel [8, 20]. Further processing of the oxygenated products depends on the scale of the FT plant.

According to Steynberg and Dry [8], the consumption of diesel has been increasing at a faster rate compared to gasoline consumption since the early 2000s, and high quality diesel motor fuel would be the dominant future product. However, recent market trends in the industrialised regions, such as the U.S. and Europe, show a slight decline in the diesel consumption, mainly due to the emergence of alternative fuels. On the other hand, it is expected that the developing nations, in the process of industrialisation, would undergo oil-driven economic expansion, which would make up for the slight decline in demand from the advanced economies [4, 21]. Diesel can be produced by the hydrocracking of primary FT products. Hydrocracking of wax or oligomerisation of olefins in naphtha using modern catalysts would also yield a high selectivity to diesel [20]. For all FT process variations, the combination of all these diesel sources with straight run diesel range products can produce similar diesel amounts. These products burn much cleaner than the crude-derived counterparts and is also free from sulphur.

Overall, FT products would result in lower greenhouse gas impact than conventional oil refinery products (according to ISO 14040 standard) [8], and the secondary products such as lubricant oils and olefinic hydrocarbons from the FT plant have wide applications in the chemical industry. The properties of the crude oil-derived diesel can be significantly enhanced by blending non-conventional diesel fuels like biodiesel or diesel derived synthetically from other carbon sources.

2.2 Catalysts

Metals, to find application as catalysts in FT synthesis, require sufficiently high activities for the hydrogenation of carbon monoxide. Only iron (Fe), cobalt (Co), nickel (Ni) and ruthenium (Ru), from group VIII of the periodic table, have shown similar activities and have been chosen for the purpose of catalysing FT reactions. Despite being the most active metal among the four, ruthenium is not a preferred catalyst in large scale applications due to its high cost and low availability. Nickel is also not commercially used as FT catalysts due to their strong hydrogenating property which results in higher methane formations than with Co or Fe catalysts. The formation of volatile carbonyls at normal FT operating temperatures and pressures, which leads to continuous loss of the metal, is another reason why Ni is not preferred as an FT catalyst. Thus, only cobalt and iron find practical applications as FT catalysts. The FT plants in South Africa use iron-based catalysts, whereas the Malaysian plant of Shell uses cobalt-based catalysts [8]. The future plants aiming to produce FT diesel would probably prefer Co as catalyst due to its higher activity. But the plants aiming to produce high value linear olefins would prefer HTFT fluidised bed reactors based on iron catalyst. Coal-derived syngas conversion would also see applications of LTFT iron catalyst in the coming years.

The three commercially significant catalysts in the FT processes are fused iron catalysts, precipitated iron catalysts and supported cobalt catalysts, and some important aspects of cobalt catalysts are covered in the following section (see Appendix A for iron catalysts). The factors affecting the performance of catalysts during FT reaction are also briefly covered in a later section.

2.2.1 Supported Cobalt Catalysts

Preparation of modern cobalt catalysts involves the deposition of cobalt on pre-shaped refractory oxide supports such as silica, alumina, titania, zinc oxide or combinations of these oxides. The desired particle sizes for applications in a slurry reactor are achieved by preparing the support using a spray drier. The prepared catalyst particles may be classified in the next step for refining of the size distribution. Catalysts supports for fixed bed reactors are usually extruded to obtain the desired shapes [22].

The mechanical strength of the shaped support is enhanced by heat treatment techniques, and the amount of cobalt deposited on the support is determined by controlling the pore size in the support, which would ultimately determine the catalyst performance. Metals such as lanthanum, platinum, palladium, rhenium and ruthenium are used as promoters and are impregnated with the cobalt catalyst onto the oxide support [22]. It is desirable to have the cobalt metal on the surface of the catalyst, and the impregnated metal promoters would prevent the cobalt metal from being oxidised. For a silica-supported cobalt catalyst, zirconium has been proven to be effective. Similarly, lanthanum, rhenium and ruthenium have been proven to enhance the re-reduction of the catalyst. However, a good cobalt catalyst with oxide support need not necessarily require promoters, but the effects of catalyst oxidation and support geometry are considerable issues. The final catalyst is prepared by drying and then reducing the impregnated support with hydrogen at high temperatures [23].

Controlling the size of cobalt crystallites on the support during the preparation of catalyst is considered to be very important. There are several methods to control the size and also to stabilise the catalyst under commercial FT reactor conditions. Cobalt catalysts have been known to have found applications in the oldest as well as the modern commercial plants. Thoria was used as the promoter in the first commercial cobalt catalyst and it was supported on kiselguhr (a powdered form of a naturally occurring, soft, siliceous sedimentary rock). Due to the understandings about geometry, cobalt distribution and reduction techniques, modern cobalt catalysts are of considerably high activity compared to the old catalysts [24].

Based on the type of reactor, several approaches have been adopted to make the process with cobalt catalysts more efficient [25]. Intra-particle temperature and concentration gradients in a fixed bed reactor can be significantly reduced by depositing cobalt only as a thin layer on the outer surface of the catalyst support. The catalysts for fixed bed reactors are always designed accounting for long term stability as continuous regeneration of the catalyst is not possible in a fixed bed. Whereas, in the case of slurry reactors, it is sometimes possible to continuously rejuvenate the catalyst by reducing the oxidised non-active cobalt metal using hydrogen contact at high temperatures. Simultaneous removal of heavy hydrocarbon depositions is also achieved during this rejuvenation step. Thus, the sizes of cobalt crystallites can be made very small, which results in a relatively more active catalyst. However, the catalyst activity of the first commercial cobalt catalyst, for use in slurry reactors, was compromised for its stability [24].

Cobalt catalysts generally produce paraffins as main products in FT synthesis, as opposed to iron catalysts which predominantly produce olefins as FT products. Cobalt catalysts can also produce sufficiently justifiable quantities of olefins with the use of small sized catalyst particles and CO-rich syngas. The selectivity to methane and the selectivity to oxygenates in the aqueous phase are higher and lower, respectively, compared to the LTFT precipitated iron catalyst. The cobalt catalysts with the highest performance could achieve a methane selectivity of about 5% of the hydrocarbon products [22].

In the case of LTFT cobalt catalysts, the water gas shift (WGS) reaction is nearly absent or is in negligible amounts, as opposed to LTFT precipitated iron catalysts, where a considerable amount of CO_2 is produced via WGS reaction. This is not an issue with HTFT fused iron catalysts as CO_2

gets converted back to CO via the reverse WGS reaction due to higher operating temperatures, which is desirable [8, 22]. Hence, fused iron catalysts tend to compete with cobalt catalysts for applications of natural gas in the FT synthesis. As discussed before, coal-derived syngas contains catalyst poisons which may be detrimental to cobalt catalysts, and since it is difficult to remove these impurities to desired low levels, iron catalysts are more preferred for coal applications.

2.2.2 Catalyst Deactivation during FT Synthesis

Several factors have been identified to affect the performance of catalysts during the time it stays in the reactor (time on-stream), and the important ones are listed below.

- Diffusion restrictions caused by the presence of high molecular mass waxes and/or aromatic coke precursors in the catalyst pores.
- Fouling of the catalyst surface by coke deposits.
- Poisons in the feed gas such as H_2S and organic sulphur compounds.
- Hydrothermal sintering.
- Oxidation of the active metal/carbide to the inactive oxide.
- Carbon deposition by Boudouard reaction.

The pores of all types of catalysts used in FT processes have high molecular mass hydrocarbons in liquid phase under normal operating conditions [8, 26]. This can be seen even in the case of HTFT iron catalysts where the products are only in gas phase, and results in a low FT conversion due to the reduced rates of diffusion in and out of the catalyst particles. This issue becomes severe only when the liquid products build-up continuously in the pores, as with the case of HTFT iron catalysts [27]. When the bulk of the products move out of the catalyst pores in the gas phase, heavy products, such as coke precursors, could build-up on the pores at high temperatures. In the case of LTFT iron or cobalt catalysts, there is a large production of heavy liquid hydrocarbons which flow out of the catalyst pores continuously, resulting in little or no build-up. Thus, in LTFT operations where no aromatics are formed, the formation of coke deposits and coke precursors are absent [26].

Sulphur compounds present in the syngas feed can poison all types of catalysts irrespective of the FT operating conditions. With time on-stream, the crystallites of metal catalyst or carbides undergo oxidation and result in loss of catalyst activity. Similarly, the catalyst particles also undergo hydrothermal sintering with on-stream time [26]. During high temperature operations, the catalysts can also be prone to elemental carbon depositions [27]. Thus, it is important to understand the catalyst behaviour and its consequences under desired operating conditions in order to increase their effectiveness during the synthesis process.

2.3 FT Reactors

Fischer-Tropsch technology has seen the applications of two types of reactors commercially, high temperature and low temperature FT reactors (HTFT and LTFT), where GTL plants mainly use the LTFT reactors [5, 9]. The typical operating temperature ranges are 593 to 623K (320 to 350°C) for HTFT and 473 to 493K (200 to 240°C) for LTFT reactors. Due to the higher temperatures in the HTFT reactors, it usually deals only with gas and solid phases in the bulk (two-phase process), and liquid phase can only be seen in the catalyst pores, as discussed before in Section 2.2. In the case of LTFT process, all the three phases (gas-liquid-solid) exist simultaneously in the bulk of the reactor.

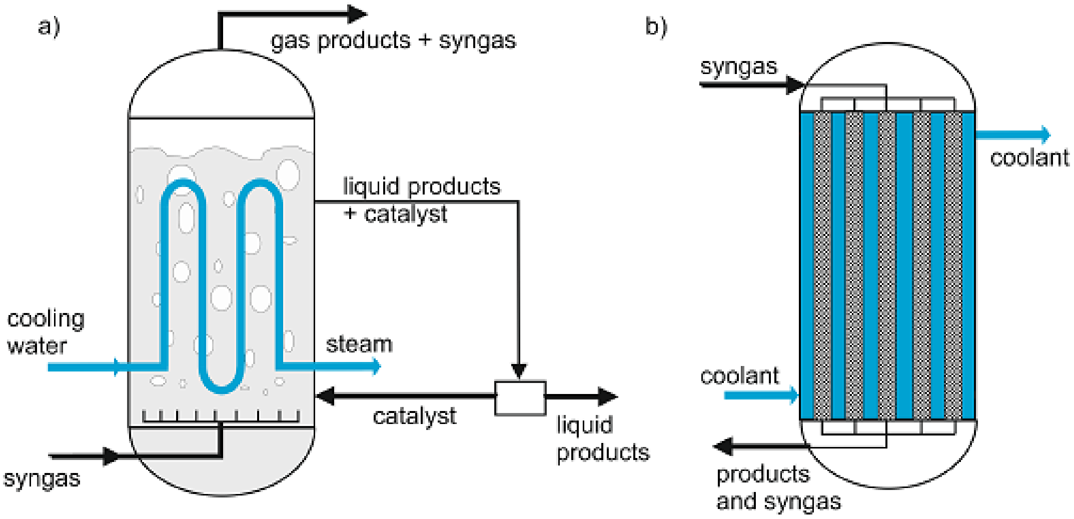

Figure 2.3: Types of commercially used LTFT reactors: (a) Slurry Bubble Column Reactor (SBCR) and (b) Multi-Tubular Fixed-Bed Reactor (MTFBR) [1].

It is undesirable to have condensation of liquid during HTFT operations, hence it is performed in fluidised-bed reactors with high temperatures, ensuring lower chain growth probability α values, thus limiting the heaviest HTFT product fractions to be in the gasoline/diesel fuel range (maximum up to C_{20}). High temperatures in the reactor can also lead to the excess formation of carbon which affects the catalyst performance; hence, the maximum temperature in the HTFT process is kept below 623K (350°C) [8]. In the case of LTFT process, slurry bubble column (SBCR) and multi-tubular fixed-bed reactors (MTFBR) are the commonly used commercial reactors, and are shown in Figure 2.3 [1]. In a SBCR, the syngas is fed into the vertical column vessel through a sparger at the bottom, and the syngas moves up through a column of liquid hydrocarbons (slurry or wax). The gas thoroughly mixes the slurry phase during its upward motion, and thus removes the need for mechanical agitation. The slurry phase consists of small sized catalyst particles suspended in it which gets removed from the reactor continuously along with the slurry. Hence, it is necessary to separate the catalyst particles from the slurry outlet and recycle them back to the reactor in the case of SBCRs. Operation of MTFBRs is relatively less complicated as it doesn't involve any separation/recycle of catalysts [1]. A fixed-bed is formed by the packing of large catalyst particles (1-3 mm) in a small diameter (2.5-5 cm) reactor tube. Several thousands of such tubes are arranged together in certain configurations to make MTFBRs. The syngas is fed to the reactor at the top, reacting as it passes through the catalyst bed to produce gas and liquid phase products, which can then be collected at the bottom of the packed bed.

There are several challenges associated with the use of these reactors for FT synthesis. Heat removal is one of the main challenges due to the highly exothermic nature of the FT reaction, making the reactor selection a difficult task. Other issues to be highlighted include the decrease in effectiveness of the catalyst due to mass transfer resistances, pressure drop in the reactor and deactivation of the catalyst. Apart from the fact that SBCR requires a complicated catalyst separation/recycle at the slurry outlet, it is difficult to scale up a SBCR. Also, the attrition of catalyst particles in the reactor reduces the effectiveness of the catalyst particles [28, 29]. Whereas, in the case of MTFBR, the capital cost is high and the removal of heat from the reactor is not that effective. Also, the pressure drop across the packed bed and the mass transfer resistances in the MTFBR are high [29].

2.4 Stoichiometry and Syngas Composition

The FT synthesis is a complicated process because it involves several simultaneous reactions giving various products. The selectivities of these reactions depend on the process conditions and mainly on the H_2/CO usage ratio of the syngas feed. The following sections will cover the stoichiometries of basic FT reactions, and the syngas compositions required for various FT processes and reactions.

2.4.1 Reaction Stoichiometry

The stoichiometry of a chemical reaction, in general, describes the molar proportion of reactants or products that are consumed or produced in that chemical reaction. While dealing with Fischer-Tropsch synthesis, the term stoichiometric ratio mainly refers to the ratio in which H_2 and CO combine to give the desired FT products. For simplicity, this ratio is generally referred to as the usage ratio. In cases when CO_2 is a reactant, the stoichiometric ratio also includes the CO_2 term and will be different from the usage ratio. The reactions taking place in an FT reactor are complicated, but can be represented in a simplified manner as given below [8].

$$\text{Methane}: \quad CO + 3\,H_2 \rightarrow CH_4 + H_2O \tag{2.1}$$

$$\text{Heavy HC}: \quad n\,CO + 2n\,H_2 \rightarrow (-CH_2-)_n + n\,H_2O \tag{2.2}$$

$$\text{Alcohols}: \quad n\,CO + 2n\,H_2 \rightarrow C_nH_{(2n+1)}OH + (n-1)\,H_2O \tag{2.3}$$

$$\text{Heavy Alkanes}: \quad n\,CO + (2n+1)\,H_2 \rightarrow C_nH_{(2n+2)} + n\,H_2O \tag{2.4}$$

$$\text{Water Gas Shift}: \quad CO + H_2O \rightleftharpoons CO_2 + H_2 \tag{2.5}$$

It is desirable to obtain heavier hydrocarbons in the LTFT process, hence Reaction 2.2 is considered to be the most desirable reaction. The consumption ratios in the above equations are based on simple stoichiometries; however, the consumption ratio of the whole FT process would be considerably different depending on the extent of all the above mentioned reactions along with the secondary reactions.

The water gas shift (WGS) reaction, shown by Reaction 2.5, has a considerable effect on the usage ratio. The negligible WGS activity in the case of cobalt catalysts would mean that the slight amount of carbon dioxide formed in the reaction could only be considered as a carbon-containing product. Whereas, while using iron catalysts at higher temperatures, the WGS reaction approaches equilibrium and the carbon dioxide formed could also be considered as a reactant. The composition of syngas and the prevailing conditions in the reactor determine the direction of WGS reaction [8].

The usage ratio in the case of cobalt catalysts depends on the extent of methane formation, olefin content in the longer chain hydrocarbons and the negligible WGS activity. Reaction 2.2 is mainly responsible for the usage ratio in cobalt catalysts, with considerable influence from Reaction 2.1. In the case of iron catalysts, the usage ratio is determined by combining the usage ratios required for the FT reaction as well as the WGS reaction. As discussed before, CO_2 needs to be considered as a reactant in this case, making the usage ratio also depend on the reverse WGS reaction.

The stoichiometric equations for some special cases and some ideal equations for coal and natural gas feedstocks have been derived by Steynberg and Dry [8] and are not discussed here. The reaction mechanism and the detailed kinetic model for FTS product distribution are discussed in detail in Section 4.1.

2.4.2 Syngas Composition and Usage Ratio

The production of syngas, for utilisation in an FT reactor as feed, is one of the major cost factors in the whole of the FT plant. Depending on the complexity of the FT plant and irrespective of the type of source (coal or natural gas) used for the production, up to 70% of the capital and operating costs may be comprised by the syngas production process. Hence, it is necessary to ensure maximum conversion of reactants (CO, H_2, and CO_2) to useful hydrocarbon products in the FT reactor [8]. Also, it is important to control the selectivity of reactions producing any undesirable products like methane.

Making the conversion of syngas an efficient process requires the feed to have an optimum usage ratio. Usage ratio is the ratio of H_2 to CO in the syngas required to maximise the product selectivity of a specific product, according to the stoichiometry of the reaction [8]. Table 2.1 represents the H_2 to CO usage ratios for typical FT products.

Table 2.1: Usage ratios for typical FT reactions [8].

FT Product	Reactions	Usage ratio
Methane	$CO + 3H_2 \rightarrow CH_4 + H_2O$	3
Ethylene	$2CO + 5H_2 \rightarrow C_2H_6 + 2H_2O$	2.5
Alkanes	$nCO + (2n+1)H_2 \rightarrow C_nH_{(2n+2)} + nH_2O$	(2n+1)/n
Alkenes	$nCO + 2nH_2 \rightarrow C_nH_{2n} + nH_2O$	2
Alcohols	$nCO + 2nH_2 \rightarrow C_nH_{(2n+1)}OH + (n-1)H_2O$	2

It can be seen from the above table that the usage ratio of alkanes decreases as the chain length increases, whereas for alcohols and alkenes, the usage ratio is independent of the chain length and is always equal to 2. But these usage ratios may slightly differ depending on the extent of water gas shift reaction in the FT reactor [8]. As discussed before, Co catalysts have very little or negligible WGS reaction, and hence typical usage ratio for the production of heavy hydrocarbons under normal FT operating conditions lie in the range of 2 to 2.15.

In the case of precipitated iron catalysts at low temperatures, the presence of WGS reaction along with the normal FT reactions results in a lower H_2 to CO usage ratio. During LTFT (493K or 220°C) operations in a fixed-bed reactor with iron based catalysts, typical usage ratio is around 1.65. Whereas, during HTFT (613K or 340°C) operations in a fluidised-bed reactor using iron catalysts, WGS reaction occurs rapidly and attains equilibrium which makes it possible to convert the CO_2 back to CO via the reverse WGS reaction [8].

$$\text{Reverse WGS reaction}: \quad CO_2 \; + \; H_2 \; \rightleftharpoons \; CO \; + \; H_2O \tag{2.6}$$

The CO produced via reverse WGS can then be converted to FT products via normal FT reactions. Hence, in order to produce FT products from the CO_2 formed, the H_2 usage ratio required for alkenes and CH_4 are 3 and 4, respectively. Overall, for HTFT iron catalysts, it is possible to achieve a high conversion in the FT reactor provided the usage ratio is optimised accordingly. A new ratio called Ribblett ratio was introduced to determine the performance of the FTS reactions based on the reaction stoichiometries and usage ratios. It is defined as the ratio of H_2 supplied to the amount of H_2 consumed by CO and CO_2 to make a -CH_2- product, i.e., $H_2/(2CO + 3CO_2)$ [8]. It can be seen that the production of one unit of -CH_2- requires three units of the sum of (H_2 + CO) for any FTS route.

$$2\,H_2 \; + \; 1\,CO \rightarrow \; (-CH_2-) \; + \; H_2O \tag{2.7}$$
$$1\,H_2 \; + \; 2\,CO \rightarrow \; (-CH_2-) \; + \; CO_2 \tag{2.8}$$
$$3\,H_2 \; + \; 1\,CO_2 \rightarrow \; (-CH_2-) \; + \; 2\,H_2O \tag{2.9}$$
$$3\,CO \; + \; 1\,H_2O \rightarrow \; (-CH_2-) \; + \; 2\,CO_2 \tag{2.10}$$

It can be observed that the sum of (H_2 + CO) remains unchanged during a WGS reaction, and the formation of CO_2 from CO or H_2O from H_2 cannot be regarded as a waste of reactants [8]. The partial pressures of H_2 and CO in the syngas affect the rates of FT reaction differently depending on the catalyst used. From experiments, it has been observed that effect of H_2/CO ratio on the activity of Co catalysts is considerably higher than that in the case of iron catalysts.

2.5 Primary and Secondary FT reactions

The product spectrum in the case of Fischer-Tropsch synthesis has been observed to be very different from the thermodynamic predictions and has been known to produce a wide range of hydrocarbon and oxygenated products. The experiments conducted by Tillmetz [30] with an H_2/CO ratio of 1.0, 0.1 MPa pressure and at typical LTFT temperature, and by Christoffel [31] with an H_2/CO ratio of 2, 1.6 MPa pressure and at 600K, respectively, showed the formation of high quantities of C_2 and higher products along with methane, as opposed to the predictions. Hence, it was concluded that the FT reactions were not even close to the thermodynamic equilibrium at normal LTFT or HTFT operating conditions.

Steynberg and Dry [8] performed several calculations to determine the quantities of various FT products formed and establish a relation between all the events happening in the FT process. They observed that alkenes, which were theoretically supposed to get hydrogenated to alkanes, in fact, were the dominant products formed. Thus, it was concluded that the formation of alkenes was primary, and their subsequent hydrogenation, even if it occured, was a slower process in the prevailing FT conditions with iron catalysts. Even with the cobalt catalysts, a higher fraction of alkenes over alkanes was found in the lower molecular range, despite its higher activity towards hydrogenation. It was predicted that the ratio of alkene to alkane would decrease with increasing chain lengths, and in practice, even though a bit higher than predicted, it actually declined with increasing carbon numbers until the ratio fell to really low values at very high carbon numbers.

Several co-feeding experiments were also conducted by Stenynberg and Dry [8] where ethene and octene were separately co-fed along with the syngas to determine the extent of hydrogenation. They observed around 50% and 15% hydrogenation for the added ethene and octene, respectively. Thus, it was concluded that the probability of hydrogenation of heavier molecular mass alkenes is less in a secondary reaction. It was also observed that when these alkenes were fed to the reactor only in the presence of H_2 (without CO), they were extensively hydrogenated or hydrocracked, according to the temperature. In the case of growing long chain primary FT species, it was predicted that these species would already be completely hydrogenated owing to the longer times these species spend on the surface of the catalyst, and the experimental results obtained were in accordance with these predictions.

Similar experiments also showed a higher ratio of ethanol to ethene than the thermodynamically predicted values, indicating that alcohols were not produced by the secondary hydration reactions of alkenes. However, the possibility of formation of alkenes by the dehydration of alcohols were studied and was justified by Steynberg and Dry [8]. Thus, it was concluded that alcohols were primary FT products as well. Also, when the experiments were conducted at 600K (327°C), it was observed that ethanol, actetic acid and acteldehyde established a thermodynamic equilibrium with each other, indicating that these three compounds were readily inter-convertible. When the same experiments were conducted at 510K (237°C), the ratios of these compounds were still higher than expected which implied that acetaldehyde and acetic acid were not formed by the de-hydrogenation and subsequent oxidation of ethanol, respectively. However, the formation of ethanol from acetic acid or acetaldehyde, via the reverse process, was possible. Hence, aldehydes and acids were also considered to be among the primary products of FTS.

The experimental data also showed the linear nature of the FT hydrocarbons. This was explained by the fact that the FT mechanism favoured the production of linear hydrocarbons over branched hydrocarbons, despite both being primary reactions. Also, the secondary isomerisation or branching of the linear primary alkanes or alkenes, which is a slow process at normal FT temperatures, increased with the FT operating temperature. This was verified with the iron catalyst at both HTFT and LTFT operating conditions.

During high temperature operations, considerable amounts of ketones and iso-alcohols were also found, and due to the slower formation rates of these products at normal FT temperatures, they were regarded as secondary products. It was observed that the ketonisation of acetic acid increased as the temperature was increased up to 633K (360°C), and a further increase in temperature resulted in the hydrogenation of these ketones to form iso-alcohols. An increase in the production of acetone was also observed when ethanol was additionally fed to the FT reactor at 610K (337°C), which can be interpreted as the conversion of ethanol to acetic acid due to the initial equilibrium achieved, followed by the ketonisation of the formed acetic acid. [32]. Analysis of data also showed that the majority of the ketones present in the FT products were methyl ketones. It was also observed that the dominant acid produced was acetic acid and that the amount of acid produced declined with increasing carbon numbers [8]. Hydrogenation of ketones to iso-alcohols was a slow process at low temperatures which supported the assumption that iso-alcohols were secondary products.

Aromatisation has been known to be a highly endothermic process, hence an increase in temperature would result in an increased aromatic content in the products. Experimental data obtained with iron catalysts showed that there was hardly any aromatic content below 500K (227°C), but at around 650K (377°C), the gasoline cut had around 25% aromatics [8]. It was also observed that the alkene content decreased with an increase in aromatics, indicating that aromatics were formed by the linkage of fist and last carbon atoms in an alkene, followed by its dehydrogenation to give stable resonating structures. The presence of large amounts of unsaturated ring compounds in the gasoline cut also supported the proposed route of aromatics formation. The majority of the aromatics found in the gasoline cut were C_7 to C_{10} alkyl benzenes. During experiments with aromatics, it was observed that the amount of aromatics did not change when recycled back into the reactor, indicating that aromatics formation was a slow primary reaction that occurred at around 600K (327°C).

The presence of large amounts of very long chain hydrocarbons at around 493K (220°C), considering the fact that short chain hydrocarbons are thermodynamically favoured, indicated that secondary hydrocracking hardly occurred in the reactor. Experiments conducted by Anderson [33] showed that hydrocracking occurred with $Ni/Co/SiO_2$, but only at very high FT conversion levels. The inhibition of FT hydrocracking process by chemisorbed CO was also reported later from the experiments conducted by Craxford [34]. Thus, it was concluded that hydrocracking, if any, occurred only at a very minimal level in the FT reactor at normal operating conditions.

The main participants in the FT secondary reactions have been observed to be 1-olefins, 2-olefins and alcohols. Since 1-olefins are far more active and also since they are the major products of FTS, generally, FTS secondary reactions refer to the secondary reactions of 1-olefins [1, 35]. Hydrogenation to n-paraffins, isomerisation to 2-olefins, re-adsorption followed by continuous growth (also called reincorporation), and cracking to lower products are some of the possible secondary reactions of 1-olefins [35, 36]. Reincorporation usually takes place on the primary FTS active sites, unlike hydrogenation and isomerisation which occur on the secondary FTS active sites [36].

Co-feeding the syngas with labelled or unlabelled olefins, and measuring the concentrations at the inlet and outlet is one of the methods to study the secondary reactions. These results are then compared with the baseline experiments (without co-feeding) to determine the activity and selectivity of these reactions [37]. It was observed that Co catalyst was more active in secondary reactions, followed by ruthenium and iron, respectively [38]. The reactivity of olefins was also determined to be in the order:

$$\textit{ethene} >> \textit{propene} > \textit{1-butene} \sim C_{5+}\ \textit{1-olefins}$$

Several theories have been proposed in order to explain the distribution of primary and secondary products in the FT synthesis and the exceptional behaviour of ethene compared to other FT products. The relevant ones are discussed in the following section.

2.6 FTS Product Distribution

The selectivity trends and product distribution in the FT synthesis have been defined and characterised by a chain growth mechanism, in which a C_1 monomer species on the catalyst surface gets inserted into the growing C_n chain. This mechanism has been observed to be dependent on the number of carbon atoms in the chain, and a simple model, called Anderson-Schulz-Flory (ASF) model, was developed to calculate the molar fractions of hydrocarbons as a function of carbon number [39, 40]:

$$y_n = (1-\alpha) \cdot \alpha^{n-1} \tag{2.11}$$

where y_n is the molar fraction of hydrocarbons with n carbon atoms and α is the chain length independent chain growth probability. This can also be represented in its logarithmic form as:

$$log(y_n) = log(\frac{1-\alpha}{\alpha}) + n \cdot log(\alpha) \tag{2.12}$$

The above Equation 2.12 represents a straight line with $log(y_n)$ along the y-axis, number of carbon atoms (n) along the x-axis, and with a constant slope of $log(\alpha)$. However, in reality, the FTS product distribution is often reported to deviate from the classical ASF distribution, as shown in Figure 2.4(a). A higher-than-expected fraction of methane, a lower-than-expected yield of C_2, and a positive bend in the ASF plot (increasing slope) are the main deviations observed in the distribution. The lower C_2 yield can be attributed to the lower fraction of ethene, and the positive bend can be attributed to the increasing chain growth probability (α) with carbon number, leading to a greater-than-expected yield of higher hydrocarbons. However, the higher methane fraction has been attributed to the presence of secondary reaction sites on the catalyst [1, 41]. Apparently, all catalysts used in the FT synthesis have been reported to show these deviations, generally termed as non-ASF behaviour [42].

Several theories have been proposed to explain the shift towards heavier products in FTS distribution [1], and some of them include: the existence of two parallel FTS mechanisms (with two separate active sites, pathways or monomers) [43, 44], the accumulation of heavy wax products in the reactor and presence of experimental VLE artefacts [44, 45], the existence of inter-particle and intra-reactor concentration gradients [46, 47], and most importantly, the secondary reactions of 1-olefins [48].

Studies showed that experimental artefacts could be the main reason for the non-ASF behaviour of FTS products [45, 49]. The negative and positive deviations from ASF have been attributed to the experimental errors in gas chromatography [49] and the operation of slurry reactor in transient state, respectively. It was observed that the lighter gas phase had a significantly lower residence time compared to the heavy molecules during the transient state operation [50]. Researchers also performed several experiments with deuterium (D_2), replacing hydrogen, to study the deviations from ASF arising due to accumulation of heavy wax in the reactor, and later found out that the properties of deuterium were significantly different from that of hydrogen, rendering them to be non-interchangeable [45, 51]. Positive deviations from ASF were also observed in lower hydrocarbon ($< C_{10}$) products which led to the conclusion that accumulation of heavy wax affected

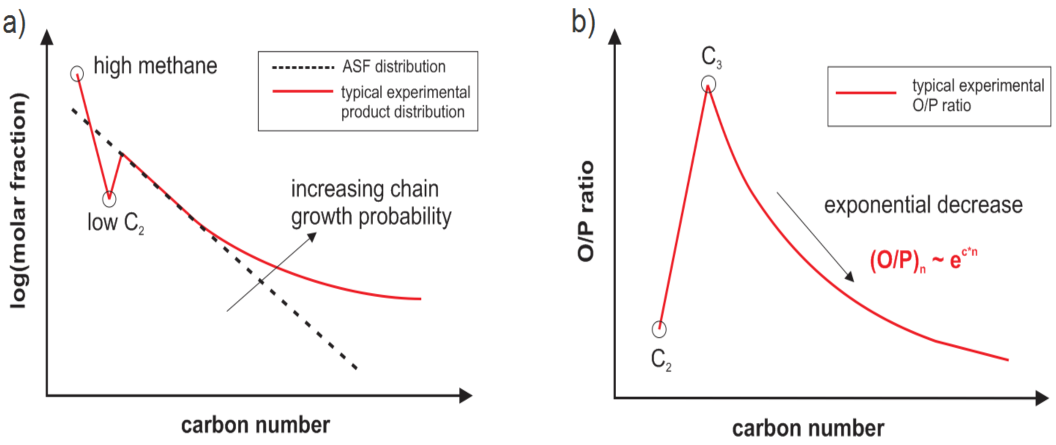

(a) ASF distribution and experimental deviations with carbon number

(b) Olefin-to-Paraffin ratio (OPR) with carbon number

Figure 2.4: Deviations from classical ASF model in FTS product distribution and the olefin-to-paraffin ratio (OPR) [1].

the product distribution only in the higher hydrocarbon (> C_{15+}) range [42].

Some researchers also came up with a new concept, called the double-α concept, where two distinct α values, α_1 and α_2, determined the FTS product distribution in the lower and higher carbon number ranges, respectively [44, 49]. It was assumed that these two α values corresponded to the two different pathways that existed in the FTS [52]. An exponential decrease in the olefin-to-paraffin ratio (OPR) with increasing carbon number was also observed in the FTS product distribution for all FT catalysts, as shown in Figure 2.4(b). One of the main drawbacks with the double-α model was its inability to distinguish between various product types (only total hydrocarbon distribution was available) as well as predict the OPR [1].

The concept considering the existence of inter-particle and intra-reactor concentration and temperature gradients was based on the fact that the α-value remained constant at constant temperatures and pressures [46, 47]. According to this concept, the gradients that existed across the bed in fixed bed reactors and the inter-particle gradients that existed in the slurry reactors resulted in different characteristic α-values at each point in these reactors, leading to non-ASF product distribution [46]. However, studies claiming the existence of non-ASF behaviour, even in systems without these gradients (such as well mixed CSTR with very fine catalyst particles), rendered this theory questionable [53, 54] and favoured more fundamental kinetic explanations.

Another explanation for the non-ASF behaviour was put forward by Herington [55], who claimed that secondary reactions of 1-olefins, such as hydrogenation, readsorption and isomerisation, were mainly responsible for such a deviation. As discussed before in Section 2.5, the olefins produced initially can get readsorbed onto the FTS active sites on the catalyst surface and grow continuously to yield heavy hydrocarbons. Also, the longer residence time of the higher olefins was assumed to contribute to their better readsorption onto the FTS sites, justifying the exponential decrease in OPR with increasing carbon numbers. Hence, the olefin readsorption concept has been widely accepted and used often to model the FTS product selectivity [42, 48, 56].

Botes [57] recently came up with a new concept, based on chain length dependent olefin desorption, where the activation energy required for the desorption of 1-olefins increased linearly with the carbon number, causing the 1-olefin desorption rate constant to decrease exponentially. This concept could successfully provide a mathematical explanation for the deviations from ASF and the exponential decrease in OPR with carbon number, even without considering the effects of secondary reactions [1].

3. Basis of Design

Before starting the modelling of MTFB reactor, it is necessary to define the basis of design. This mainly include the battery limits of the project, the feed and product specifications, and the selection of process, reactor, catalyst and utilities. These are explained in the following sections of this chapter.

3.1 Battery Limits

As discussed before in Section 2.1, the application of FT technology requires an integration of several complex process steps which include mainly syngas generation, FT synthesis and syncrude refining or upgrading. Figure 3.1 shows an overview of the main steps involved in the conversion of WAGs into syncrude via FTS process and refining of produced syncrude to obtain various fractions.

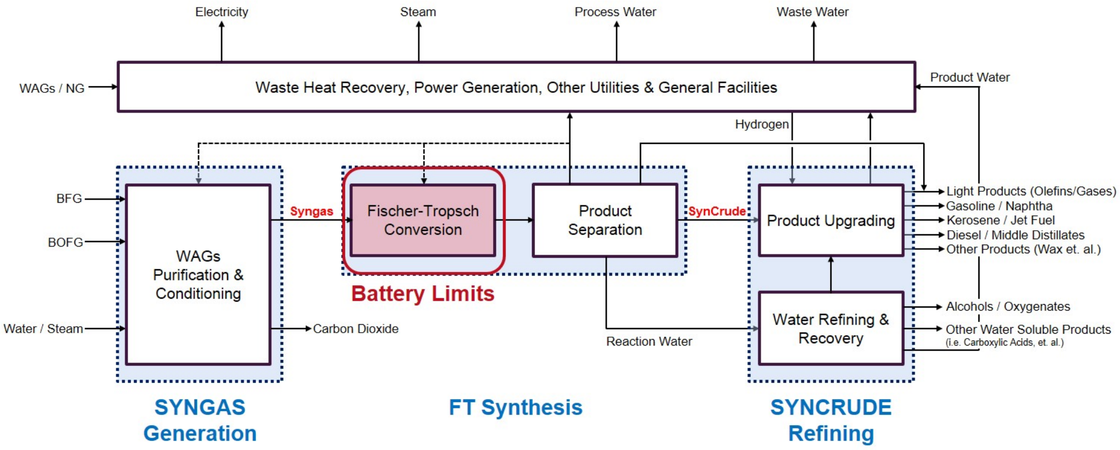

Figure 3.1: Various process steps involved in the conversion of WAGs of an integrated steel mill into liquid fuels.

In the case of WAGs in a steel plant, the syngas generation step involves the conditioning of the BF/BOF gases with steam in a water gas shift reactor to produce syngas with the desired ratio of H_2/CO for the FT synthesis. The CO_2 present in the syngas stream is then removed in a carbon capture unit to produce required feed for conversion in the FTS unit. After the FT conversion step, the syncrude from the reactor is then separated and processed further to produce liquid fuels such as gasoline, kerosene, diesel, etc. A part of the tail gas, after product separation, is recycled back to the FTS reactor and also the syngas generation unit in order to improve the efficiency of the overall process. The water produced in the FTS reactor, which contains dissolved oxygenates such as acids and alcohols, is processed and a part of it is utilised for steam generation or as process water in the plant.

The scope of this project is limited only to the FT conversion section of the FT synthesis unit (shown in Figure 3.1), which starts with the syngas feed stream, includes the FT conversion step and ends with the syncrude leaving the reactor. The product separation section under the FT synthesis unit is not included in the battery limits of this project. However, since the effect of recycle on the reactor performance is also estimated, a simplified product separation section is modelled later in this project to extract the recycle stream for the reactor from FT tail gas.

3.2 Feed & Product Specifications

The feed stream to the reactor comes from the syngas generation unit and the specifications of the feed stream are given in Table 3.1.

Table 3.1: Specifications of the syngas feed stream from the syngas generation unit.

Feed Composition		Feed Conditions	
Component	**Mole Fraction (%)**	Temperature (K)	319
CO	14.8	Pressure (bar)	15
H_2	29.5	Flow rate (kg/h)	393,242
H_2O	0.7		
N_2	47.1		
CO_2	5.6		
O_2	0.9		
CH_4	1.4		

It can be seen from the above table that the syngas obtained from the WAGs processing contains around 50% N_2 by mole, which may have a negative effect on the partial pressures of CO and H_2 in the reactor. Also the H_2 to CO ratio in the feed is around 2, which is in the desired range (2 to 2.15) for LTFT process catalysed by cobalt catalysts. Since the WAGs processing section includes a water gas shift reactor operating at 16 bar, followed by a CO_2 capture unit operating at the same pressure, the pressure of the syngas feed obtained is around 15 bar. Also, the temperature of the syngas feed is around 319K as it is obtained as the exhaust stream during the adsorption cycle in the CO_2 capture unit. The syngas feed temperature and pressure have to be adjusted in order to meet the FT reaction conditions (473-493K and 20-30 bar) before feeding into the reactor.

The desired product from the multi-tubular fixed-bed reactor is syncrude with a selectivity of at least 85% to C_{5+} hydrocarbons. This is because the C_5 to C_{20} hydrocarbons can be processed and converted into various liquid fuels such as gasoline, kerosene, diesel, etc. in a fractional distillation column, and the wax products above C_{20} can be hydroprocessed and broken down into smaller fractions in order to blend them with the desired fuel ranges. Methane is considered to be the most undesirable product in the syncrude production process.

3.3 Process & Catalyst Selection

Low temperature (LTFT) and high temperature Fischer-Tropsch (HTFT) are the two types of FT processes used commercially for the production of synthetic fuels, as discussed before in Section 2.3. The LTFT process is the most preferred process in GTL plants due to its higher selectivity to heavy hydrocarbons or waxes, as opposed to the HTFT process which has a higher selectivity to lighter hydrocarbons or gases. Since the aim of this project is to develop a model of an FT reactor for syncrude production, the desirable choice of process would be LTFT.

In case of LTFT process, two types of catalysts have seen applications in the commercial plants: precipitated iron catalysts and supported cobalt catalysts. As discussed before in Section 2.2, cobalt catalysts generally produce paraffins as main products in the FT synthesis, as opposed to iron catalysts which predominantly produce olefins as FT products. Also, in case of cobalt catalysts, the water gas shift (WGS) reaction is nearly absent or is in negligible amounts, as opposed to precipitated iron catalysts where a considerable amount of CO_2 is produced via WGS reaction. The cobalt catalysts also have a higher reactivity compared to iron catalysts and are mostly preferred in GTL processes for syncrude production, despite its relatively higher costs. Hence, owing to all the above facts, it has been decided to use supported cobalt catalysts for the reactor model in this project.

The kinetic model developed by Todic et al. [58] for supported cobalt catalysts, based on CO-insertion mechanism, has a decent fit with the experimental data and also explains the non-ASF behaviour in FT product distribution. Todic et. al have estimated all the parameters in their kinetic model using the experimental data with 25%Co-0.48%Re/Al_2O_3 catalysts, which have been specifically manufactured for their project in the Center for Applied Energy Research (CAER), University of Kentucky. Since the values of kinetic parameters are known only for the above mentioned CAER catalysts, the composition and properties of the cobalt-based catalysts used in this project are assumed to be the same as that of the CAER catalysts. Hence, the values of the kinetic parameters determined by Todic et al. can be used in this project (see Section 4.1).

3.4 Reactor & Utilities Selection

Slurry bubble column and multi-tubular fixed-bed reactors are the commonly used commercial reactors in LTFT process, and there are several challenges associated with the use of both these reactors, as discussed before in Section 2.3. Heat removal, catalyst effectiveness due to mass transfer resistances, pressure drop and catalyst deactivation are some of the main challenges involved in the use of these reactors, making the reactor selection a difficult task. However, in this project, a model of multi-tubular fixed-bed reactor is developed in order to establish the benchmark performance of the FT Synthesis using cobalt catalysts and syngas from WAGs as feedstock.

Fischer-Tropsch synthesis is a highly exothermic process and the removal of heat from the reactor is considered to be a major challenge while using a fixed-bed reactor. Hence, it is desirable to have an efficient cooling system for the effective transfer of heat from the packed bed to the coolant, which is very crucial for the optimal performance of the reactor. It has been observed that tubes up to 5 cm diameter are usable in MTFBRs with iron catalysts as they are less active and thus produce less heat, but since cobalt catalysts are far more active, it is optimal to use smaller diameter tubes [59].

Several methods have been proposed to facilitate the removal or control the generation of heat in an FT reactor. These include the partial recycle of tail gas into the reactor, which increases the gas velocity, and thus, improving the heat transfer characteristics; or the addition of inert gas (N_2) into the syngas to suppress the reaction by reducing the partial pressures of the reactants. However, in all these cases, it is recommended to operate the reactor at higher pressures to avoid loss in productivity [59, 60].

In this project, it is assumed that the temperature at the wall remains constant throughout the length of the reactor tube. This is achieved with a sufficiently high flow rate of pressurised boiling water (saturated water) in the outer shell of the MTFB reactor. The saturated water acts as a coolant here, by utilising the heat from the reactor tube to change the phase, and thus producing wet saturated steam. Since all the heat absorbed by the saturated water is only utilised for the phase change process, and not as sensible heat, the temperature of the coolant remains the same throughout the length of the reactor [59, 61]. Also, it is assumed that the heat transfer resistances between the wall and the cooling medium, and through the steel wall, are negligible. Hence, the temperature of the inner reactor tube wall can be considered to be equal to that of the cooling medium, i.e., $T_{wall} = T_{coolant}$ (see Appendix C for derivation). The inlet temperatures and pressures of saturated water considered in this project are in the ranges of 465-485K (192-212°C) and 13-19 bar, respectively, depending on the process conditions used.

4. Modelling & Simulation

Modelling of a reactor involves several steps such as modelling of the kinetics, selection of suitable heat, mass and momentum equations for the reactor along with their associated parameters and boundary conditions, implementation of the kinetics in the reactor modelling equations, etc. Initially, a basic reactor model is developed, followed by the development of a more sophisticated reactor model by improving the basic reactor model. The following sections of this chapter explain the various equations used to model the FTS kinetics and the MTFB reactor.

4.1 Kinetic Modelling

As discussed before in Section 3.3, the detailed kinetic model developed by Todic et al. [58], based on CO-insertion and chain length-dependent olefin desorption mechanism, has a reasonably good fit with the experimental data and also explains the observed deviations from the ASF model. Hence, the kinetic model of Todic et al. is used in this project to model the FTS product distribution.

The kinetic model has been developed based on the experiments performed on rhenium-promoted cobalt catalysts supported on alumina (25%Co/0.48%Re/Al_2O_3). Due to experimental limitations such as heavy product accumulation, the kinetic analysis focuses mainly on C_1-C_{15} hydrocarbons. The relevant species considered for developing the kinetic model are n-paraffins and 1-olefins until C_{15}, whereas minor products such as 2-olefins and oxygenates (alcohols, acids, ketones, etc.) are assumed to be negligible [58]. The CO-insertion reaction mechanism and the equations used for the kinetic model are covered in the following sections.

4.1.1 Reaction Mechanism

The basic steps involved in the FTS reaction mechanism are: reactants (CO and H_2) adsorption, CO activation (or chain initiation), chain propagation, and chain termination (or product formation). In the case of CO-insertion mechanism, the activation step involves the step-wise hydrogenation of the CO (see Figure 4.1), followed by the dissociation of the C-O bond to form the chain starter (CH_3-S, where S is a vacant active site on the catalyst surface). Subsequently, new CO molecules that are adsorbed onto the catalyst surface get inserted into the growing chain, thus forming continuous long hydrocarbon chains [58]. The elementary reaction steps and the corresponding reaction rate/ equilibrium constants involved in the derivation of the FTS kinetics are shown in Table 4.1.

The insertion of CO-S into the growing chain (step 1), the formation of n-paraffins by hydrogenation of adsorbed alkyl chain (step 7), and the formation of 1-olefins by dehydrogenation of C_nH_{2n+1}-S followed by its subsequent desorption (step 8), have been assumed to be the rate determining steps (RDS) in the whole reaction process [58].

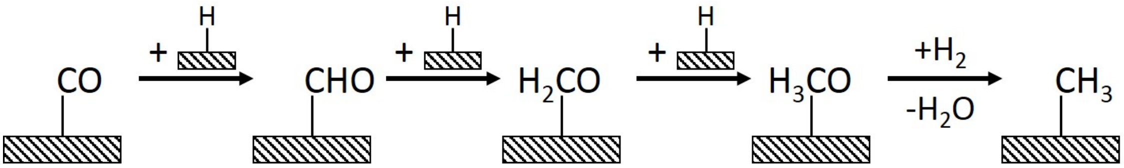

Figure 4.1: CO activation step involving the step-wise hydrogenation of CO-S, followed by the dissociation of C-O bond, to produce the chain starter (CH_3-S).

Table 4.1: The elementary steps involved in CO-insertion mechanism, used by Todic et al. [58] for developing the detailed kinetic model (RDS = Rate Determining Step).

No.	Elementary Step	Rate and Equilibrium Constants
1	CO + S ↔ CO-S	K_1
2	H_2 + 2S ↔ 2H-S	K_2
3^{RDS}	CO-S + H-S → CHO-S + S CO-S + CH_3-S → CH_3CO-S + S CO-S + C_nH_{2n+1}-S → C_nH_{2n+1}CO-S + S, n = 2, 3, ...	k_3
4	CHO-S + H-S ↔ CH_2O-S + S CH_3CO-S + H-S ↔ CH_3CHO-S + S C_nH_{2n+1}CO-S + H-S ↔ C_nH_{2n+1}CHO-S + S, n = 2, 3, ...	K_4
5	CH_2O-S + 2H-S ↔ CH_3-S + OH-S + S CH_3CHO-S + 2H-S ↔ CH_3CH_2-S + OH-S + S C_nH_{2n+1}CHO-S + 2H-S ↔ $C_nH_{2n+1}CH_2$-S + OH-S + S, n = 2, 3, ...	K_5
6	OH-S + H-S ↔ H_2O + 2S	K_6
7^{RDS}	CH_3-S + H-S → CH_4 + 2S C_nH_{2n+1}-S + H-S → C_nH_{2n+2} + 2S, n = 2, 3, ...	k_{7M} k_7
8^{RDS}	C_2H_5-S → C_2H_4 + H-S C_nH_{2n+1}-S → C_nH_{2n} + H-S, n = 3, 4, ...	k_{8E} k_8

4.1.2 Model Equations

The final model equations developed by Todic et al. [58] based on the CO-insertion mechanism are summarised in this section. The chain growth probability of hydrocarbons depends on the carbon number, unlike single-alpha and double-alpha models, and are calculated as:

$$\alpha_1 = \frac{k_3 K_1 P_{CO}}{k_3 K_1 P_{CO} + k_{7M}\sqrt{K_2 P_{H_2}}} \tag{4.1}$$

$$\alpha_2 = \frac{k_3 K_1 P_{CO}[S]}{k_3 K_1 P_{CO}[S] + k_7\sqrt{K_2 P_{H_2}}[S] + k_{8E}e^{c\cdot 2}} \tag{4.2}$$

$$\alpha_n = \frac{k_3 K_1 P_{CO}[S]}{k_3 K_1 P_{CO}[S] + k_7\sqrt{K_2 P_{H_2}}[S] + k_8 e^{c\cdot n}} \qquad n \geq 3 \tag{4.3}$$

where α_1, α_2 and α_n are the chain growth probabilities of C_1, C_2 and C_{3+} hydrocarbons; P_{CO} and P_{H_2} are partial pressures of CO and H_2, respectively; and c is a constant that accounts for the weak van der Waals interactions, given by the formula:

$$c = -\frac{\Delta E}{RT} \tag{4.4}$$

where ΔE is the contribution of van der Waals interactions of the hydrocarbon chain with the surface for every carbon atom (-CH_2-); and $[S]$ is the fraction of vacant sites on the surface of the catalyst, calculated from the overall site balance as:

$$\begin{aligned}[S] = 1/\{1 + K_1 P_{CO} + \sqrt{K_2 P_{H_2}} + (\frac{1}{K_2^2 K_4 K_5 K_6}\frac{P_{H_2O}}{P_{H_2}^2} + \sqrt{K_2 P_{H_2}}) \\ \cdot(\alpha_1 + \alpha_1\alpha_2 + \alpha_1\alpha_2\sum_{i=3}^{n}\prod_{j=3}^{i}\alpha_j)\}\end{aligned} \tag{4.5}$$

Since Equation 4.5 is an implicit non-linear function of a single variable $[S]$, it is estimated by solving the function $g([S]) = f([S]) - [S]$ using the MATLAB *fzero* function in the range of 0 to 1. The formation rates of hydrocarbon products are calculated using the following equations:

$$R_{CH_4} = k_{7M} K_2^{0.5} P_{H_2}^{0.5} \alpha_1 \cdot [S]^2 \tag{4.6}$$

$$R_{C_nH_{2n+2}} = k_7 K_2^{0.5} P_{H_2}^{0.5} \alpha_1 \alpha_2 \prod_{i=3}^{n} \alpha_i \cdot [S]^2 \qquad n \geq 2 \tag{4.7}$$

$$R_{C_2H_4} = k_{8E} e^{c \cdot 2} \alpha_1 \alpha_2 \cdot [S] \tag{4.8}$$

$$R_{C_nH_{2n}} = k_8 e^{c \cdot n} \alpha_1 \alpha_2 \prod_{i=3}^{n} \alpha_i \cdot [S] \qquad n \geq 3 \tag{4.9}$$

The reaction rates of CO, H_2 and H_2O are calculated from the stoichiometric relation with the products (see Table 2.1) as:

$$R_{CO} = R_{H_2O} = \sum_{n=1}^{\infty} n \cdot (R_{C_nH_{2n+2}} + R_{C_nH_{2n}}) \tag{4.10}$$

$$R_{H_2} = \sum_{n=1}^{\infty} \left[(2n+1) \cdot R_{C_nH_{2n+2}} + 2n \cdot R_{C_nH_{2n}} \right] \tag{4.11}$$

The reaction rate constants and the equilibrium constants depend only on the temperature, and are calculated using Arrhenius equation as:

$$k_i(T) = A_i \ \exp(-\frac{E_i}{RT}) \tag{4.12}$$

$$K_i(T) = A_i \ \exp(-\frac{\Delta H_i}{RT}) \tag{4.13}$$

where k_i and/or K_i are the reaction rate constant and/or the equilibrium constant, respectively, of the elementary reaction step i (see Table 4.2); A_i is the pre-exponential factor in Arrhenius equation; E_i is the activation energy; and ΔH_i is the adsorption enthalpy. The values of these parameters estimated by Todic et al. [58] are summarised in Table 4.2.

Table 4.2: Parameter values estimated by Todic et. al [58] for the calculation of reaction rates and equilibrium constants.

Parameter	Value	Unit	Parameter	Value	Unit
A_1	6.59×10^{-5}	MPa^{-1}	**ΔH_1**	-48.9	kJ/mol
A_2	1.64×10^{-4}	MPa^{-1}	**ΔH_2**	-9.4	kJ/mol
A_3	4.14×10^{8}	-	**E_3**	92.8	kJ/mol
A_4	3.59×10^{5}	-	**ΔH_4**	16.2	kJ/mol
A_5	9.81×10^{-2}	MPa	**ΔH_5**	11.9	kJ/mol
A_6	1.59×10^{6}	mol/(gcat-h)	**ΔH_6**	14.5	kJ/mol
A_7	4.53×10^{7}	mol/(gcat-h)	**E_7**	75.5	kJ/mol
A_8	4.11×10^{8}	mol/(gcat-h)	**E_8**	100.4	kJ/mol
A_{7M}	7.35×10^{7}	mol/(gcat-h)	**E_{7M}**	65.4	kJ/mol
A_{8E}	4.60×10^{7}	mol/(gcat-h)	**E_{8E}**	103.2	kJ/mol

The value for ΔE has also been estimated to be 1.1 kJ/mol/CH_2. The accuracy of the kinetic model and fit quality relative to the experimental data have also been estimated by Todic et al. using the mean absolute relative residual (MARR). The MARR value for the kinetic model based on CO-insertion mechanism has been reported to be 23.5%, which is better than the kinetic model based on carbide mechanism (MARR = 26.6%) developed by Todic et al. previously [62].

4.2 Basic Reactor Modelling

The FTS reactor model needs to meet several demands in order to render it comparable with the commercial reactors. The most important one is that the model should be capable of describing the complex interplay between the reaction kinetics and various physical phenomena that exist within these reactors. Several models have been developed so far for the purpose, but one of the major limitations with those models is the lack of a detailed kinetic model that is capable of predicting the FTS product distribution. Most of the developed models use simple reaction kinetics, with an overall conversion of CO, to estimate the product formation. Some of the models even assume a constant chain growth probability for the hydrocarbons, i.e., single-alpha or double-alpha models (see Section 2.6), instead of a varying chain growth probability that depends on the pressure, temperature and the hydrocarbon chain length, as in the model of Todic et al. [1].

In this project, the detailed kinetic model developed by Todic. et al [58] (discussed in Section 4.1) is used to develop the MTFBR model for FT synthesis. The fixed-bed reactor model developed by Todic during his PhD work [1] is considered as the reference model to develop a basic MTFBR reactor model. Once the basic reactor model is developed and validated, it is then further improved to develop a more sophisticated reactor model that performs detailed calculations and simulates the reactor conditions in a more accurate and realistic way. The assumptions and modelling equations considered for the basic reactor model are summarised in the following sections.

4.2.1 Model Assumptions

Fixed bed reactor models can be generally classified into pseudo-homogeneous and heterogeneous models, where the first assumes the catalyst to be a part of the bulk of the fluid (assumes thermal and concentration equilibrium between catalyst and fluid bulk) and does not account for its presence, while the the latter considers the presence of catalyst explicitly and uses separate conservation equations for fluid and catalyst (considers heat and mass transport to and within the catalyst). Also depending on the type of mixing (axial or radial) considered in the reactor, it can be either one- or two-dimensional, where the first assumes a plug flow in the axial direction without or with axial mixing (to account for non-ideality), while the latter also considers radial mixing in addition to the axial plug flow [1, 63]. The complexity of the model increases as it moves from the pseudo-homogeneous one-dimensional to the heterogeneous two-dimensional model, the latter being the most complex one. According to Steynberg et al. [8], the interfacial heat and mass transport in large catalyst particles (> 1 mm) with liquid filled pores can be neglected due to the low volumetric reaction rates, making the pseudo-homogeneous model sufficient in the case of an FTS reactor model.

Due to the typical large sizes of catalyst particles (1-3 mm), small diameters of tube (2.5-5 cm) and large lengths of tube (6-12 m), it has been considered reasonable to assume a plug flow model without axial mixing [8]. Also from the studies performed by Todic et al. [59] on the heat management in FTS reactor tubes, it is evident that the effect of heat transfer in the radial direction can be neglected in the case of smaller tube diameters (< 5 cm). Since reactors for Co-based catalyst use small diameters, it is assumed that one-dimensional approach is adequate. The intra-particle heat and mass transport are also assumed to be negligible in the basic model, which is generally valid only for small catalyst particles (< 200 μm), making the catalyst 100% efficient. Also, it is assumed that all molecular species in the gas phase follow ideal gas behaviour in the reactor.

From the experiments performed by Visconti et al. [64], it has been observed that more than 99% of all hydrocarbons in the reactor remain in the vapour phase under FTS conditions, thus making it justifiable to assume only the presence of gas phase in the model. However, the presence of even trace amounts of liquid in the reactor have been observed to considerably improve the heat transfer inside the reactor [65]. Hence, the presence of a thin layer of liquid is assumed in the reactor for heat transfer calculations. Also, since the syngas feed comes in contact with the reactor tube even before it reaches the catalyst bed, it is assumed that the feed and the tube wall attain a thermal equilibrium. Hence, T_w is assumed to be equal to the inlet temperature T_{in}.

4.2.2 Model Equations

The fixed-bed reactor model for FTS mainly consists of mass, heat and momentum balance equations. These are discussed in the following sections.

4.2.2.1 Mass Balance Equations

$$-\frac{dF_i}{dz} = A_{cs}\eta\rho_b R_i L \tag{4.14}$$

where F_i is the molar flow rate of component i (i = CO, H_2, H_2O and all product hydrocarbons), z is the dimensionless length of reactor, A_{cs} is the cross-sectional area of the reactor tube, η is the catalyst effectiveness factor (assumed to be 1), ρ_b is the bulk density of catalyst bed, L is the reactor length, and R_i is the rate of disappearance or formation of components. The rates of product formation and reactant disappearance are calculated for every element of the reactor using the detailed kinetic model discussed in Section 4.1. Also, the formation rates of n-paraffins and 1-olefins for every carbon number are summed up, and at the same time, the formation rates of every component with carbon number above and including 5 are summed up to obtain lumped formation rates for components C_1, C_2, C_3, C_4 and C_{5+} [1].

4.2.2.2 Heat Balance Equation

$$u_s\rho c_p\frac{dT}{dz} = \left[(-\Delta H_r)\eta\rho_b(-R_{CO}) - \frac{4U}{d_t}(T - T_w)\right]L \tag{4.15}$$

where u_s is the superficial velocity of fluid, ρ is the density of fluid, c_p is the heat capacity of fluid, T is the temperature in the reactor, $(-\Delta H_r)$ is the enthalpy of reaction (assumed to be 157 kJ/mol-CO considering C_9 to be the product formed [1, 60]), U is the overall heat transfer coefficient inside the reactor, d_t is the diameter of reactor tube, and T_w is the temperature at the reactor wall.

4.2.2.3 Momentum Balance Equation

$$-\frac{dP_t}{dz} = f\,\frac{\rho u_s^2}{d_p}L \tag{4.16}$$

The pressure drop in the reactor is calculated using the Ergun equation [1, 66], as given above, where P_t is the total pressure in the reactor, f is the friction factor for the flow of fluid through the packed bed (see Section 4.2.4.3), and d_p is the diameter of catalyst particle.

4.2.3 Model Implementation

With all the above balance equations, the FTS MTFBR model comprises of 10 ODEs that are solved using the Runge-Kutta method in MATLAB, with the *ode15s* implicit solver for stiff problems. The reactor is assumed to be a PFR with 100 elements ($\Delta z = 0.01$), and the equations are solved for every reactor element. The boundary conditions at the inlet of the reactor are as follows:

$$F_{CO}(z=0) = F_{CO}^{in} \tag{4.17}$$

$$F_{H_2}(z=0) = F_{H_2}^{in} \tag{4.18}$$

$$F_{H_2O}(z=0) = 0 \tag{4.19}$$

$$F_{CH_4}(z=0) = 0 \tag{4.20}$$

$$F_{C_2}(z=0) = 0 \tag{4.21}$$

$$F_{C_3}(z=0) = 0 \tag{4.22}$$

$$F_{C_4}(z=0) = 0 \tag{4.23}$$

$$F_{C_{5+}}(z=0) = 0 \tag{4.24}$$

$$T(z=0) = T^{in} \tag{4.25}$$

$$P(z=0) = P^{in} \tag{4.26}$$

For developing the basic model, only H_2 and CO (with an H_2/CO ratio of 2) are assumed to be present in the syngas feed. Later, in the detailed model, actual syngas feed with additional components such as CH_4, H_2O, N_2, etc., will be considered.

4.2.4 Parameter Estimation

Several parameters, such as thermodynamic and transport properties of components, and pressure drop parameters have to be calculated in order to solve the model equations. These are discussed in the following sections.

4.2.4.1 Thermodynamic and Transport Properties

The temperature-dependent physical properties of the system components (CO, H_2, H_2O, CH_4, C_2, C_3, C_4 and C_{5+}) in the vapour phase, such as heat capacity, viscosity and thermal conductivity, are estimated using correlations mainly obtained from Perry's Chemical Engineer's Handbook [1, 67] (see Table D.1). The properties of C_{5+} components are assumed to be equal to that of octane, and the thin liquid layer present in the reactor is assumed to be of C_{20} n-paraffin, for which the property values are taken from Aspen Properties and assumed to be constant throughout the reactor.

4.2.4.2 Overall Heat Transport

The heat transport calculations are performed considering the conductive, convective and diffusive transports of heat, through the reactor, in the radial direction. The heat transfer characteristics at the reactor wall and the central axis of the reactor are considerably different; hence, an overall heat transport coefficient (U), which takes into account the effective radial thermal conductivity in the core of the reactor (λ_{er}) as well as the heat transfer at the reactor wall (h_{wall}), is used [1, 68]. It is calculated as:

$$\frac{1}{U} = \frac{1}{h_{wall}} + \frac{d_t}{8\lambda_{er}} \tag{4.27}$$

where the effective radial thermal conductivity (λ_{er}) in the core of the reactor is estimated using the correlation suggested by Matsuura et al. [69], based on the work of Yagi et al. [70], as shown below:

$$\lambda_{er} = \lambda_{er}^{s} + \lambda_{er}^{g} + \lambda_{er}^{l} \tag{4.28}$$

where λ_{er} accounts for the static contribution (λ_{er}^{s}) of heat transport by conduction and diffusion, and the dynamic contribution of the heat transport by convection in the gas (λ_{er}^{g}) and liquid (λ_{er}^{l})

phases [68]. Since diffusion contributions are negligible for gas-liquid phases at FT conditions, Matsuura et al. [69] simplified the λ_{er}^{s} as:

$$\lambda_{er}^{s} = 1.5\lambda_{l} \tag{4.29}$$

where λ_l is the thermal conductivity of the liquid layer in the reactor. The values of λ_{er}^{g} and λ_{er}^{l} are estimated as a function of Reynolds (Re) and Prandtl (Pr) numbers (defined in Appendix E), as they account for the radial mixing of gas and liquid phases within the void spaces of the packed bed:

$$\lambda_{er}^{g} + \lambda_{er}^{l} = (\alpha\beta)_g \lambda_g Re_g Pr_g + (\alpha\beta)_l \lambda_l Re_l Pr_l \tag{4.30}$$

The coefficients required for the calculations are given in Table 4.3.

Table 4.3: Coefficients required for the calculation of dynamic contribution convective of heat transport in gas and liquid phases [68, 69].

d_p	$(\alpha\beta)_g$	$(\alpha\beta)_l = a*(1+b*Re_g)$	
(cm)	-	a	b
0.12	0.412	0.201	$2.83*10^{-2}$
0.26	0.334	0.167	$1.34*10^{-2}$
0.43	0.290	0.152	$6.32*10^{-3}$

The interaction of all three phases with the wall of reactor tube is given by the effective heat transfer coefficient at the wall (h_{wall}), and since the flow rate of liquid is negligible, the following equation is used [1, 63, 68]:

$$h_{wall} = \frac{10.21\lambda_{er}^{s}}{d_t^{4/3}} + 0.033\frac{\lambda_g}{d_p} Re_g Pr_g \tag{4.31}$$

where the two terms represent the static and dynamic contributions to heat transfer at the wall, respectively.

4.2.4.3 Fixed-Bed Pressure Drop

The pressure drop inside the reactor is calculated using the Ergun equation (4.16) [71], and the friction factor (f) in the packed bed is calculated as:

$$f = \frac{1-\varepsilon_w}{\varepsilon_w^3}\,(1.75 + 150\,\frac{1-\varepsilon_w}{Re_g}) \tag{4.32}$$

where ε_w is the effective bed porosity, which takes into account the holdup of liquid inside the reactor bed (ε_l), such that:

$$\varepsilon_w = \varepsilon_b - \varepsilon_l \tag{4.33}$$

where the porosity of the bed (ε_b) is estimated as a function of catalyst particle diameter and the tube geometry [1, 68]:

$$\varepsilon_b = 0.1504 + \frac{0.2024}{\phi_p} + \frac{1.0814}{(\frac{d_t}{d_p} + 0.1226)^2} \tag{4.34}$$

where ϕ_p is the sphericity of the catalyst particle (assumed to be 1). It has been observed that the contribution of liquid holdup (ε_l) to effective bed porosity in FT reactors is less than 3-4% [72], hence, a contribution of 1% is considered in this model. Some miscellaneous formulas and relations are also provided in Appendix E.

4.3 Detailed Reactor Modelling

The detailed reactor model is essentially an improved version of the basic reactor model. The values of certain parameters used directly from the literature, while developing the basic reactor model, are estimated using exhaustive calculations in the detailed reactor model. The detailed model is also integrated with Aspen Plus for developing the process model, with a gas loop to provide a recycle stream back to the FTS reactor. The following sections will explain these in detail.

4.3.1 Model Improvements

The main improvements incorporated in the reactor model include: extended component calculation; integration of the model with Aspen Properties for estimation of thermodynamic physical and transport properties, vapour-liquid equilibrium, dynamic liquid holdup, and actual enthalpy of FT reaction; calculation of catalyst effectiveness factor; improved h_{wall} calculation; and improved pressure drop calculation.

4.3.1.1 Extended Component Model

In the basic reactor model, the formation rates of n-paraffins and 1-olefins, with carbon atoms 1, 2, 3, 4 and above 5, are summed up to obtain lumped formation rates for components C_1, C_2, C_3, C_4 and C_{5+} (see Section 4.2.2.1). In the detailed model, the formation rates of n-paraffins and 1-olefins are separately calculated, i.e., the rates of C_n n-paraffin and C_n 1-olefin are not added up to get an overall rate for C_n hydrocarbon. Also, all the components above C_5 are not lumped to form a C_{5+} component, instead, they are considered as individual components. Due to lack of available data in the Aspen Properties database, the components considered for the detailed model include: all n-paraffins from $C_{1\text{-}50}$, excluding C_{39}, C_{41}, C_{47} and C_{49}; all 1-olefins from $C_{2\text{-}40}$, excluding C_{25}, $C_{31\text{-}35}$ and $C_{37\text{-}39}$; and other components like H_2, CO, CO_2, H_2O, O_2, N_2 and Ar. Thus, the detailed model considers a total of 83 components, including 76 hydrocarbons.

4.3.1.2 Vapour-Liquid Equilibrium

In the basic reactor model, existence of a thin layer of C_{20} liquid is assumed throughout the reactor in order to facilitate heat transfer inside the reactor, whereas in the detailed model, the actual vapour-liquid equilibrium (VLE) composition inside the reactor is estimated for every element of the reactor, which makes the reactor model more accurate. The VLE data for the system, based on Peng-Robinson equation of states, is extracted from an Excel Add-in of Aspen, called Aspen Properties and MATLAB extracts these data during every iteration of the solver. Peng-Robinson equation of states has been known to predict the properties of hydrocarbons and petroleum fractions with a reasonable accuracy [73]. The process of extracting VLE data from Aspen Properties is explained in detail in Section 4.3.3. Ideally, the liquid fraction should increase along the reactor length, reaching its maximum towards the exit of the reactor, as more heavy hydrocarbons are formed.

4.3.1.3 Thermodynamic and Transport Properties

The thermodynamic and physical properties of components in the basic reactor model are calculated using correlations from Perry's Chemical Engineer's Handbook [67] (see Section 4.2.4.1), whereas in the detailed model, the properties of all components are directly extracted from the Aspen Properties. The heat capacities, densities and thermal conductivities of all system components (extended model), in both vapour and liquid phases, are extracted dynamically and used for calculations in every element of the reactor, during every iteration of the MATLAB solver. The process of extracting thermodynamic data from Aspen Properties is also explained in Section 4.3.3.

4.3.1.4 FTS Reaction Enthalpy

The reaction enthalpy (ΔH_r) for FT synthesis in the basic model is assumed to be 157 kJ/mol-CO, assuming an average C_9 product [1, 60], whereas in the detailed model, the enthalpy of reaction is estimated for every element of the reactor by iterating and solving the modified heat balance equation (4.35) in MATLAB, instead of Equation 4.15. As discussed before, the thermodynamic properties of the components are obtained from Aspen Properties, and thus, an accurate value for the ΔH_r can be estimated for every reactor element. The derivation of the modified heat balance equation can be found in Appendix F.

$$(\dot{m}_g c_{p,g} + \dot{m}_l c_{p,l})\frac{dT}{dz} = \frac{dH_{tot}}{dz} - U\pi d_t (T - T_w)L \tag{4.35}$$

where $\dot{m}$ is the mass flow rate, c_p is the specific heat capacity, dz is the dimensionless length of differential reactor element, and dH_{tot} is the total heat released during the reaction at reference state conditions (considered to be at inlet conditions). dH_{tot} is calculated as follows:

$$dH_{tot} = (F_g^{in} H_g^{in} + F_l^{in} H_l^{in})_{T_{in}} - (F_g^{out} H_g^{out} + F_l^{out} H_l^{out})_{T_{in}} \tag{4.36}$$

where F and H are the flow rate and enthalpy, respectively, of the gas/liquid phase in the inlet/outlet stream. Equation 4.35 is a more accurate heat balance equation than Equation 4.15, however, the computational time required to simulate the whole reactor with Equation 4.35 (more than 30 min) is considerably higher than that with Equation 4.15 (less than a minute). Hence, Equation 4.15 is used for heat balance in the detailed model, but with a more accurate reaction enthalpy (ΔH_r) value, which is calculated as the weighted average of reaction enthalpy estimated for every reactor element ($\Delta H_\mathrm{r,e}$) with the rate of CO consumption ($-R_{CO}$) in every reactor element. $\Delta H_\mathrm{r,e}$ is calculated as follows:

$$-\Delta H_{r,e} = \frac{dH_{tot}}{dz}\frac{1}{\rho_b(-R_{CO})A_{cs}L} \tag{4.37}$$

4.3.1.5 Heat Transfer at Wall

Experiments performed by Todic et al. [59] show that the values of h_{wall} predicted using Equation 4.31 are considerably lower than that obtained from correlations developed for two-dimensional models [74, 75]. The results of Matsuura et al. [69] at trickle-bed conditions under low liquid flow rates show that h_{wall} can be dependent on the flow rates of both gas and liquid phases. They observed two regions: a region of low liquid flow rate ($Re_l < 10$) where h_{wall} is determined by the flow of gas, and a region of high liquid flow rate ($Re_l > 10$) where h_{wall} is determined by the flow of liquid [59]. Hence, it is justifiable to assume that for FTS conditions (where $Re_l = < 2$), h_{wall} is entirely determined by the gas phase flow rate. The following gas-phase h_{wall} correlation has been observed to adequately predict the heat transport model for a range of process conditions and reactor geometries [59, 75]:

$$h_{wall} = h_{wall,o} + h_{wall,g} \tag{4.38}$$

where $h_{wall,o}$ and $h_{wall,g}$ are the stagnant and convective contributions, respectively, to the radial heat transfer at the wall. These are calculated as:

$$h_{wall,o} = \frac{\lambda_g}{d_p}\left(2\,\varepsilon_b + \frac{1-\varepsilon_b}{\frac{\lambda_g}{\lambda_c}\gamma_w + \phi_w}\right) \tag{4.39}$$

$$h_{wall,g} = \frac{\lambda_g}{d_p} \cdot 0.0835 \cdot Re_g^{0.91} \tag{4.40}$$

where $\gamma_w = 1/3$ and $\phi_w = 0.00240.(d_t/d_p)^{1.58}$ for spherical particles, and λ_g is the thermal conductivity of the gas phase. Equation 4.40 has been observed to be valid in the range of $10 < Re_g$

<1200, which is within the range of Re_g observed under typical FTS conditions [75, 68]. Thermal conductivity of the catalyst particles (λ_c) is estimated using the correlation provided by Wu et al. for cobalt based FT catalysts [76]:

$$\lambda_c = 0.8652 + 0.00108 \cdot (T - 273.15) \tag{4.41}$$

where T is the temperature in K.

4.3.1.6 Dynamic Liquid Holdup

The contribution of liquid holdup to the bed porosity (ε_l) is assumed to be 1% in the basic model, whereas in the detailed model, the dynamic liquid holdup in the reactor is estimated using a correlation determined by Satterfield and reported by Froment et al. [68, 66]:

$$\varepsilon_l = \left(\frac{\mu_l u_{s,l}}{d_p^2 g \rho_l}\right)^{\frac{1}{3}} \tag{4.42}$$

where μ_l, $u_{s,l}$ and ρ_l are viscosity, superficial velocity and density of the liquid, respectively, and g is the gravitational constant.

4.3.1.7 Fixed-Bed Pressure Drop

It has been observed that the Ergun equation (4.32) is valid only if $Re_g/(1 - \varepsilon_w) < 500$, as the equation assumes a constant turbulent contribution to friction in the packed bed [77]. Since the typical values of $Re_g/(1 - \varepsilon_w)$ for FTS are well above 500 [68], Ergun equation is not usable as such for estimating the pressure drop in the packed bed. Tallmadge [78] modified the turbulent contribution in the Ergun equation to incorporate the dependence of Reynolds number to the packed-bed friction, and thus, extending the valid range of the correlation to $0.1 < Re_g/(1 - \varepsilon_w) <$ 100,000 [68].

$$f = \frac{1 - \varepsilon_w}{\varepsilon_w^3} \left(4.2 \left(\frac{1 - \varepsilon_w}{Re_g}\right)^{\frac{1}{6}} + 150\,\frac{1 - \varepsilon_w}{Re_g}\right) \tag{4.43}$$

The above Tallmadge equation (4.43) is used to calculate the packed-bed friction factor in the detailed reactor model.

4.3.1.8 Catalyst Effectiveness Factor

The intra-particle heat and mass transfer are neglected in the case of basic reactor model, whereas the catalyst particles are assumed to be completely filled with hydrocarbon wax in the case of detailed reactor model. Mandic et al. [79] assumed the properties of the hydrocarbon wax to be same as that of n-octacosane ($C_{28}H_{58}$), but in this project, the actual properties of the wax, which mainly contains all heavy hydrocarbons, are estimated using Aspen Properties. The diffusion coefficients of species in the wax, based on Wilke-Chang correlation [80], are also estimated using Aspen Properties. The effective diffusivities of the components are then calculated as:

$$D_{e,i} = D_{wax,i}\,\frac{\varepsilon_c}{\tau} \tag{4.44}$$

$D_{wax,i}$ is the diffusivity of the component i in the hydrocarbon wax, ε_c is the porosity of the catalyst (assumed to be 0.5), and τ is the tortuosity factor (assumed to be 2) [79]. A generalised Thiele Modulus based on the characteristic diffusion length has been proposed as [79, 81]:

$$\phi = \phi_{CO} = L_c \sqrt{\frac{\rho_c \cdot (-R^s_{CO})}{D_{e,CO} \cdot C^s_{CO}}} \tag{4.45}$$

where L_c is the characteristic diffusion length ($L_c = V/S$; V = volume in which the catalyst is located and S = surface area exposed to surrounding fluid). For a spherical catalyst, L_c is calculated to be $d_p/6$; ρ_c is the catalyst density, C^s_{CO} is the liquid phase concentration of CO at the catalyst surface, and $(-R^s_{CO})$ is the rate of disappearance of CO at the catalyst surface [59, 79]. The CO concentration is estimated using the liquid phase composition obtained from Aspen Properties. The effectiveness factor for a spherical particle is then calculated using the formula [82]:

$$\eta = \frac{3}{\phi}\left[\frac{1}{\tanh(\phi)} - \frac{1}{\phi}\right] \tag{4.46}$$

Every component has to diffuse into the hydrocarbon wax filled in the catalyst pores in order to reach the catalyst surface for reaction. Since the diffusivity of every component in wax is not the same, effectiveness factor must be calculated for every component individually. However, for simplicity, the effectiveness factor for all components are assumed to be equal to that of CO, i.e., $\eta_i = \eta_{CO}$ in the mass balance equation (4.14). Todic et al. [59] observed that the effects due to the use of a generalised effectiveness factor is negligible considering the thermal behaviour of FTS FBRs.

4.3.2 Gas Loop & Recycle

Generally, the per pass conversion in an FTS reactor with cobalt catalysts is limited by the partial pressure of water. Hence, it is recommended to keep the per pass conversion below 60% in order to keep the partial pressure of water in the reactor under desirable ranges (< 5 bar, in some cases) [8]. Internal or an external recycle may also be introduced into the process to obtain an overall conversion of about 90%, while still keeping the per pass conversion under 60%. Internal recycle involves the recycling of a part of the FTS product stream directly back into the reactor along with the feed, whereas, external recycle involves the recycling of a part of the product stream after separating the undesirable components from it. The recycle stream can be either directly introduced to the reactor inlet or to the syngas generation unit, depending on the process and stream specifications, forming a gas loop. The optimisation of the recycle streams is very crucial to obtain maximum productivity of the desired products, in this case, C_{5+} hydrocarbons.

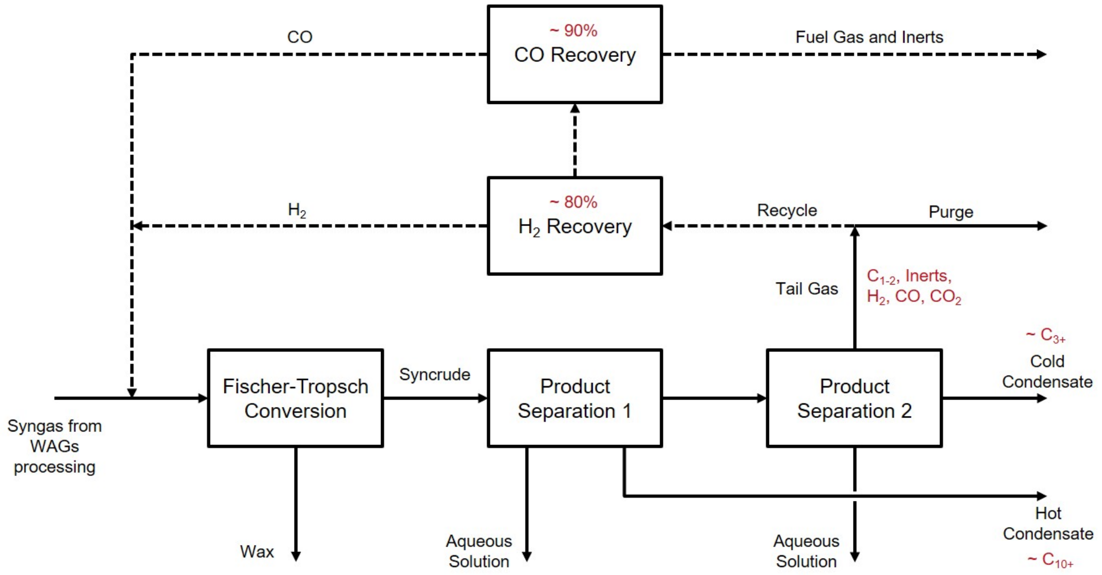

Figure 4.2: Gas loop design for the FTS process.

Since the separation and refining of syncrude are beyond the scope of this project, a simplified gas loop design, with basic separation processes, is considered in order to determine the effect of recycling on the per pass and the overall conversion. Figure 4.2 shows the block flow diagram of the simplified gas loop design for the FTS process.

The syngas, generated from the processing of WAGs, is fed to the MTFBR reactor where it gets converted to syncrude and wax products via the FTS process. The wax stream mainly contains heavy hydrocarbons ($\sim C_{20+}$) in the liquid phase and is directly sent to the refining section, whereas the syncrude stream contains all light hydrocarbons ($< C_{20}$) and unreacted syngas in the gas phase, which is partly recycled after separation. The syncrude stream initially enters a separation unit where hydrocarbons above C_{10} are efficiently extracted as a hot condensate. The remaining gases from the first separation unit are sent to a cryogenic separation unit where hydrocarbons above C_3 are efficiently separated as a cold condensate. Aqueous streams, which mainly contain dissolved oxygenates, are also removed from both the separation units.

The tail gas obtained after the separation processes mainly contain fuel gases ($C_{1\text{-}2}$), unreacted CO and H_2, inerts and CO_2. It is partly purged, and the rest is sent to the H_2 recovery unit, where an H_2 recovery of 80% is considered. The H_2-lean exhaust stream from the H_2 recovery unit is then sent to the CO recovery unit, where a CO recovery of 90% is considered. The recovered H_2 and CO streams are recycled back into the FTS reactor to complete the gas loop. The recycle/purge ratio of the tail gas can be varied to obtain different conversion values; this is later optimised to determine the best configuration with respect to the productivity of C_{5+}.

4.3.3 Model Implementation

As discussed in Section 4.1.2, the chain growth probability of hydrocarbons (α_n) and the fraction of vacant sites on the catalyst surface ($[S]$) are inter-dependent, and thus, need to be solved simultaneously using the *fzero* function in MATLAB. Since these parameters are necessary to calculate the rates of reactants and products, they must be solved for every element of the reactor, i.e., within every iteration of the *ode*15*s* solver. Thus, there is a non-linear implicit solver within the ODE solver, which is quite cumbersome, but can be easily handled in MATLAB. Aspen Plus does not have a provision to deal with such type of reaction kinetics, and therefore, it is necessary to use an external solver to perform the kinetic calculations. Hence, the MTFBR reactor model is basically developed in MATLAB and then integrated into Aspen Plus as a user-defined reactor model, which acts like a black box with respect to Aspen Plus. The data required to perform calculations in MATLAB are passed on from Aspen Plus, and the final data from MATLAB, after solving the balance equations, are passed back to Aspen Plus. The Aspen Plus-MATLAB connection is established using VBA (Visual Basic for Applications) macros in Excel, which acts as an intermediate platform to control and exchange data between the two.

The basic reactor model assumes constant properties for the liquid-phase and uses correlations to calculate temperature-dependent properties of the gas-phase components (see Section 4.2.4.1). Since the detailed model deals with every component individually, the properties of every individual n-paraffins and 1-olefins have to be calculated. Also, the calculation of VLE inside the reactor requires the thermodynamic properties of all components, and since MATLAB does not have any in-built fluid property package to extract these properties from, an external fluid property package is essential. AspenTech has a consistent and robust software to generate fluid physical property packages that are of industrial standards, and is used in the process simulation software Aspen Plus. AspenTech also has made the fluid property packages available as an Excel Add-in called Aspen Properties [83], which is very convenient to integrate it with most of the computational software. Hence, the MATLAB reactor model is linked to an excel file, which in turn extracts the required component properties via the Aspen Properties tool, to perform calculations in the MATLAB during every iteration of the ODE solver. The MATLAB-Aspen Properties connection is established using the ActiveX COM (Component Object Model) server, which is an in-process server that provides a framework for integrating resuable, binary software components into an application [84]. The flow of control and data exchange between Aspen Plus, MATLAB and Aspen Properties are illustrated in Figure 4.3.

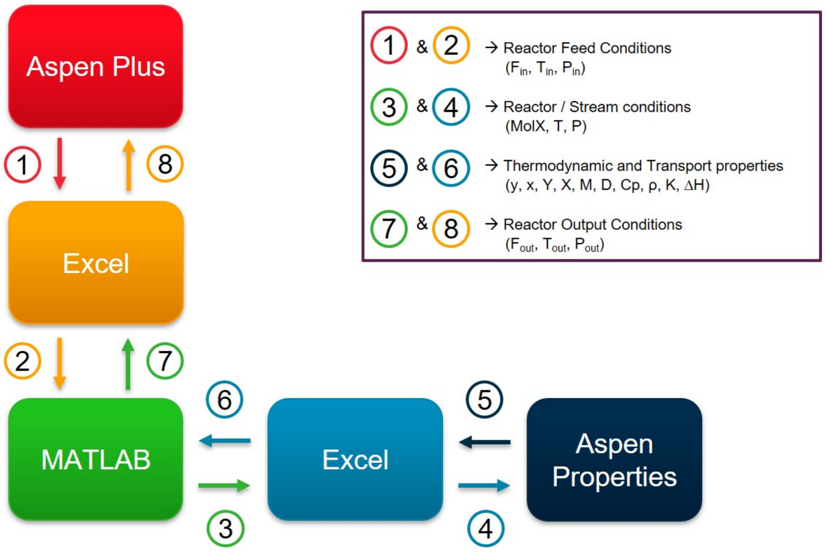

Figure 4.3: Flow of control and data exchange between Aspen Plus, MATLAB and Aspen Properties.

The user-defined reactor model in Aspen Plus passes the reactor feed conditions (step 1), such as molar flow rates of components (F_{in}), inlet temperature (T_{in}) and inlet pressure (P_{in}), to an excel file which interacts with the MATLAB server and passes these values (step 2) to the MATLAB model. The MATLAB model then interacts with Aspen Properties via the same excel file and extracts the component properties during every iteration of the solver. Aspen Properties requires MATLAB to pass on the reactor/stream conditions (steps 3 & 4), such as mole fraction of components ($MolX$), temperature (T) and pressure (P), in order to retrieve thermodynamic and transport properties (steps 5 & 6), such as vapour and liquid composition (y and x), vapour and liquid fraction (Y and X), molar masses (M), diffusivities (D), heat capacities (C_p), densities (ρ), thermal conductivities (K), and enthalpies (H) of both gas and liquid phases. All the thermodynamic and physical properties in Aspen Properties are estimated using the Peng-Robinson equation of states, which has been known to predict the properties of hydrocarbons and petroleum fractions with a reasonable accuracy [73]. Steps 3-6 repeat until MATLAB completes all the solver iterations, and the reactor output conditions, such as molar flow rates of components (F_{out}), outlet temperature (T_{out}) and outlet pressure (P_{out}), are passed back to the Aspen Plus via the Excel-VBA link (steps 7 & 8), where they become the output of the user-defined reactor model in Aspen Plus. A schematic showing the sequence of calculations and operations performed in MATLAB is shown in Figure 4.4.

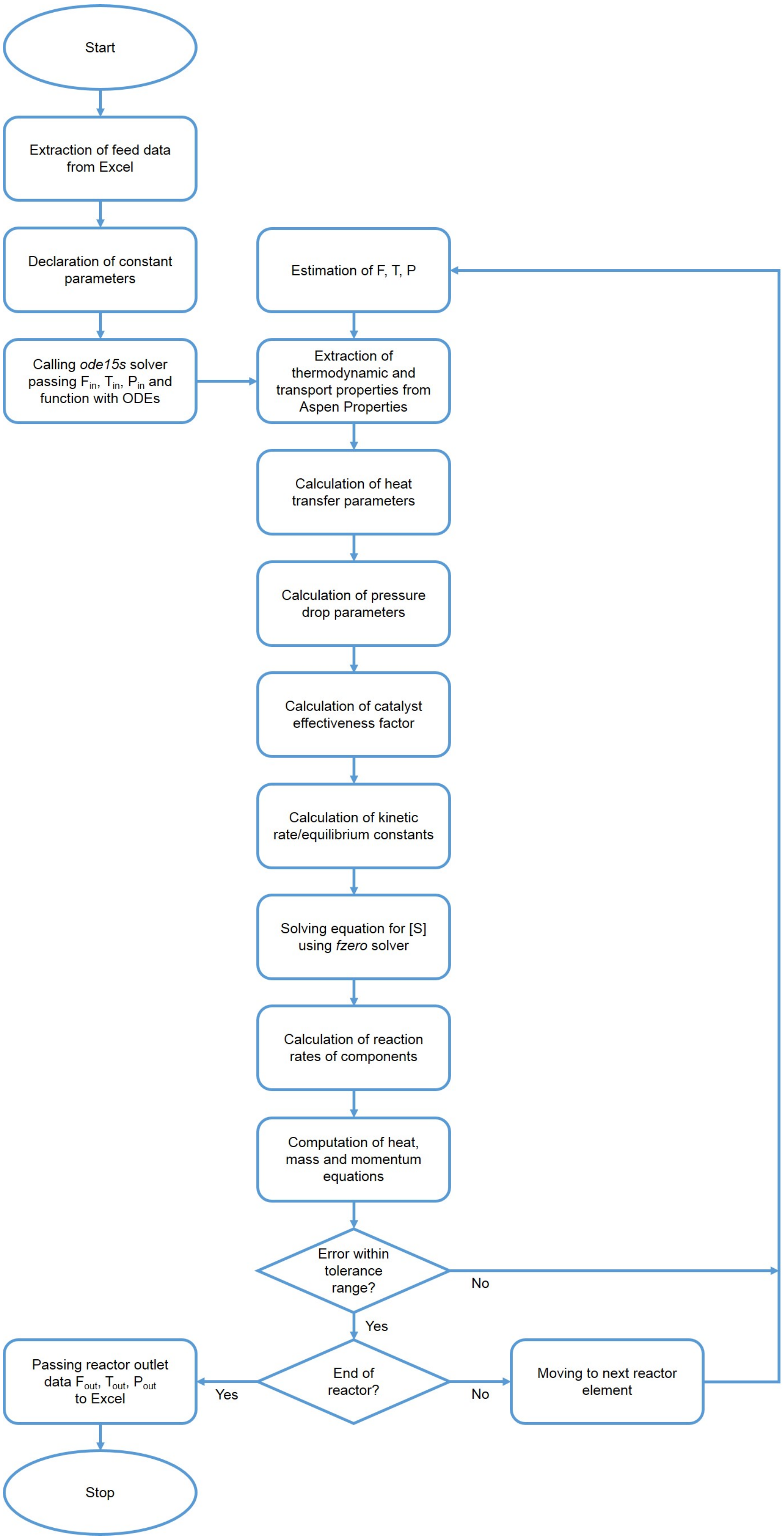

Figure 4.4: Sequence of calculations and operations performed in MATLAB.

5. Results & Discussion

As discussed before in the previous chapters, a kinetic model is developed in MATLAB initially, followed by the modelling of the basic and the detailed reactors. A sensitivity analysis is also performed on the design and process parameters of the reactor, followed by the optimisation of the detailed reactor model to yield maximum productivity of C_{5+}. The results obtained for various models and cases during the modelling and simulation of the reactor are summarised in this chapter.

5.1 Kinetic Model Validation

The CO-insertion mechanism based kinetic model developed by Todic et al. [58] is used to model the FTS product distribution in the reactor model. A MATLAB model for FTS kinetics is developed based on the model equations discussed in Section 4.1.2 and is validated with the kinetic model developed by Todic et al. The validation is perfomed for three different conditions: T = 478K, P = 1.5 MPa, H_2/CO = 2.1 and WHSV = 3.7 NL/gcat/h; T = 493K, P = 1.5 MPa, H_2/CO = 1.4, WHSV = 5.6 NL/gcat/h; and T = 503K, P = 1.5 MPa, H_2/CO = 2.1, WHSV = 11.3 NL/gcat/h; where WHSV is the weighted hourly space velocity of the syngas feed. The results for the first validation case are shown in Figure 5.1, and the results for the second and third validation cases are shown in Appendix G.

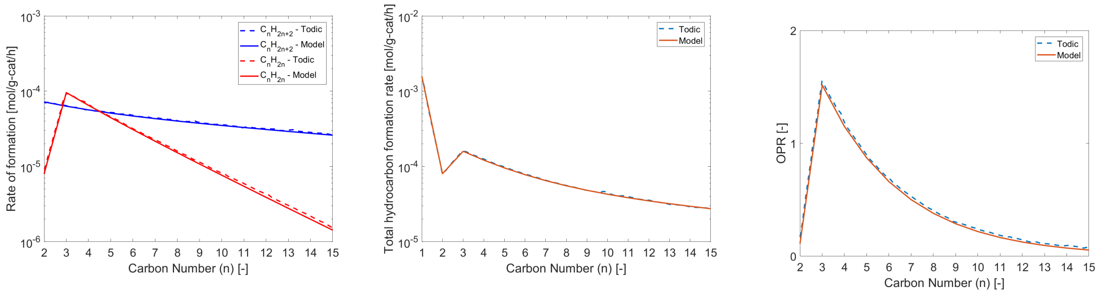

(a) Formation rates of n-paraffins and 1-olefins

(b) Total hydrocarbon formation rate

(c) Olefin-to-Paraffin ratio (OPR)

Figure 5.1: Validation of kinetic model with results of Todic et al. (Process conditions: T = 478K, P = 1.5 MPa, H_2/CO = 2.1, WHSV = 3.7 NL/gcat/h, X_{CO} = 37%) [58].

The product distribution and the chain growth probability obtained using the kinetic model are also validated in a similar way, as shown in Figure 5.2. The process conditions used are: T = 493K, P = 1.5 MPa, H_2/CO = 2.1 and WHSV = 8 NL/gcat/h.

It can be seen from the Figures 5.1 and 5.2 that the OPR ratio reaches a maximum at C_3 and then decreases further with increasing the carbon number. The low OPR ratio of C_2 can be attributed to the high reactivity of ethene, which results in the readsorption of ethene to undergo chain growth (forming longer hydrocarbons) or hydrogenation (forming paraffins). It can also be seen that the chain growth probability increases with carbon number and reaches a maximum of around 0.93 at C_{15}, leading to the higher than expected production of heavy hydrocarbons, justifying the non-ASF behaviour. Thus, the results produced by the kinetic model are very similar to that obtained by Todic et al [58], rendering the kinetic model suitable for modelling the multi-tubular fixed-bed reactor.

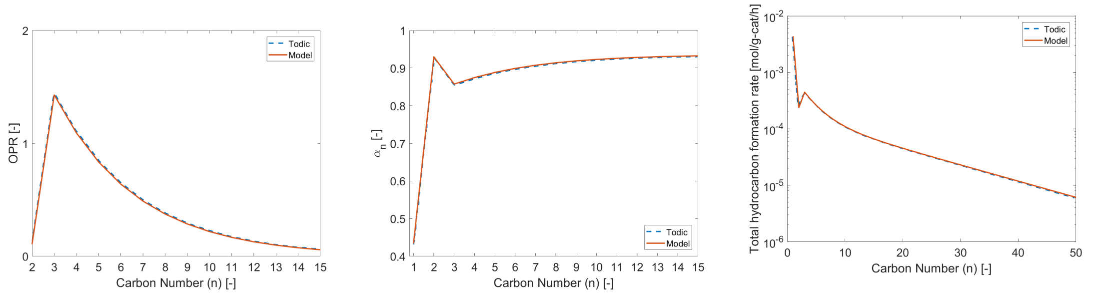

(a) Olefin-to-Paraffin ratio (OPR) **(b) Chain growth probability (α_n)** **(c) Total hydrocarbon formation rate (ASF Plot)**

Figure 5.2: Validation of model product distribution with results of Todic et al. (Process conditions: T = 493K, P = 1.5 MPa, H_2/CO = 2.1, WHSV = 8 NL/gcat/h, X_{CO} = 45%) [58].

5.2 Basic Reactor Model Results

The main objective of the basic reactor model is to provide a starting point for developing a detailed reactor model that is comparable to the commercial FTS reactors. Since the basic reactor model uses the same model equations and assumptions used by Todic [1], the process conditions and reactor geometry used for validation of the reactor model are also the same. The parameters used for the initial validation of the model (base case) are also similar to that used in the MTFBR of Shell in Bintulu plant and are summarised in Table 5.1 [1, 8, 68, 85, 86].

Table 5.1: Process parameters and reactor geometry used for the base case simulation

Process Conditions		Reactor Geometry	
Inlet temperature (K)	475	Tube length (m)	12.86
Inlet pressure (bar)	30	Tube diameter (cm)	2.6
Feed H_2/CO ratio (mol/mol)	2	Particle diameter (mm)	2.5
Inlet syngas flow rate per tube (mol/s)	0.15*	Number of tubes	26150
Wall temperature (K)	475		

* flow rate per tube is chosen to obtain approximately 60% conversion

The results obtained from the simulation of the basic reactor model for the base case conditions are shown in Figure 5.3. It can be observed from Figure 5.3(c) that the temperature profile is slightly higher in case of the basic reactor model (by 5-6K), compared to the results obtained by Todic [1]. This may be attributed to the difference in thermal properties of the liquid layer used, which plays a vital role in the transfer of heat inside the reactor. The liquid properties for the model are taken from Aspen Properties for the inlet conditions and are assumed to be constant throughout the reactor length, i.e., independent of the temperature, resulting in inaccurate heat values. The higher temperature in the reactor has also resulted in a slightly higher conversion (by 1-2%) (see Figure 5.3(a)), but it is still closely comparable. The molar flow rates of CH_4 and C_{5+} obtained in the basic model are also very similar to that obtained by Todic. However, despite similar conversion and molar flow rates, the pressure drop obtained in case of the basic reactor model ($\sim$ 1.4 bar) is around 9 times lower than that obtained by Todic ($\sim$ 12 bar). Considering the fact that the feed stream used comprises only H_2 and CO, and that it does not contain any inerts or liquids, a pressure drop of 12 bar along the packed bed seems unjustifiable. Todic [1] has also commented about the higher pressure drop obtained in his model and attributes it to the pressure drop equation considered. However, using the same model equations, the basic reactor model is able to simulate a pressure drop which is more realistic when compared to packed bed reactors [68].

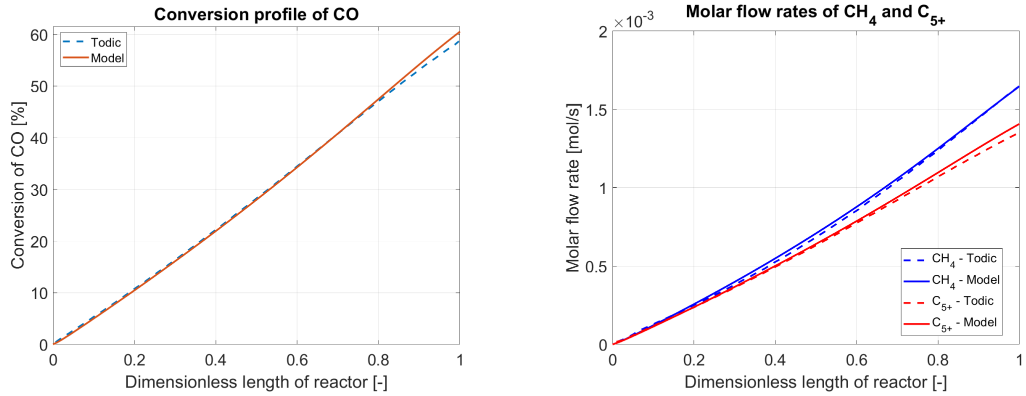

(a) Conversion profile of CO **(b) Molar flow rates of CH_4 and C_{5+} per tube**

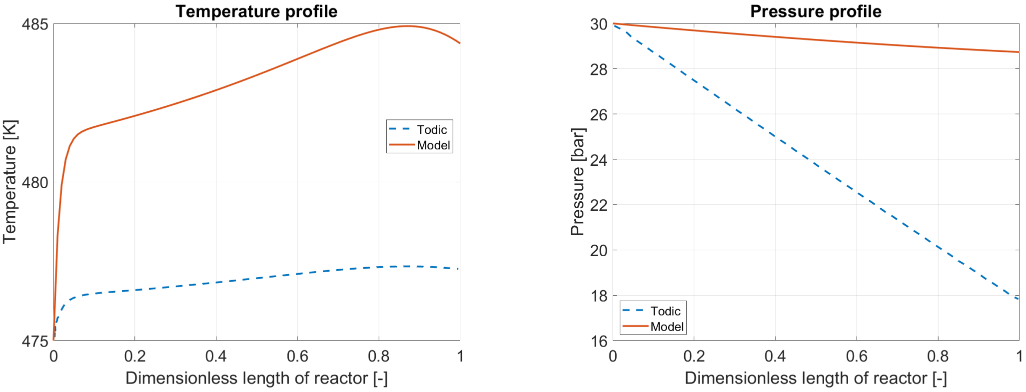

(c) Temperature profile **(d) Pressure profile**

Figure 5.3: Results of basic reactor model and that of Todic et al. [1].

The selectivities of CH_4 and C_{5+} obtained in the basic reactor model are 5.4 and 89.8%, respectively, which is comparable to that obtained by Todic (5.6 and 89.7%, respectively). Assuming the average C_{5+} products to be in the C_9 fuel range, the productivity of the reactor calculated is 142,800 tonnes/y (assuming 350 days of production), which is also comparable to that of Todic (151,670 tonnes/y). The slight difference in productivity may be due to the difference in number of production days assumed, as the production days assumed by Todic is unknown. Interestingly, the selectivities of CH_4 and C_{5+}, in the MTFBR of Shell in Bintulu plant, are in the ranges of 5-10% and 85-92%, respectively. Also the annual production of C_{5+} is known to be 144,000 tonnes/y with around 80% total conversion [1, 8, 68]. The basic model produces results in similar ranges to that of Shell, even with a 60% conversion in the reactor. This can be mainly due to the fact that the syngas feed in this model is assumed to be pure, without any inerts or other hydrocarbons which can have a negative impact on the production, or because the effectiveness of catalyst is assumed to be 100%, which, according to literature, should be in the range of 60 to 90% [68]. However, considering all the results of the basic reactor model, it can be seen that it is sufficiently representative of the large-scale commercial reactors, and thus, it can be used as a starting design to develop a detailed reactor model that represents the commercial reactors even more closely.

5.3 Detailed Reactor Model Results

The detailed reactor model is developed by incorporating several improvements to the basic reactor model, as discussed before in Section 4.3. The simulations in the detailed reactor model are performed with the same base case process conditions and the reactor geometry as used with the basic reactor model. An initial simulation is performed using the pure syngas feed used to simulate the basic model, and later, the actual syngas feed produced from the work's arising gases is used. The results for the two cases are discussed in the following sections.

5.3.1 Pure Syngas Feed

As discussed before in Section 4.2.3, the syngas feed used in the case of basic reactor model is assumed to be a mixture of only H_2 and CO, with an H_2/CO ratio of 2. The same feed, base case conditions and reactor geometry are used for simulation in the detailed model, and the results are shown in Figure 5.4.

It can be seen that the conversion in the detailed reactor model is around 40%, while the conversion in the basic reactor model, for the same feed and process conditions, is around 60%. The low conversion in the detailed model can be attributed mainly to the lower temperature inside the reactor (maximum around 480K near the outlet) compared to the basic model (maximum around 485K near the outlet), which in turn, is an effect of improved heat transfer in the detailed reactor model. Since the kinetics is favoured by higher temperatures, a lower temperature in the reactor thus results in a lower conversion level, also resulting in lower flow rates of product hydrocarbons. However, the pressure drop in the packed-bed appear to be the same (1.4 bar) in case of both the reactors, despite the difference in conversion levels. This can be attributed to the fact that the pressure drop mainly depends on the superficial velocity of the gas phase and the size of catalyst particles (or bed voidage). Since these parameters are the same, the effect of other parameters, like the gas density, on the pressure drop is not evidently visible. The selectivities of CH_4 and C_{5+} obtained in the advanced reactor are 5.8 and 89%, respectively, which are also similar to those obtained with the basic reactor model (5.4 and 89.8%). The productivity of C_{5+} obtained in the case of detailed model is 198,890 tonnes/y, which is much higher than that obtained in case of the basic model (142,800 tonnes/y), despite a lower conversion. This can be attributed to the fact that the productivity in case of basic model is calculated assuming C_9 as the average C_{5+} product, leading to the multiplication of total number of C_{5+} moles produced with the mass of just C_9 hydrocarbon. It can be seen from Figure 5.4(f) that the mass fraction of hydrocarbons above C_5 reaches a maximum between C_{25} and C_{30}. Thus, assuming the average C_{5+} product to be C_{28}, for instance, would be more accurate than assuming it to be C_9. However, in the case of detailed model, the molecular mass of every individual component (from C_1 until C_{50}) is multiplied by its corresponding moles produced to calculate the productivity, thus, leading to more accurate results. It can be seen from Figure 5.4(f) that the mass fraction of C_2 1-olefin is very low compared to its corresponding n-paraffin and also the C_3 1-olefin, which can be attributed to its higher reactivity, as discussed before in Section 2.6. Also, it can be observed that the 1-olefin fraction decreases from C_3 until around C_{25}, and thereafter, only n-paraffins are present in the heavy wax range. Thus, the product distribution in the detailed reactor model closely follows the non-ASF behaviour observed in actual FTS reactors.

The improvements incorporated in the basic reactor model have considerable effects on the results obtained. The presence of a heavy wax layer in the reactor, which increases along the reactor length, improves the heat transfer compared to a thin uniform layer of C_{20} liquid throughout the length. The improved heat transfer inside the reactor, in turn, results in a better temperature control, allowing the reactor to be operated at higher temperatures than in the case of basic reactor model, without leading to a thermal runaway. Also, over 99% of all components inside the reactor are observed to be in the vapour phase at FTS conditions, verifying the results obtained by Visconti et al [64]. The new average reaction enthalpy (ΔH_r) estimated using Equations 4.35 and 4.37,

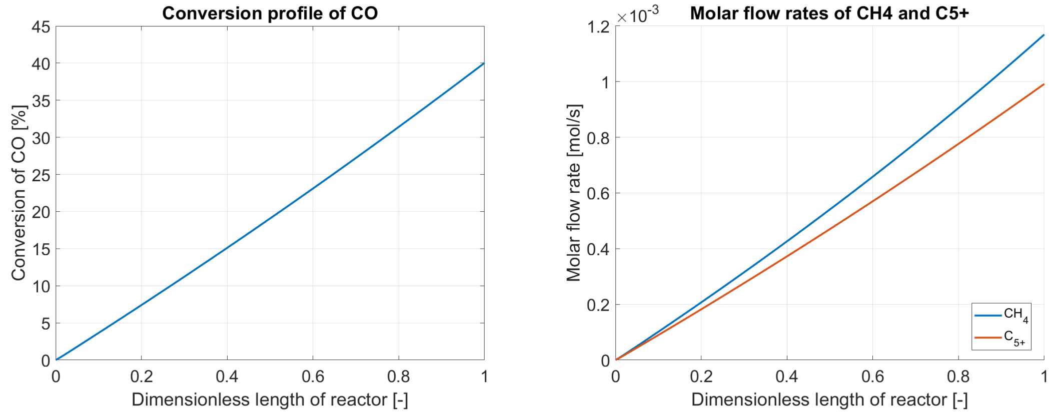

(a) Conversion profile of CO **(b) Molar flow rates of CH_4 and C_{5+} per tube**

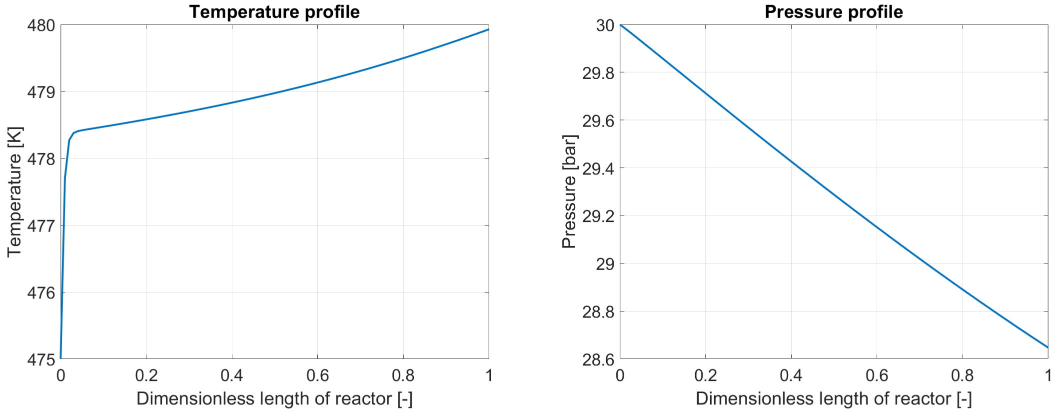

(c) Temperature profile **(d) Pressure profile**

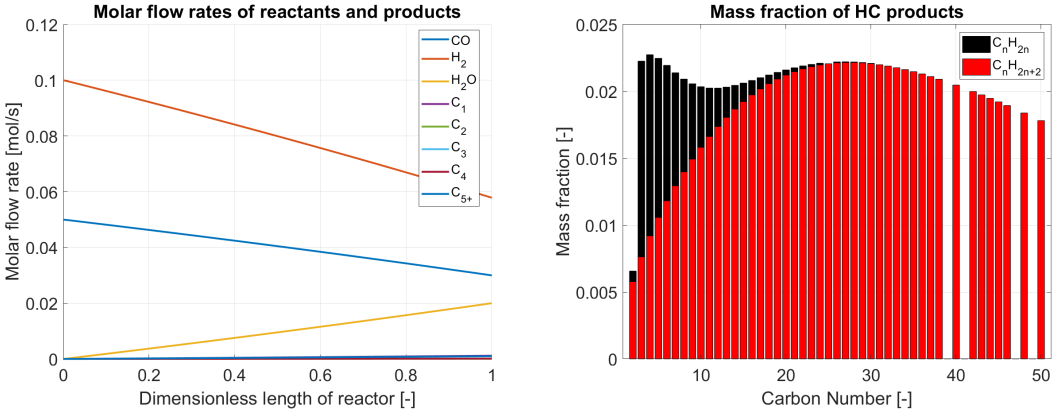

(e) Molar flow rates of components per tube **(f) Mass fraction of hydrocarbon products**

Figure 5.4: Results of detailed reactor model for base case process conditions and reactor geometry with pure syngas feed.

taking into account all hydrocarbon products formed, is around 167 kJ/mol-CO, which is around 10 kJ/mol-CO higher than that calculated for an average C_9 product (157 kJ/mol-CO) and also corresponds to the literature [87, 88]. However, the catalyst effectiveness factor estimated is in the range of 95-100%, as opposed to 60-90% estimated by Brunner et al. [68]. This can be due to the fact that the calculations performed by Brunner et al. assumed only $C_{28}H_{58}$ as the wax product filled in catalyst pores, in which CO must diffuse to reach the catalyst surface for reaction. This assumption can lead to a lower diffusion coefficient than the case where CO diffuses into all hydrocarbons present in the liquid phase, as calculated in the detailed model. The diffusion coefficient for CO in wax estimated in the detailed model is several magnitudes higher (10^3-10^4) than that estimated for CO in $C_{28}H_{58}$ alone due to the presence of more liquid hydrocarbons. Thus, the intra-particle mass transport resistances reduce considerably, resulting in higher catalyst effectiveness factors.

Owing to all the above facts, the detailed reactor model can be considered to be more accurate than the basic reactor model in simulating multi-tubular fixed bed reactors used in commercial GTL plants.

5.3.2 WAGs Syngas Feed

Following the development of the detailed reactor model and verification of its improved features, the actual syngas feed, obtained from the processing of WAGs, is fed into the detailed reactor model to determine the effect of impure syngas on the performance of MTFBR. The composition of the WAGs syngas feed can be found in Table 3.1, and the simulation results obtained for the base case conditions and reactor geometry are shown in Figure 5.5.

Ideally, higher flow rates result in lower reactor conversions as the residence time of reaction molecules decreases with increase in space velocity. However, despite the higher flow rate of WAGs syngas feed (0.2 mol/s/tube) compared to the pure syngas feed (0.15 mol/s/tube), the single pass conversion in the reactor is much higher ($\sim$ 68%) compared to that with the pure syngas feed ($\sim$ 40%). This can be mainly attributed to the fact that only around 45% of the WAGs syngas feed is comprised of pure syngas ($\sim$ 15% CO and $\sim$ 30% H_2), and the rest is comprised of inerts that do not take part in the reaction and contribute only to the pressure drop. Thus, the effective flow rate of pure syngas in the WAGs syngas feed is only around 0.09 mol/s/tube, which is much lower than the pure syngas feed at 0.15 mol/s/tube, resulting in a higher conversion in the reactor. The lower partial pressures of reactants in the case with WAGs syngas feed should have resulted in a lower conversion; however, in this case, the effect of the residence time of reactants appears to be more dominant than the effect of reactant partial pressures on the conversion. A higher conversion does not always guarantee a higher productivity of C_{5+}, as lower effective flow rate of pure syngas results in lower flow rates of hydrocarbon products, ultimately resulting in a lower productivity. The productivity of C_{5+} obtained is 182,300 tonnes/y with the WAGs syngas feed, which is lower than that with the pure syngas feed (198,890 tonnes/y), as expected. The selectivities of CH_4 and C_{5+} obtained are 10.8 and 81.2%, respectively, which shows that the presence of impurities have a negative impact on the selectivity towards heavy hydrocarbons. This can also be seen in Figure 5.5(f) where the mass fraction has increased in the lower hydrocarbon ranges and decreased in the higher hydrocarbon ranges. Higher flow rates also contribute to increased heat transfer inside the reactor, as can be seen in Figure 5.5(c), where the maximum temperature is restricted to around 481K. A peak can be observed in the temperature profile near the entrance of the reactor which shows that most of the conversion occurs in the first half of the reactor, and that the formation rate gradually slows down as more products are produced along the reactor, due to the decrease in partial pressure of the reactants. The pressure drop in the packed-bed is higher ($\sim$ 4 bar) than that with pure syngas ($\sim$ 1.4 bar), due to the higher overall flow rate.

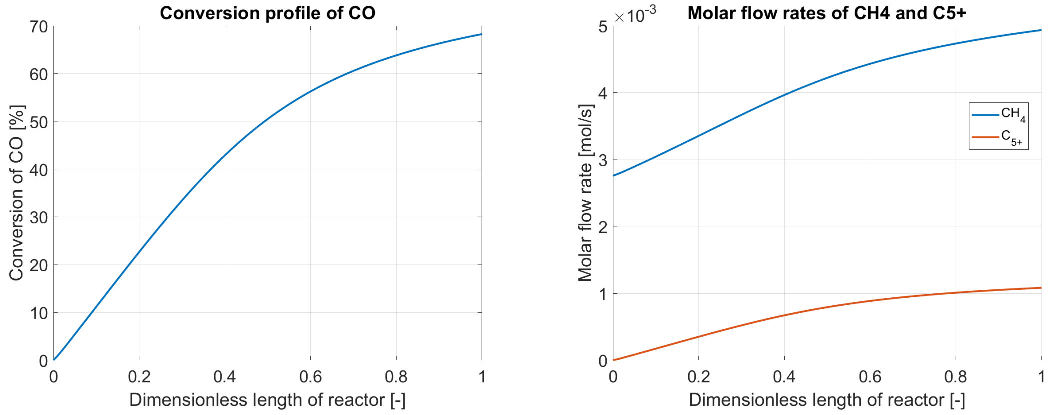

(a) Conversion profile of CO **(b) Molar flow rates of CH_4 and C_{5+} per tube**

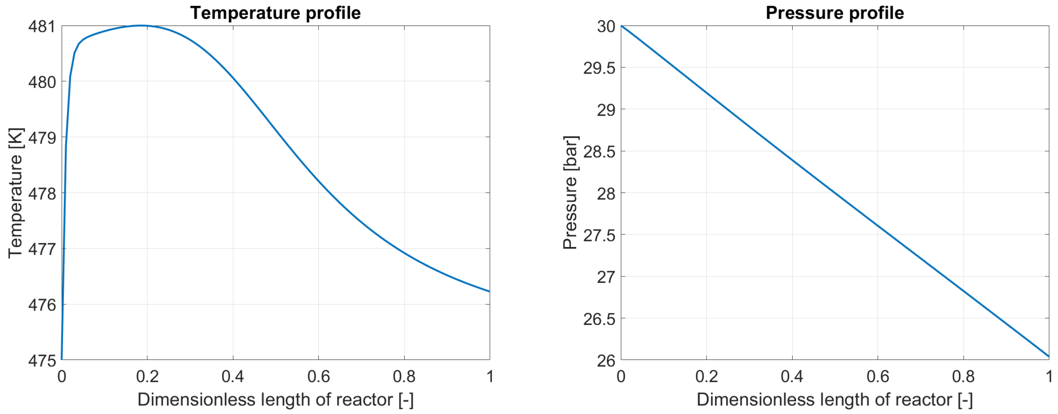

(c) Temperature profile **(d) Pressure profile**

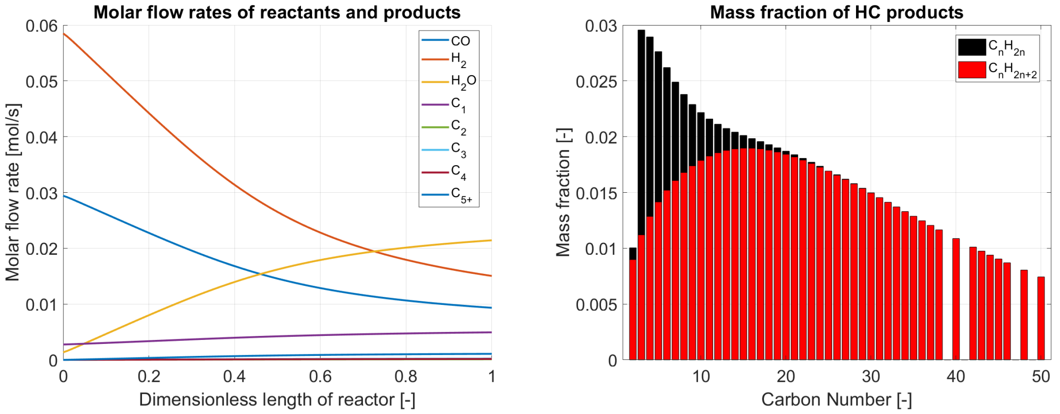

(e) Molar flow rates of components per tube **(f) Mass fraction of hydrocarbon products**

Figure 5.5: Results of detailed reactor model for base case process conditions and reactor geometry with syngas from WAGs as feed.

5.4 Gas Loop & Recycle

After performing simulations with the detailed reactor model using WAGs syngas feed and analysing the results for a single pass reactor, a process model for the gas loop is developed in Aspen Plus V10 in order to introduce a recycle stream into the MTFB reactor. Since the product separation and refining units are beyond the scope of this project, several assumptions are made during the process model development (see Section 4.3.2). The process flow diagram (PFD) of the FTS gas loop process with MTFBR is shown in Figure 5.6.

The process starts with the WAGs syngas feed stream (1), which is compressed to the required inlet pressure of 30 bar in an isentropic compressor (C-101). The compressed feed stream (2) is heated to the required inlet temperature in a heater (E-101), after which the conditioned stream (4) is fed to the FTS MTFB reactor (R-101). The product stream (5) from the reactor, which is a gas-liquid mixture, is sent to a two-phase flash drum (D-101) which is operated at the same temperature as the reactor outlet, in order to separate the gas (6) and the liquid (7) streams. The liquid stream (7) mainly contains heavy wax products and is sent to the hydroprocessing unit for further refining, whereas the gas stream (6) is cooled (E-102) and condensed in a three-phase flash drum (D-102) in order to separate the aqueous phase (11), the organic phase (10) with C_{10+} hydrocarbons, and a gas stream (9) with rest of the components. The gas stream (9) is further cooled (E-103) to cryogenic temperatures and condensed in a three-phase flash drum (D-103) to separate the tail gas stream (13), the organic phase (14) with C_{3+} hydrocarbons, and the aqueous stream (15). The tail gas stream (13), which mainly contains unreacted H_2 and CO, fuel gas ($C_{1\text{-}2}$), CO_2 and inerts, is partly purged (17) and the rest (16) is sent to the H_2 recovery unit. Since the H_2 recovery (assumed to be an H_2-PSA) requires a temperature less than 100°C, the recycled tail gas stream (16) is cooled (E-104) before feeding it to the H_2 recovery unit. An H_2 recovery of 80% is considered in this unit (see Section 4.3.2). The exhaust gases from the H_2 recovery unit (19) are then sent to the CO recovery unit, where a CO recovery of 90% is considered. Since CO recovery (assumed to be COSORB process) is performed at atmospheric pressures, the pressure of the exhaust stream (19) from the H_2 recovery unit is reduced to 1 atm using a valve (V-101), before feeding it to the CO recovery unit. The exhaust gas stream (23) from the CO recovery unit, which mainly contains fuel gas, unrecovered H_2 and CO, CO_2 and inerts, is purged out. The recovered H_2 (20) and CO (24) streams are both compressed and mixed with the feed stream (2) in order to complete the gas loop. Since the recovered CO stream (24) is at atmospheric pressure and since the temperature of the stream rises during the isentropic compression process, a multi-stage compression with intermediate cooling is required to pressurise it to 30 bar. A two-stage compressor system (C-103 and C-104), with a compression ratio of 5.5 in each stage, is considered in this model for representational purposes.

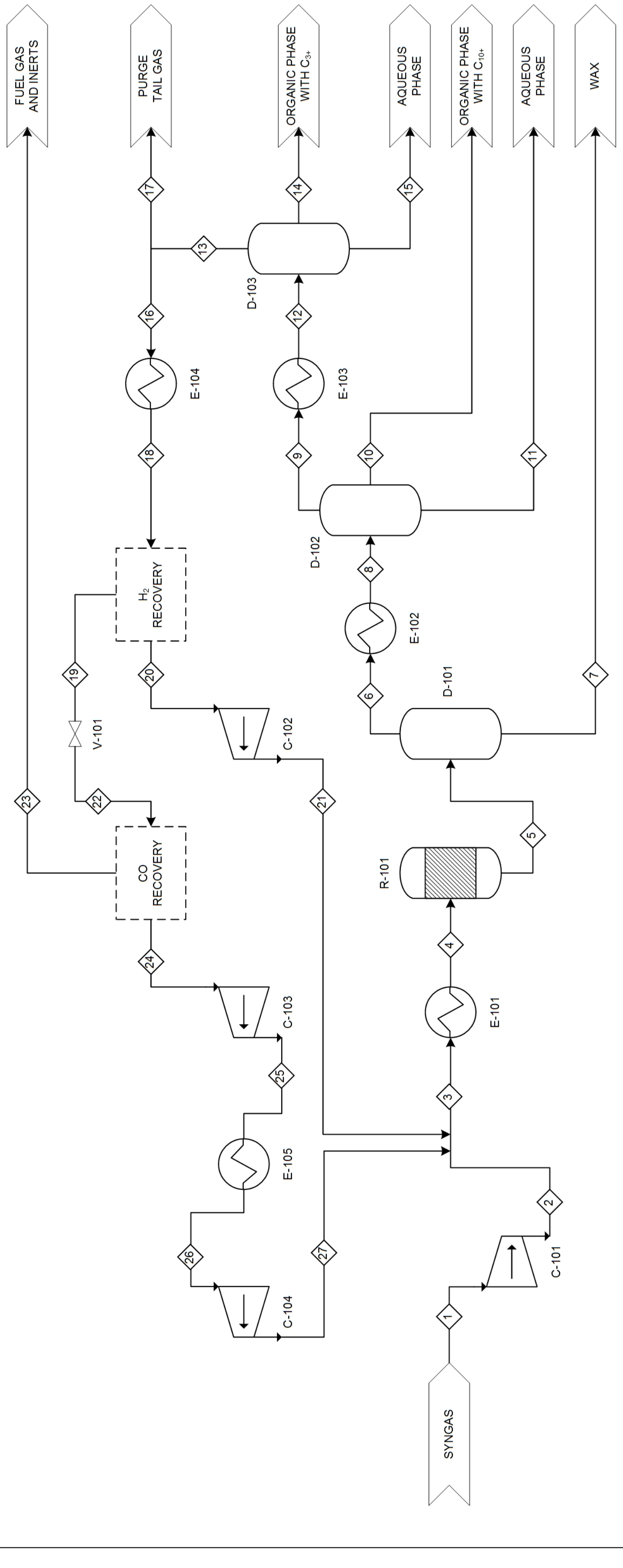

Figure 5.6: The process flow diagram (PFD) of the FTS gas loop process with MTFBR.

5.5 Sensitivity Analysis

The MTFB reactor performance is influenced by several parameters, such as catalyst particle size, tube diameter, inlet temperature, inlet pressure and feed flow rate, feed H_2/CO ratio, etc. These can be generally classified as reactor design and process parameters, and the effect of these parameters on the reactor performance is studied by performing a sensitivity analysis. All simulations are performed with the WAGs syngas feed (specifications in Table 3.1) using the base case process conditions and reactor geometry (see Table 5.1), except for the parameter under consideration, for which a lower and a higher value than the base case are used. The simulation results are compared with the base case results (see Figure 5.5) in order to understand the degree of influence of the desired parameter on the reactor performance. After performing the sensitivity anaysis on the reactor parameters, a sensitivity analysis is also performed on the tail gas recycle ratio, which is an FTS gas loop process parameter, in order to study its effects on the overall FTS process. These are discussed in the following sections.

5.5.1 Reactor Design Parameters

The reactor design parameters considered for sensitivity analysis in this project are the catalyst particle size (d_p) and the diameter of the reactor tube (d_t). The analysis results for these parameters are explained in the following sections.

5.5.1.1 Particle Size

The three cases considered for the sensitivity analysis on the catalyst particle size (d_p) are: base case (B) = 2.5 mm, case (1) = 1.5 mm, and case (2) = 3.5 mm; and the simulation results obtained are shown in Figure 5.7.

It can be seen from Figure 5.7(a) that the conversion in all the three cases is around 67-68% which shows that the effect of catalyst particle size on the reactor conversion is relatively negligible. The pressure drop in the packed-bed is considerably affected by the particle size, as can be seen from Figure 5.7(d), where the pressure drop in the case of smaller particle size ($\sim$ 9 bar) is much higher compared to that with larger particle size ($\sim$ 2 bar). This can be attributed to the fact that the smaller particles get packed very closely in the bed, resulting in a low bed porosity, thus providing more resistance to the flow of fluid through the bed. It can also be seen from Figure 5.7(c) that the peak in the reactor temperature profile, near the entrance of the reactor, is higher for smaller catalyst particles. This can be attributed to the decrease in radial thermal conductivity of the bed with decrease in particle size, which makes it difficult to remove heat effectively from the reactor. A detailed study on the effect of particle size on the heat management in a fixed-bed has been performed by Todic et al. [59], and the results obtained confirm the simulation results obtained in this project. Several studies also suggest the use of large catalyst particles for better heat management in the reactor, allowing operations at even higher temperatures, leading to higher productivities [8, 59, 89]. The reduction in the catalyst effectiveness factor with large catalyst particles, due to increase in intra-particle heat and mass transfer resistances, also contributes to the lower heat in the reactor [89, 90]. The selectivities of CH_4 and C_{5+} are around 11 and 81%, respectively, in all the three cases, with a negligible increase in C_{5+} selectivity with particle size, as can be seen from Figure 5.7(b). According to Todic et al. [59], the recommended size of particles to have optimum heat management and productivity is in the range of 1-3 mm for Co catalysts.

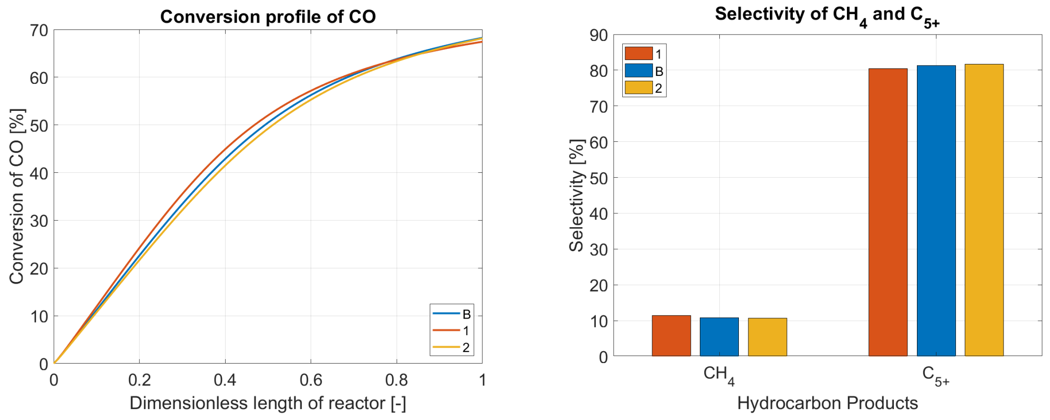

(a) Conversion profile of CO **(b) Selectivities of CH_4 and C_{5+}**

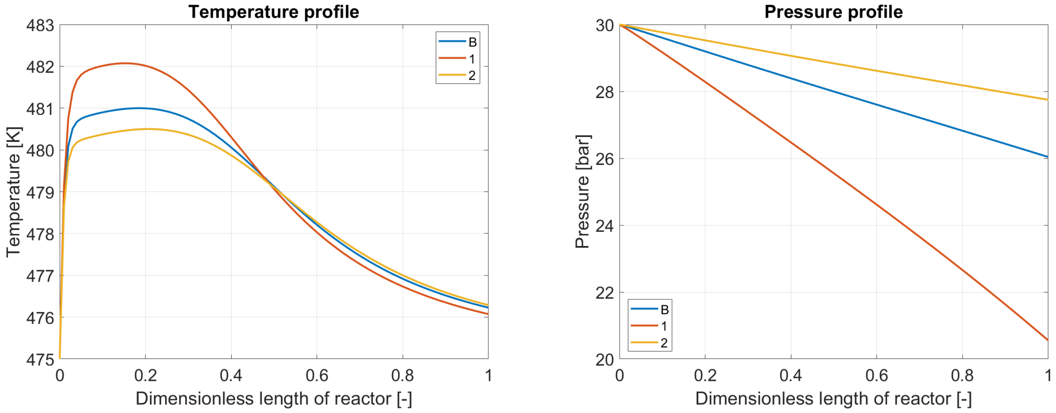

(c) Temperature profile **(d) Pressure profile**

Figure 5.7: Results of sensitivity analysis performed on catalyst particle size (d_p) (Base case (B) = 2.5 mm, Case (1) = 1.5 mm, Case (2) = 3.5 mm).

5.5.1.2 Tube Diameter

The three cases considered for the sensitivity analysis on the tube diameter (d_t) are: base case (B) = 2.6 cm, case (1) = 2 cm, and case (2) = 3 cm; and the simulation results obtained are shown in Figure 5.8. It can be seen from Figure 5.8(c) that the temperatures near the entrance in the case of larger tube size are considerably higher than that in the base case. This can be attributed to the combination of lower values of heat transport coefficients due to reduced fluid velocities and increased radial heat transport resistance due to larger size of the tube. Thus, heat is not effectively removed from the reactor in the case of a larger tube size, resulting in higher reactor temperatures, especially near the entrance of the reactor where most of the conversion occurs. However, in the case of smaller tubes, heat is effectively removed from the bed due to lower heat transport resistance, and thus results in a steady temperature profile throughout the reactor (see Figure 5.8(c)). A higher temperature in the reactor also results in a higher conversion, as can be seen in Figure 5.8(a), where around 75% conversion takes place in the larger tube compared to around 68% in the base case. The conversion in the smaller tube barely reaches 50% even with the same conditions.

The selectivity to C_{5+} products is generally favoured by lower temperatures, hence, larger tubes with high temperatures result in lower selectivity to C_{5+}, as can be seen in Figure 5.8(b). The selectivity to C_{5+} decreases from around 83 to 79% as the tube size increases from 2 to 3 cm. However, the pressure drop in the smaller tube is considerably higher ($\sim$ 12 bar) than that in the

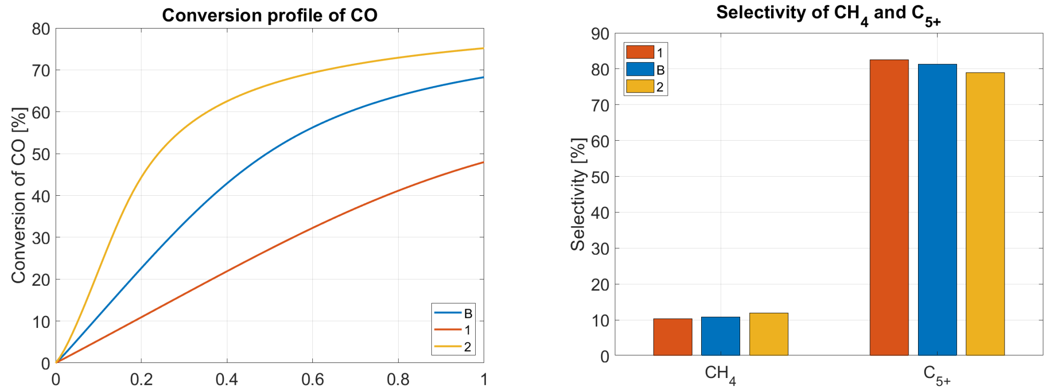

(a) Conversion profile of CO **(b) Selectivities of CH_4 and C_{5+}**

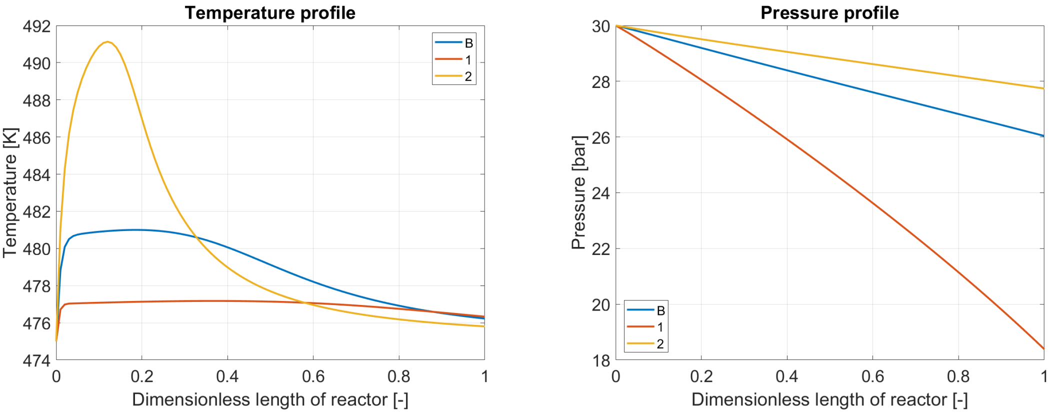

(c) Temperature profile **(d) Pressure profile**

Figure 5.8: Results of sensitivity analysis performed on tube diameter (d_t) (Base case (B) = 2.6 cm, Case (1) = 2 cm, Case (2) = 3 cm).

larger tube ($\sim$ 2 bar). This can be mainly attributed to the decrease in flow area per tube in the case of smaller tube diameters. As the flow area in the tube decreases, the flow rate in the tube increases, which ultimately leads to a higher pressure drop in the tube. The decrease in density of the fluids, due to higher temperatures in the case of larger tube diameters, can result in a lower pressure drop. However, the effect of density on the pressure drop is considerably negligible compared to that of the flow rate. Typical tube sizes for MTFBRs are in the range of 2.5-5 cm (1-2 in), where larger tubes are used for Fe catalysts and smaller tubes are used for Co catalysts, due to the higher reactivity of Co compared to Fe [8, 59].

5.5.2 Reactor Process Parameters

The reactor process parameters considered for sensitivity analysis in this project are: inlet temperature (T_{in}), inlet pressure (P_{in}), inlet flow rate (F_{in}) and inlet H_2/CO ratio. The analysis results for these parameters are explained in the following sections.

5.5.2.1 Inlet Temperature

The three cases considered for the sensitivity analysis on the inlet temperature (T_{in}) are: base case (B) = 475K, case (1) = 465K, and case (2) = 485K. The tube wall temperature is assumed to

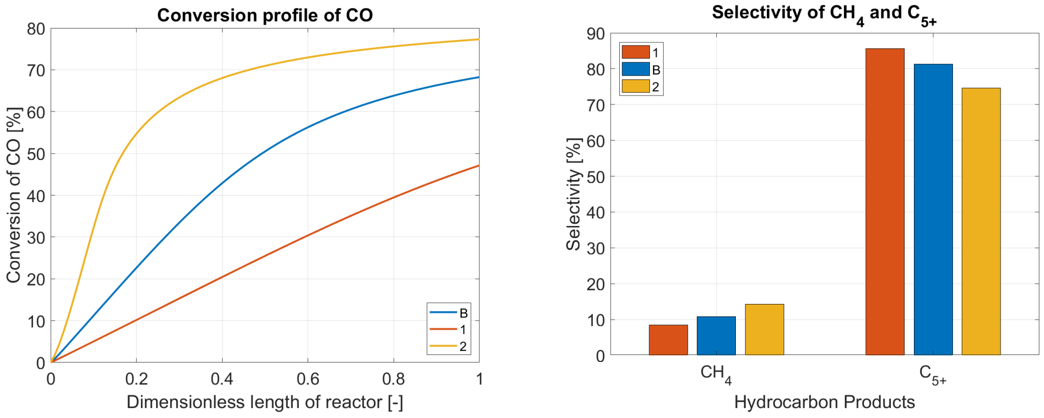

(a) Conversion profile of CO **(b) Selectivities of CH_4 and C_{5+}**

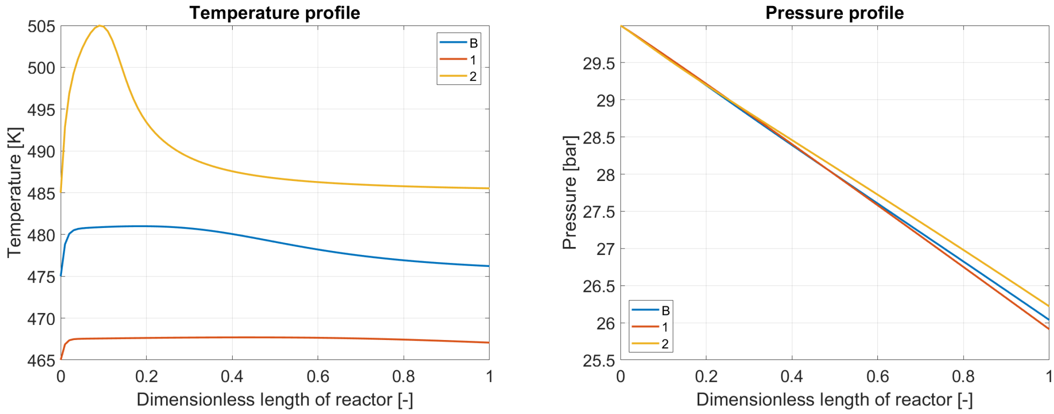

(c) Temperature profile **(d) Pressure profile**

Figure 5.9: Results of sensitivity analysis performed on inlet temperature (T_{in}) (Base case (B) = 475K, Case (1) = 465K, Case (2) = 485K).

be constant throughout its length and equal to the inlet temperature in all the three cases, i.e., $T_w = T_{in}$; and the simulation results obtained are shown in Figure 5.9.

It can be seen from Figure 5.9(c) the temperatures near the entrance of the reactor, in the case of higher inlet temperature, reaches a maximum of 505K, which is very high compared to the base and the lower cases, where it reaches only around 480K and 467K, respectively. A higher inlet temperature results in a higher reaction rate, which further results in large amounts of heat released due to the higher rate of exothermic FTS reaction. The removal of heat from the reactor would be relatively difficult in such conditions, leading to a thermal runaway. Simulations with inlet temperatures above 487K (plots not shown here) result in much poorer heat removal and thermal runaways, unless the wall temperature is reduced to cope with the increased heat generated from the exothermic FTS reaction. It can be seen from Figure 5.9(a) that the conversion increases from around 48 to 78% as the inlet temperature increases from 465 to 485K. This can also be attributed to the increase in reactor temperature with increase in the inlet temperature, thus leading to a higher rate of reaction and conversion. It can also be observed that in the case of higher inlet temperature, the slope of the conversion curve is higher in the first half of the reactor, and then, reduces gradually in the second half of the reactor. This is also a consequence of higher reaction rates in the first half of the reactor due to higher reactor temperatures. The selectivity of C_{5+} decreases from 86 to 75% as the inlet temperature increases from 465 to 485K, as can be seen in Figure 5.9(b), thus implying that low temperatures are favourable for the production of liquid hydrocarbons. The pressure drop in the packed-bed is not significantly affected by the inlet temperature, however, the pressure drop in the case of higher inlet temperature is slightly lower than that of the base case due to lower density of fluids (see Figure 5.9(d)). Thus, an optimal inlet temperature is desirable for maximising the selectivity towards C_{5+} products without compromising on the reactor conversion.

5.5.2.2 Inlet Pressure

The three cases considered for the sensitivity analysis on the inlet pressure (P_{in}) are: base case (B) = 30 bar, case (1) = 20 bar, and case (2) = 40 bar; and the simulation results obtained are shown in Figure 5.10.

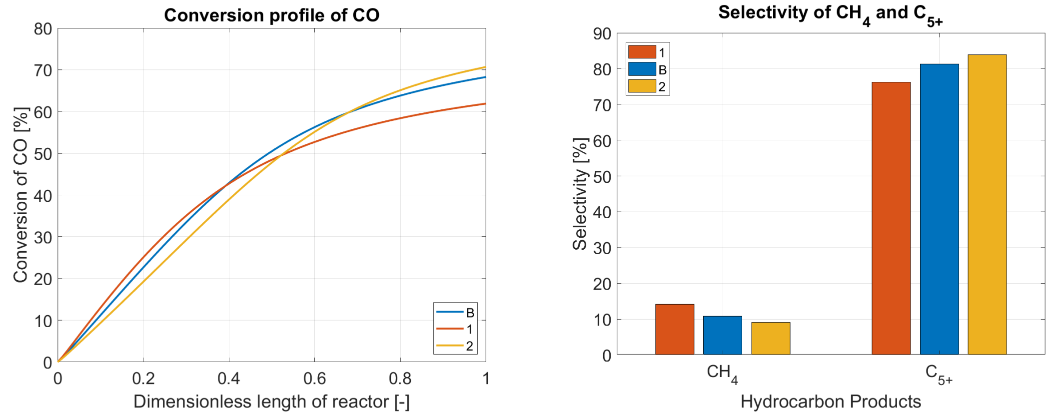

(a) Conversion profile of CO **(b) Selectivities of CH_4 and C_{5+}**

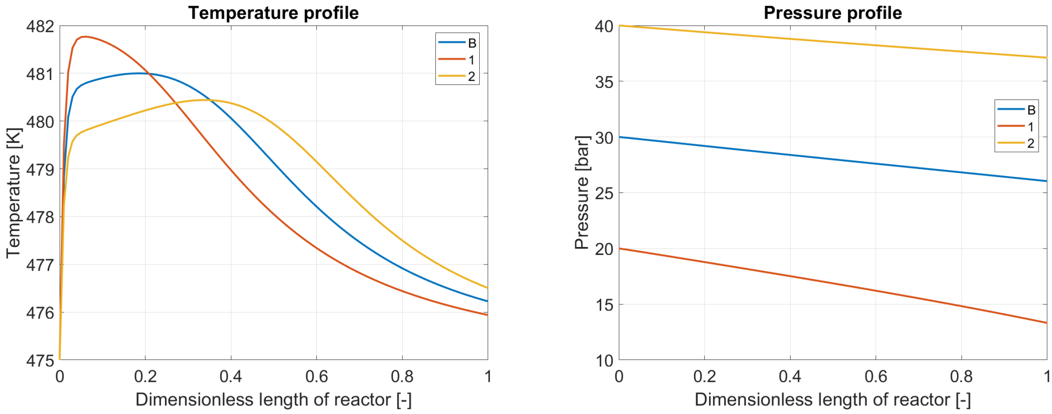

(c) Temperature profile **(d) Pressure profile**

Figure 5.10: Results of sensitivity analysis performed on inlet pressure (P_{in}) (Base case (B) = 30 bar, Case (1) = 20 bar, Case (2) = 40 bar).

As can be seen from Figure 5.10, the effect of inlet pressure on the performance of MTFBR is only positive. The conversion in the reactor increases from around 62 to 70% as the inlet pressure increases from 20 to 40 bar. This can be mainly attributed to the increase in partial pressure of the reactants with increase in total pressure, leading to higher reaction rates. Increase in total pressure can also lead to higher partial pressures of water, which may inhibit the FTS reaction to an extent. However, the simulations show that the increase in reaction rates with pressure is more prominent than the inhibition by water, leading to better conversions. The selectivity of C_{5+} also increases from around 76 to 84% as the inlet pressure increases from 20 to 40 bar. This can also be attributed to the intrinsic kinetic effects like in the case of conversion. The temperature in the reactor is not considerably affected by pressure, except for the slight shift in the peak towards the centre of the reactor and the slight decrease in the peak temperature. It can also be seen from Figure 5.10(d) that the pressure drop in the case of lower inlet pressure (∼ 6 bar) is relatively higher than that in the base case (∼ 4 bar) and also the case with higher inlet pressure (∼ 3 bar). Thus, it is optimal to have maximum allowable pressure in the reactor to maximise the productivity of C_{5+}, especially while using a syngas feed with almost 50% N_2, which reduces the partial pressure of reactants.

5.5.2.3 Inlet Flow Rate

The three cases considered for the sensitivity analysis on the inlet flow rate per tube (F_{in}) are: base case (B) = 0.2 mol/s, case (1) = 0.15 mol/s, and case (2) = 0.25 mol/s; and the simulation results obtained are shown in Figure 5.11.

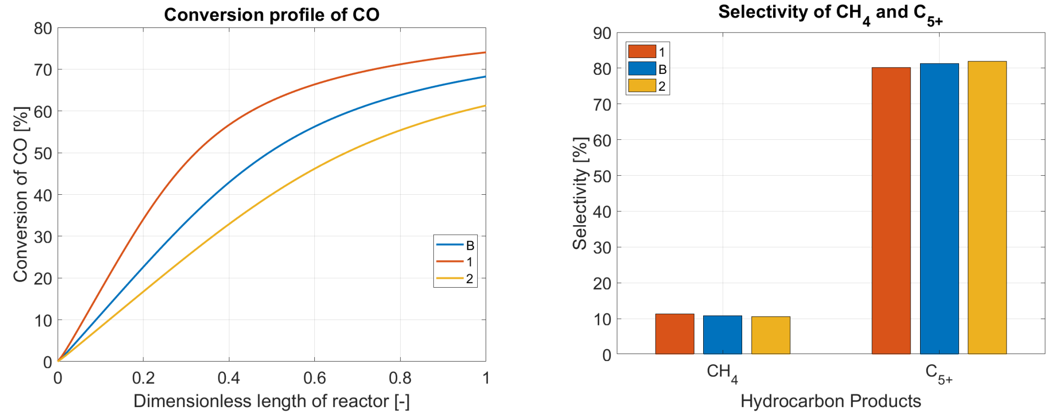

(a) Conversion profile of CO

(b) Selectivities of CH_4 and C_{5+}

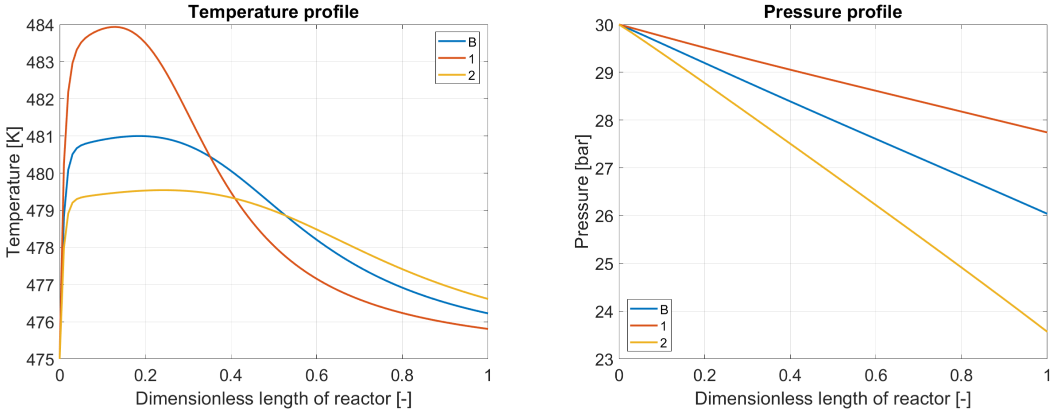

(c) Temperature profile

(d) Pressure profile

Figure 5.11: Results of sensitivity analysis performed on tube inlet flow rate (F_{in}) (Base case (B) = 0.2 mol/s, Case (1) = 0.15 mol/s, Case (2) = 0.25 mol/s).

It can be seen from Figure 5.11(c) that the temperatures near the reactor entrance are much higher in the case of lower flow rate (∼ 484K) than in the base (∼ 481K) and the higher flow rate (∼ 480K) cases. This can be mainly attributed to the lower superficial velocities of fluids in the case of a lower flow rate. Lower superficial velocities of fluids can have two possible effects: firstly, they lead to higher contact times of the reactants with the catalyst, resulting in higher reaction rates, and subsequently, in higher energy release; secondly, they lead to lower Reynolds numbers, which result in lower heat transfer coefficients inside the reactor. The combination of both these effects results in higher reactor temperatures in the case of lower flow rates. Higher temperatures in the case of lower flow rates also lead to higher conversions near the reactor entrance, which gradually slow down as more products are formed (see Figure 5.10(a)). The selectivity of C_{5+} is not considerably affected by the inlet flow rate, as the simulations show a selectivity increase of only around 1% with an increase in flow rate from 0.15 to 0.25 mol/s/tube (see Figure 5.10(b)). However, the packed-bed pressure drop in the case of higher flow rate ($\sim$ 6 bar) is considerably higher than that in the case of lower flow rate ($\sim$ 2.2 bar) due to to higher flow resistance offered by the packed-bed in the latter case.

5.5.2.4 Inlet H_2/CO ratio

The three cases considered for the sensitivity analysis on the inlet H_2/CO ratio are: base case (B) = 2, case (1) = 1.8, and case (2) = 2.2; and the simulation results obtained are shown in Figure 5.12.

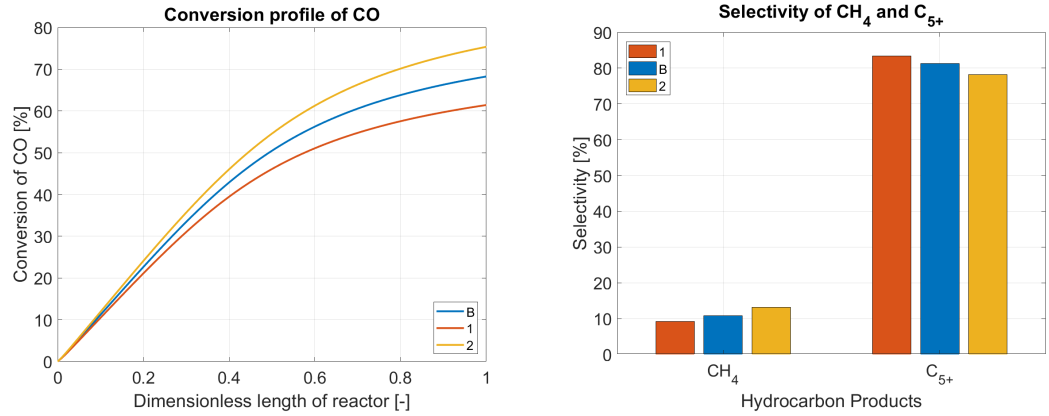

(a) Conversion profile of CO **(b) Selectivities of CH_4 and C_{5+}**

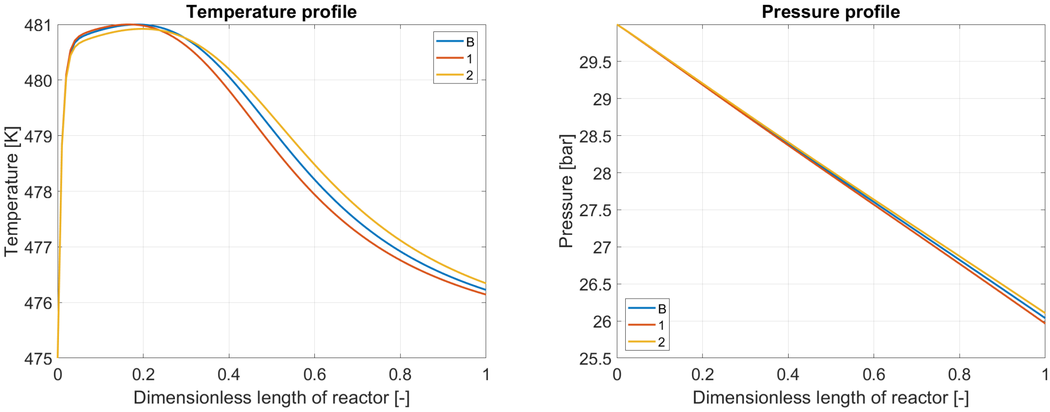

(c) Temperature profile **(d) Pressure profile**

Figure 5.12: Results of sensitivity analysis performed on H_2/CO ratio (Base case (B) = 2, Case (1) = 1.8, Case (2) = 2.2).

The H_2/CO ratio is adjusted in the syngas feed stream keeping the same flow rate and other parameters as in the base case. It can be seen from Figures 5.12(c) and 5.12(d) that the temperature and the pressure profiles in the reactor are barely affected by the H_2/CO ratio, whereas the effect on conversion and selectivity of C_{5+} is considerable. The conversion in the reactor increases with an increase in H_2/CO ratio, as can be seen in Figure 5.12(c), where the conversion improved from around 62 to 75% as the H_2/CO ratio increased from 1.8 to 2.2. However, H_2/CO ratio has a negative effect on the selectivity of C_{5+}, as can be seen in Figure 5.12(b), where the selectivity decreases from around 83 to 78% as the H_2/CO ratio increases from 1.8 to 2.2. Thus, it is desirable to maintain an optimal H_2/CO ratio in the syngas feed for maximising the productivity of C_{5+}.

5.5.3 FTS Gas Loop - Tail Gas Recycle

As discussed before in Section 5.4, the tail gas stream (S8) is partly purged out (S16), and the recovered H_2 (S14) and CO (S11) streams, from the recycled tail gas stream (S15), are mixed with the syngas feed stream to MTFB reactor (see Figure 5.6). The amount of H_2 and CO recovered depends on the amount of tail gas recycled back to the recovery units. Hence, a sensitivity analysis is performed on the tail gas recycle ratio (or fraction of tail gas recycled) to determine its effect on the MTFBR performance. The tail gas recycle ratio is varied from 0 (base case) to 1 (no tail gas purge), and the conversion of CO in the reactor and in the overall process are estimated for each value of recycle ratio, as shown in Figure 5.13.

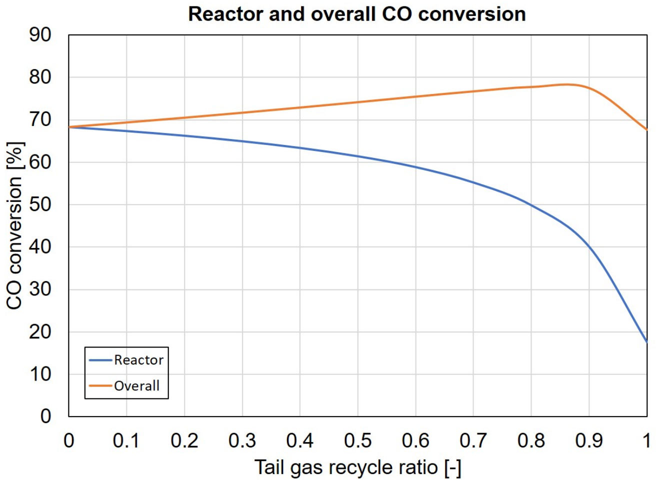

Figure 5.13: Reactor and overall CO conversion with tail gas recycle ratio.

It can be seen from Figure 5.13 that the reactor conversion and the overall conversion of CO is the same when the tail gas is not recycled (base case conditions). The conversion per pass decreases with increasing tail gas recycle, while the overall conversion increases to a limit and then decreases with increasing tail gas recycle. The maximum overall CO conversion (∼ 78%) is obtained with a tail gas recycle ratio of around 0.85. The simulation results for the base case and the case with maximum overall CO conversion are shown in Figure 5.14

It can be seen from Figure 5.14 that the conversion per pass with recycle (∼ 46%) is much lower than that without recycle (∼ 68% in base case). This is due to the combination of factors such as flow rate, reactor temperature and H_2/CO ratio. The flow rate in the case with recycle is observed to be higher than that in the base case, resulting in lower residence time of reactants, and thus leading to a lower reactor conversion. The higher flow rate in the recycle case also improves the heat transfer inside the reactor, thus resulting in a lower reactor temperature, which in turn, leads to a lower reactor conversion. The H_2/CO ratio of the feed stream reduces below 2 in the case with recycle due to the recycling of unreacted H_2 and CO recovered from the tail gas stream, which has an H_2/CO ratio lower than 2. This also contributes to the lower conversion in the reactor. However, the lower H_2/CO ratio in the feed stream with recycle results in a higher selectivity

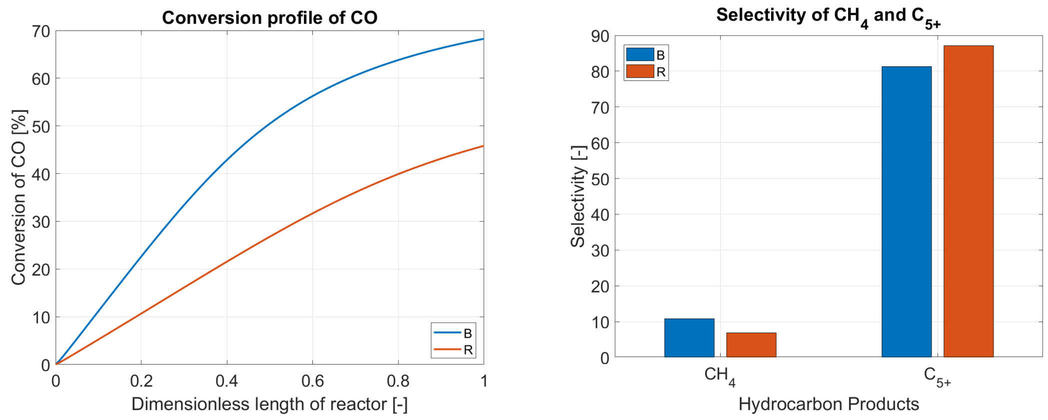

(a) Conversion profile of CO **(b) Selectivities of CH_4 and C_{5+}**

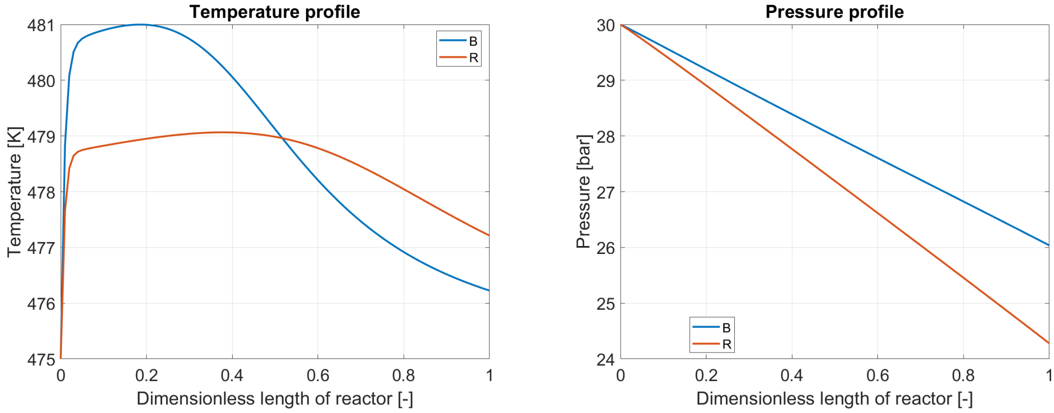

(c) Temperature profile **(d) Pressure profile**

Figure 5.14: Results of sensitivity analysis performed on tail gas recycle ratio (Base case (B) = no recycle, Recycle case (R) = tail gas recycle ratio of 0.85).

towards C_{5+} ($\sim$ 87%) compared to the base case ($\sim$ 81%), as can be seen in Figure 5.14(b). The pressure drop in the case with recycle ($\sim$ 6 bar) is higher compared to the base case ($\sim$ 4 bar) due to the higher flow rate in the reactor tube.

5.6 Process Optimisation

From the previous sections, it is evident that the process conditions play a key role in the performance of the MTFB reactors. Thus, optimising the process conditions can significantly improve the overall productivity of syncrude, which is very desirable for the sustainability and profitability of the FTS plant. In this project, the optimum reactor operating conditions are determined in order to yield maximum productivity of C_{5+} hydrocarbons for the specific syngas feed produced from the processing of WAGs. Hence, the feed parameters such as inlet flow rate and H_2/CO ratio are not considered as optimisation variables. Since the inlet pressure only has a positive effect on the reactor performance, and also since the typical operating pressures in FTS plants are between 25-30 bar, the operating pressure is considered to be 30 bar. Thus, the process variables that need to be optimised are inlet temperature and tail gas recycle ratio. Optimisation is performed using the Sensitivity Analysis tool in Aspen Plus, by varying the inlet temperature (T_{in}) from 465 to 487K and the tail gas recycle ratio (RR) from 0 to 1. As the inlet temperature increases, the overall conversion of CO also increases, but the selectivity of C_{5+} decreases. However, due to the interplay between the overall CO conversion and the C_{5+} selectivity, the productivity of C_{5+} increases initially as the inlet temperature increases and then decreases after a certain maximum, which is considered as the optimum point. Figure 5.15 shows the productivity of C_{5+} for a key range of inlet temperatures and tail gas recycle ratios.

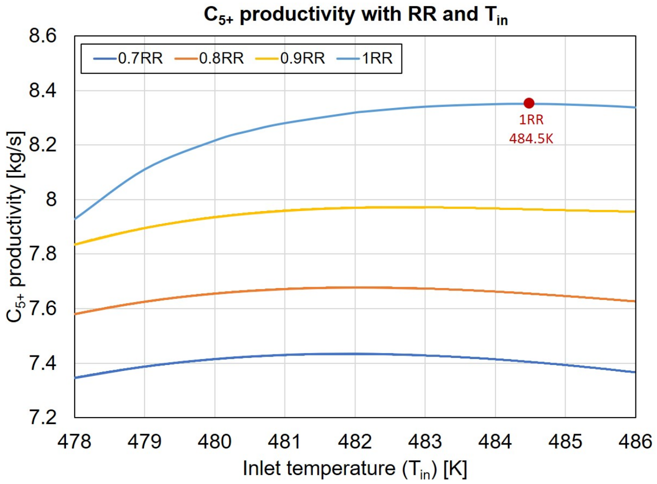

Figure 5.15: Productivity of C_{5+} with tail gas recycle ratio (RR) and inlet temperature (T_{in}). The maximum productivity of C_{5+} is achieved at RR = 1 and T_{in} = 484.5K.

It can be seen from Figure 5.15 that the maximum productivity of C_{5+}, for the given WAGs syngas feed conditions, is achieved for a 100% recycle of tail gas at an inlet temperature of 484.5K. Total recycle of tail gas does not mean the whole of tail gas stream is sent back to the reactor, it only means that the whole of tail gas is sent to the recovery section, where H_2 and CO are recovered (see Figures 4.2 and 5.6). The inerts, fuel gas, CO_2, and unrecovered H_2 and CO are removed as an exhaust stream from the recovery section, thus avoiding accumulation of inerts in the process loop. The simulation results of MTFBR with WAGs syngas feed for the optimised process conditions are shown in Figure 5.16.

The conversion of CO in the reactor with optimised process conditions is around 46%, which is considerably lower than that in the base case ($\sim$ 68%) due to similar reasons mentioned before in Section 5.5.3. Due to the total recycle of unconverted H_2 and CO recovered from the tail gas stream, the H_2/CO ratio and the flow rate of the syngas feed stream drops from 1.99 to 1.27 and increases from 0.2 to 0.24 mol/s/tube, respectively, at the reactor inlet, resulting in a lower conversion of CO in the reactor. However, the overall conversion of CO and the selectivity of C_{5+} hydrocarbons are 88.8 and 86.6%, respectively, while the selectivity of CH_4 is only 6.2%, which are all in the desired ranges. The productivity of C_{5+} is calculated to be 252,540 tonnes/y, which is much higher than the base case productivity of 182,300 tonnes/y. The peak temperature near the reactor entrance is around 494K and the pressure drop in the packed bed is around 6 bar, which are also in the desired ranges. The comparison of optimised process conditions and its results with that of the base case conditions are summarised in Table 5.2.

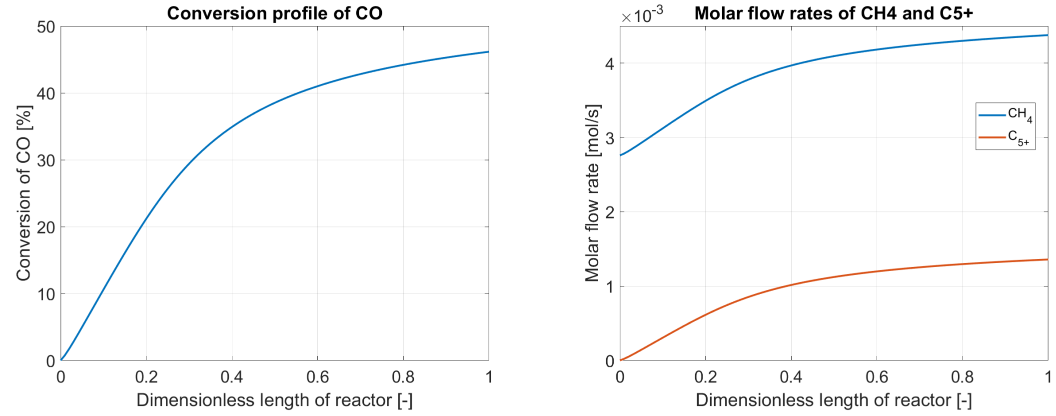

(a) Conversion profile of CO (b) Molar flow rates of CH_4 and C_{5+} per tube

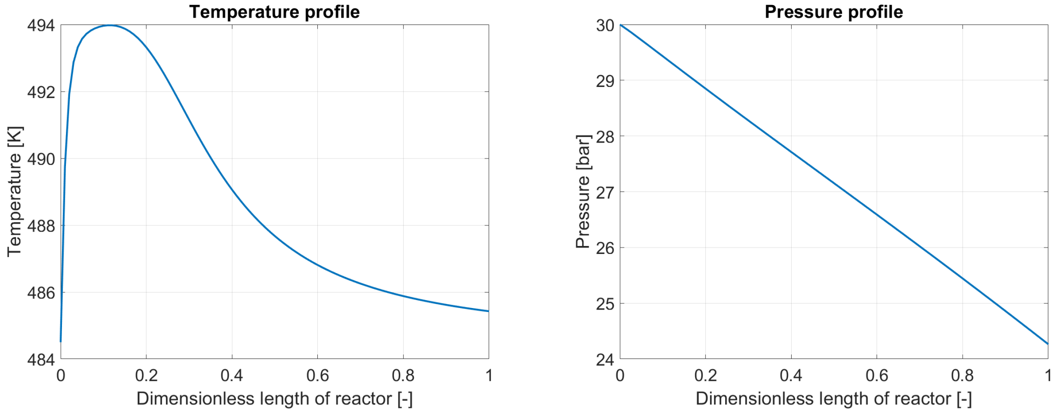

(c) Temperature profile (d) Pressure profile

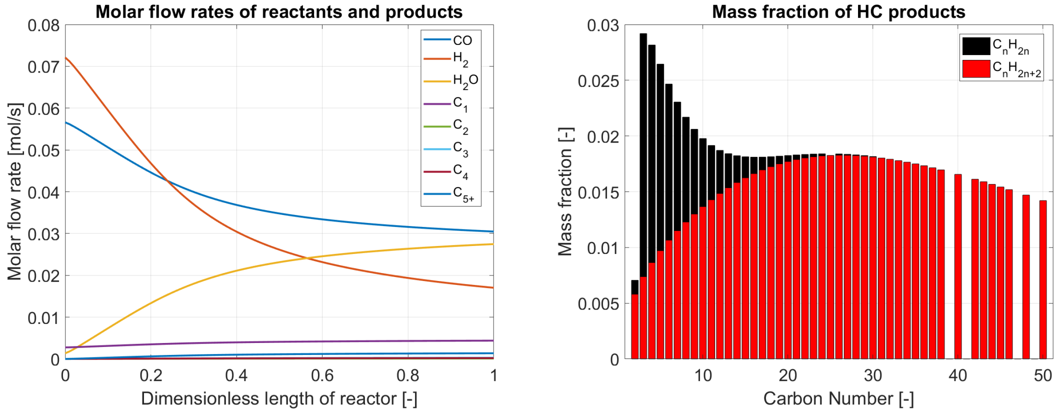

(e) Molar flow rates of components per tube (f) Mass fraction of hydrocarbon products

Figure 5.16: Simulation results with WAGs syngas feed for optimised process conditions (T_{in} = 484.5K, RR = 1 and P_{in} = 30 bar)

Table 5.2: Comparison of optimised process conditions and its results with that of the base case conditions (reactor geometry defined in Section 5.2).

Process Conditions	Base Case	Optimised Case
Inlet temperature (K)	475	484.5
Tail gas recycle ratio	0	1
Inlet pressure (bar)	30	

Model Results	Base Case	Optimised Case
Reactor CO conversion (%)	68.26	46.15
Overall CO conversion (%)	68.26	88.81
C5+ selectivity (%)	81.24	86.60
C5+ productivity (tonnes/y)	182,300	252,540
Maximum bed temperature (K)	481	494
Pressure drop (bar)	4	5.7

Among the several GTL plants established commercially (see Appendix B), the best known examples of a cobalt-based MTFB reactor design for syncrude production include the GTL plant in Bintulu, Malaysia and the Pearl GTL in Ras Laffan, Qatar. Both these plants are based on a technology developed by Shell, called Shell's Middle Distillate Synthesis (SMDS) process (see Appendix B.3). However, only very little is known about the working of the Pearl GTL plant, other than its total productivity, whereas, there is relatively more data available in the literature about the FTS reactors in Bintulu GTL plant [1, 8, 68, 85, 86]. It can be observed that the optimised results of the FTS gas loop process model with MTFBR, in terms of C_{5+} selectivity and overall CO conversion, are pretty much inline with the available data from the Shell SMDS plant in Bintulu (discussed in Section 5.2). However, a complete validation of the FTS process model is not possible at the moment due to the lack of available data in the literature about the syngas feed composition, feed flow rate and the tail gas recycle ratio used in the Shell Bintulu plant.

6. Conclusions & Recommendations

The main objective of this thesis was to develop a detailed model of a multi-tubular fixed-bed reactor (MTFBR) to produce synthetic crude from syngas via Fischer-Tropsch synthesis (FTS). The model was then used to simulate a reactor that utilises the syngas obtained from the processing of work's arising gases of an integrated steel mill to produce synthetic crude. The main research question posed at the beginning was:

What is the benchmark performance of the multi-tubular fixed-bed reactor for Fischer-Tropsch synthesis, which produces synthetic crude using syngas obtained from the processing of work's arising gases of an integrated steel mill?

The results obtained and the methodology followed are interpreted to answer the above research question and the sub-questions associated with it.

The FTS product distribution was modelled using the kinetic model based on CO-insertion mechanism, developed by Todic et al. This model had a reasonably good fit with the experimental results even though it considered only the primary FT reactions. The validation of kinetic model with the literature showed that it was capable of predicting the FTS product distribution at various conditions with high levels of accuracy. The kinetic model was then used to develop the basic and detailed MTFBR models.

The model equations and assumptions used to develop the basic MTFBR model in MATLAB were based on the fixed-bed reactor model developed by Todic. The basic MTFBR model was able to produce similar results as that of the Todic's model, except for the temperature and pressure profiles in the reactor, which were off by a slight margin. These deviations were attributed to the difference in thermodynamic and physical properties of the components used in the model. The basic MTFBR model was then further improved to render it comparable with the commercial FT reactors. The main improvements in the model include the dynamic extraction of thermodynamic and transport properties of the system components using Aspen Properties; calculation of dynamic vapour-liquid equilibrium, liquid holdup and catalyst effectiveness factor; and the use of improved heat transfer and pressure drop equations.

A sensitivity analysis was performed to determine the effect of design and process parameters on the performance of the MTFBR model. The most crucial design parameter was observed to be the tube diameter as it had a considerable effect on the heat management and the pressure drop in the reactor bed. Smaller tube diameters removed the heat generated by the highly exothermic FTS reaction more effectively. However, smaller tube diameters also resulted in relatively higher pressure drops in the packed bed. Thus, an optimum tube diameter in the case of an MTFBR is extremely desirable. At the same time, the most important process parameters for the reactor were observed to be the inlet temperature and the feed flow rate. Higher inlet temperatures resulted in higher reaction rates, which subsequently resulted in large amounts of heat released due to the highly exothermic nature of the FTS reaction, ultimately leading to thermal runaways. The conversion of CO in the reactor also increased with higher inlet temperatures; however, the selectivity towards C_{5+} decreased with higher inlet temperatures. Hence, there is a trade-off between the CO conversion and the C_{5+} selectivity, urging the need to optimise the inlet temperature for maximum productivity of C_{5+} hydrocarbons. On the other hand, lower feed flow rates, i.e., lower superficial velocities of fluids had two crucial effects: firstly, they led to higher contact times of the reactants with the catalyst, resulting in higher reaction rates, and subsequently, in higher energy release; secondly, they led to lower Reynolds numbers, which resulted in lower heat transfer coefficients inside the reactor. The combination of both these effects resulted in higher reactor temperatures in the case of lower flow rates. However, the selectivity of C_{5+} was not considerably affected by the inlet flow rate.

A simplified FTS gas loop process was also modelled in Aspen Plus in order to introduce a recycle stream into the MTFBR. The model mainly comprised of the syncrude production unit and a simplified product separation unit. The effect of tail gas recycle for the recovery of unreacted H_2 and CO was also studied, and it was observed that higher recycle ratios resulted in lower conversions per pass due to higher flow rates per pass and reduction in feed H_2/CO ratio; however, overall CO conversions were observed to increase until a maximum, and then decrease thereafter.

The optimum conditions for the simplified gas loop process, which provided maximum productivity of C_{5+} for the given WAGs syngas feed, were estimated to be with an inlet temperature of 484.5K and a total recycle of tail gas to the recovery section. The optimisation process was performed for an inlet pressure of 30 bar, which is typical in FTS reactors. Simulation using optimised process conditions resulted in a reactor CO conversion of 46%, an overall CO conversion of 89%, a C_{5+} selectivity of 86.6%, a CH_4 selectivity of 6.2%, and a C_{5+} productivity of 252,540 tonnes/y. The optimised model results were also compared with the available data from the Shell SMDS plant in Bintulu, and the C_{5+} selectivity and overall CO conversion obtained with the model were pretty much inline with the Shell data. However, a complete validation of the process model with MTFBR was not possible due to the lack of basic data, such as the feed composition, feed flow rate and the tail gas recycle ratio used in the Shell Bintulu plant.

Recommendations for future work

This thesis could answer the main research question only to a certain extent, mainly due to the lack available data in the literature about the commercial FTS process with MTFBRs. This section recommends subjects for further study that will add to the answering of the main research question.

Aspen Plus does not have the provision to solve the type of kinetics used in this model; hence, the feed stream data from the process model in Aspen Plus is transferred to MATLAB, where all calculations of the MTFBR are performed, and the outlet stream data is transferred back to the process model in Aspen plus. Also, MATLAB extracted the thermodynamic and transport properties of components from Aspen Properties during every iteration of the MATLAB solver. The integration of all these platforms and automation of the calculation involved some exhaustive coding in MATLAB and Excel VBA. Future work would focus on the simplification of the model without compromising on its accuracy level.

The kinetic based on CO-insertion mechanism, developed by Todic et al., does not consider the secondary FT reactions, such as the production of secondary methane on the secondary active sites of the catalyst, hydrogenation of 1-olefins and the formation of oxygenates. Incorporating the effect of secondary reactions into the kinetic model will make the FTS product distribution more accurate.

The heat transfer resistances between the wall and the cooling medium, and through the steel wall, are assumed to be negligible in this model. As a consequence, the temperatures of the coolant and that of the inner reactor wall are always the same. This would make the calculation of coolant flow rate required and the amount of steam produced in the shell side of the reactor inaccurate. Also, this would lead to inaccuracies while performing the process heat integration. Hence, modelling the shell side of the MTFBR with proper heat and mass characteristics is important.

The FTS gas loop process model with MTFBR is developed considering a simplified product separation unit. The unconverted H_2 and CO in the FT tail gas are recovered and directly recycled back to the MTFBR in the FTS gas loop process model, which results in the lowering of H_2/CO ratio in the feed stream. This can be avoided by purging out the excess CO in the recycle stream after its recovery to maintain an H_2/CO ratio of 2 in the recycle stream, which would make the

FTS process model more comparable with the commercial FTS processes.

Validation of the FTS process model with commercial FTS processes is very important in determining the accuracy level of the model. However, this requires sufficiently more information about the commercial FTS plants, which is scarce in the literature at present, especially since the FTS is still considered to be a novel technology. Obtaining sufficient data and validating the model is one of the crucial steps in establishing the benchmark performance of the FTS process model with MTFBR.

Bibliography

[1] B. S. Todic, "Kinetic modeling and optimization of fixed-bed reactor for Fischer-Tropsch synthesis," Ph.D. dissertation, University of Belgrade, 2015.

[2] U.S. Energy Information Administration (EIA), "Annual Energy Outlook 2014 with projections to 2040," April 2014, [Accessed 12 February 2019]. [Online]. Available: https://www.eia.gov/outlooks/aeo/pdf/0383(2014).pdf

[3] J. Rostrup-Nielsen and L. J. Christiansen, *Syngas Applications*, ser. Catalytic Science Series. Imperial College Press, 2011, vol. 10, ch. 2, pp. 73–140. [Online]. Available: https://www.worldscientific.com/doi/abs/10.1142/9781848165687_0002

[4] U.S. Energy Information Administration (EIA), "Annual Energy Outlook 2019 with projections to 2050," Jan 2019, [Accessed 12 February 2019]. [Online]. Available: https://www.eia.gov/outlooks/aeo/pdf/aeo2019.pdf

[5] M. E. Dry, "The Fischer–Tropsch process: 1950–2000," *Catalysis Today*, vol. 71, no. 3, pp. 227–241, 2002. [Online]. Available: http://www.sciencedirect.com/science/article/pii/S0920586101004539

[6] P. Sabatier and J. Senderens, "New methane synthesis," *Comptes rendus de l'Académie des Sciences*, vol. 134, pp. 514–516, 1902.

[7] F. Fischer and H. Tropsch, "The Synthesis of Petroleum at Atmospheric Pressures from Gasification Products of Coal," *Brennstoff-Chemie*, vol. 7, pp. 97–104, 1926.

[8] A. Steynberg and M. Dry, *Fischer-Tropsch Technology*, 1st ed., ser. Studies in Surface Science and Catalysis. Amsterdam: Elsevier, 2004, vol. 152.

[9] C. H. Bartholomew and R. J. Farrauto, *Fundamentals of Industrial Catalytic Processes*, 2nd ed. Hoboken: John Wiley & Sons, 2006.

[10] D. Leckel, "Diesel Production from Fischer-Tropsch: The Past, the Present, and New Concepts," *Energy & Fuels*, vol. 23, no. 5, pp. 2342–2358, 2009. [Online]. Available: https://doi.org/10.1021/ef900064c

[11] Velocys, [Accessed 13 February 2019]. [Online]. Available: https://www.velocys.com/

[12] Compact GTL, [Accessed 13 February 2019]. [Online]. Available: http://www.compactgtl.com/

[13] R. Luque, A. R. de la Osa, J. M. Campelo, A. A. Romero, J. L. Valverde, and P. Sanchez, "Design and development of catalysts for Biomass-To-Liquid-Fischer–Tropsch (BTL-FT) processes for biofuels production," *Energy Environmental Science*, vol. 5, no. 1, pp. 5186–5202, 2012. [Online]. Available: http://dx.doi.org/10.1039/C1EE02238E

[14] M. Hook and K. Aleklett, "A review on coal-to-liquid fuels and its coal consumption," *International Journal of Energy Research*, vol. 34, no. 10, pp. 848–864, 2010. [Online]. Available: https://onlinelibrary.wiley.com/doi/abs/10.1002/er.1596

[15] B. Todic, V. Ordomsky, N. Nikacević, A. Khodakov, and D. B. Bukur, "Opportunities for intensification of Fischer-Tropsch synthesis through reduced formation of methane over cobalt catalysts in microreactors," *Catalysis Science & Technology*, vol. 5, 2015. [Online]. Available: http://dx.doi.org/10.1039/C4CY01547A

[16] C. O. Bauer, "Peer Reviewed: Developing Clean Coal Technology," *Environmental Science & Technology*, vol. 37, no. 1, pp. 27A–34A, 2003. [Online]. Available: https://doi.org/10.1021/es032325w

[17] H. Schulz, “Short history and present trends of Fischer-Tropsch synthesis,” *Applied Catalysis A: General*, vol. 186, no. 1-2, pp. 3–12, 1999. [Online]. Available: https://doi.org/10.1016/S0926-860X(99)00160-X

[18] D. Xu, L. Dong, and J. Ren, “Chapter 2 - introduction of hydrogen routines,” in *Hydrogen Economy*, A. Scipioni, A. Manzardo, and J. Ren, Eds. Academic Press, 2017, pp. 35–54. [Online]. Available: http://www.sciencedirect.com/science/article/pii/B978012811132100002X

[19] S-cool: The revision website, “Chemicals from oil,” [Accessed 16 January 2019]. [Online]. Available: https://www.s-cool.co.uk/gcse/chemistry/products-from-crude-oil/revise-it/chemicals-from-oil

[20] A. de Klerk, *Fischer-Tropsch Refining*, 1st ed. Weinheim: Wiley-VCH Verlag & Co. KGaA, 2011.

[21] TMR Research, “Diesel Fuel Market: Global Industry Analysis, Size, Share, Trends, Analysis, Growth and Forecast 2017 - 2025,” [Accessed 12 February 2019]. [Online]. Available: https://www.tmrresearch.com/diesel-fuel-market

[22] M. Kraum and M. Baerns, “Fischer–Tropsch synthesis: the influence of various cobalt compounds applied in the preparation of supported cobalt catalysts on their performance,” *Applied Catalysis A: General*, vol. 186, no. 1, pp. 189–200, 1999. [Online]. Available: http://www.sciencedirect.com/science/article/pii/S0926860X99001726

[23] J. van de Loosdrecht, M. van der Haar, A. M. van der Kraan, A. J. van Dillen, and J. W. Geus, “Preparation and properties of supported cobalt catalysts for Fischer-Tropsch synthesis,” *Applied Catalysis A: General*, vol. 150, no. 2, pp. 365–376, 1997. [Online]. Available: http://www.sciencedirect.com/science/article/pii/S0926860X96003067

[24] C. H. Bartholomew, R. B. Pannell, and J. L. Butler, “Support and crystallite size effects in CO hydrogenation on nickel,” *Journal of Catalysis*, vol. 65, no. 2, pp. 335–347, 1980. [Online]. Available: http://www.sciencedirect.com/science/article/pii/0021951780903115

[25] R. Oukaci, A. H. Singleton, and J. G. Goodwin, “Comparison of patented Co F–T catalysts using fixed-bed and slurry bubble column reactors,” *Applied Catalysis A: General*, vol. 186, no. 1, pp. 129–144, 1999. [Online]. Available: http://www.sciencedirect.com/science/article/pii/S0926860X99001696

[26] J. R. Anderson and M. Boudart, *Catalysis: Science and Technology*, 1st ed., ser. Catalysis. Berlin, Heidelberg: Springer-Verlag Berlin Heidelberg, 1984, vol. 2.

[27] M. E. Dry, “Fischer-Tropsch synthesis over iron catalysts,” *Catalysis Letters*, vol. 7, no. 1, pp. 241–251, 1990. [Online]. Available: https://doi.org/10.1007/BF00764506

[28] S. T. Sie and R. Krishna, “Fundamentals and selection of advanced Fischer–Tropsch reactors,” *Applied Catalysis A: General*, vol. 186, no. 1, pp. 55–70, 1999. [Online]. Available: http://www.sciencedirect.com/science/article/pii/S0926860X99001647

[29] S. Chambrey, P. Fongarland, H. Karaca, S. Piché, A. Griboval-Constant, D. Schweich, F. Luck, S. Savin, and A. Khodakov, “Fischer-Tropsch synthesis in milli-fixed bed reactor: Comparison with centimetric fixed bed and slurry stirred tank reactors,” *Catalysis Today*, vol. 171, no. 1, pp. 201–206, 2011. [Online]. Available: https://hal-univ-lyon1.archives-ouvertes.fr/hal-01923790

[30] K. D. Tillmetz, “Über thermodynamische Simultangleichgewichte bei der Fischer-Tropsch-Synthese,” *Chemie Ingenieur Technik*, vol. 48, no. 11, pp. 1065–1065, 1976. [Online]. Available: https://onlinelibrary.wiley.com/doi/abs/10.1002/cite.330481125

[31] M. Baerns, Christoffel, and J. Surjo, “Thermodynamische berechnungen zur bildung von kohlenwasserstoffen durch hydrierung von kohlenmonoxid,” *Chemiker-Zeitung*, vol. 102, no. 1, pp. 19–23, 1978.

[32] J. R. Anderson and M. Boudart, *Catalysis: Science and Technology*, 1st ed., ser. Catalysis. Berlin, Heidelberg: Springer-Verlag Berlin Heidelberg, 1981, vol. 1.

[33] P. H. Emmett, *Catalysis*. New York: Reinhold Publishing Corporation, 1956, vol. 45.

[34] F. R. Craxford, *Fuel*. Amsterdam: Elsevier B.V., 1947, vol. 26.

[35] V. Sage and N. Burke, “Use of probe molecules for Fischer–Tropsch mechanistic investigations: A short review,” *Catalysis Today*, vol. 178, no. 1, pp. 137–141, 2011. [Online]. Available: http://www.sciencedirect.com/science/article/pii/S0920586111006778

[36] H. Schulz, “Major and Minor Reactions in Fischer-Tropsch Synthesis on Cobalt Catalysts,” *Topics in Catalysis*, vol. 26, no. 1, pp. 73–85, 2003. [Online]. Available: https://doi.org/10.1023/B:TOCA.0000012988.86378.21

[37] M. K. G, R. A. Keogh, W. Shafer, and B. Davis, “Deutero-1-pentene tracer studies for iron and cobalt Fischer-Tropsch synthesis,” *Applied Catalysis A: General*, vol. 393, no. 1-2, pp. 130–137, 2011. [Online]. Available: https://doi.org/10.1016/j.apcata.2010.11.035

[38] E. Iglesia, S. C. Reyes, and R. J. Madon, “Transport-enhanced α-olefin readsorption pathways in Ru-catalyzed hydrocarbon synthesis,” *Journal of Catalysis*, vol. 129, no. 1, pp. 238–256, 1991. [Online]. Available: http://www.sciencedirect.com/science/article/pii/0021951791900272

[39] R. B. Anderson, R. A. Friedel, and H. H. Storch, “Fischer-Tropsch Reaction Mechanism Involving Stepwise Growth of Carbon Chain,” *The Journal of Chemical Physics*, vol. 19, no. 3, pp. 313–319, 1951. [Online]. Available: https://doi.org/10.1063/1.1748201

[40] G. V. Schulz, “Über die Beziehung zwischen Reaktionsgeschwindigkeit und Zusammensetzung des Reaktionsproduktes bei Makropolymerisationsvorgängen,” *Zeitschrift für Physikalische Chemie*, vol. 30B, no. 1, pp. 379–398, 1935. [Online]. Available: https://doi.org/10.1515/zpch-1935-3027

[41] B. Todic, W. Ma, G. Jacobs, N. Nikacevic, B. H. Davis, and D. B. Bukur, “Kinetic Modeling of Secondary Methane Formation and 1-Olefin Hydrogenation in Fischer–Tropsch Synthesis over a Cobalt Catalyst,” *International Journal of Chemical Kinetics*, vol. 49, no. 12, pp. 859–874, 2017. [Online]. Available: https://onlinelibrary.wiley.com/doi/abs/10.1002/kin.21133

[42] G. P. van der Laan and A. Beenackers, “Kinetics and selectivity of the Fischer-Tropsch synthesis: A literature review,” *Catalysis Reviews-Science and Engineering*, vol. 41, no. 3-4, pp. 255–318, 1999. [Online]. Available: https://doi.org/10.1081/cr-100101170

[43] J. Patzlaff, Y. Liu, C. Graffmann, and J. Gaube, “Studies on product distributions of iron and cobalt catalyzed Fischer–Tropsch synthesis,” *Applied Catalysis A: General*, vol. 186, no. 1, pp. 109–119, 1999. [Online]. Available: http://www.sciencedirect.com/science/article/pii/S0926860X99001672

[44] G. A. Huff and C. N. Satterfield, “Evidence for two chain growth probabilities on iron catalysts in the Fischer-Tropsch synthesis,” *Journal of Catalysis*, vol. 85, no. 2, pp. 370–379, 1984. [Online]. Available: http://www.sciencedirect.com/science/article/pii/0021951784902264

[45] B. Shi and B. H. Davis, “Fischer–Tropsch synthesis: accounting for chain-length related phenomena,” *Applied Catalysis A: General*, vol. 277, no. 1, pp. 61–69, 2004. [Online]. Available: http://www.sciencedirect.com/science/article/pii/S0926860X04007586

[46] I. Puskas and R. S. Hurlbut, "Comments about the causes of deviations from the Anderson–Schulz–Flory distribution of the Fischer–Tropsch reaction products," *Catalysis Today*, vol. 84, no. 1, pp. 99–109, 2003. [Online]. Available: http://www.sciencedirect.com/science/article/pii/S0920586103003055

[47] D. Vervloet, F. Kapteijn, J. Nijenhuis, and J. R. van Ommen, "Fischer–Tropsch reaction–diffusion in a cobalt catalyst particle: aspects of activity and selectivity for a variable chain growth probability," *Catal. Sci. Technol.*, vol. 2, no. 6, pp. 1221–1233, 2012. [Online]. Available: http://dx.doi.org/10.1039/C2CY20060K

[48] E. W. Kuipers, C. Scheper, J. H. Wilson, I. H. Vinkenburg, and H. Oosterbeek, "Non-ASF Product Distributions Due to Secondary Reactions during Fischer–Tropsch Synthesis," *Journal of Catalysis*, vol. 158, no. 1, pp. 288–300, 1996. [Online]. Available: http://www.sciencedirect.com/science/article/pii/S0021951796900287

[49] C. N. Satterfield and G. A. Huff, "Carbon number distribution of Fischer-Tropsch products formed on an iron catalyst in a slurry reactor," *Journal of Catalysis*, vol. 73, no. 1, pp. 187–197, 1982. [Online]. Available: http://www.sciencedirect.com/science/article/pii/0021951782900926

[50] C. M. Masuku, W. D. Shafer, W. Ma, M. K. Gnanamani, G. Jacobs, D. Hildebrandt, D. Glasser, and B. H. Davis, "Variation of residence time with chain length for products in a slurry-phase Fischer–Tropsch reactor," *Journal of Catalysis*, vol. 287, pp. 93–101, 2012. [Online]. Available: http://www.sciencedirect.com/science/article/pii/S0021951711003927

[51] J. Yang, W. D. Shafer, V. R. R. Pendyala, G. Jacobs, W. Ma, D. Chen, A. Holmen, and B. H. Davis, "Fischer-Tropsch Synthesis: Deuterium Kinetic Isotopic Effect for a 2.5% Ru/NaY Catalyst," *Topics in Catalysis*, vol. 57, no. 6, pp. 508–517, 2014. [Online]. Available: https://doi.org/10.1007/s11244-013-0207-y

[52] R. Zhang, J. Chang, Y. Xu, L. Cao, Y. Li, and J. Zhou, "Kinetic Model of Product Distribution over Fe Catalyst for Fischer-Tropsch Synthesis," *Energy & Fuels*, vol. 23, no. 10, pp. 4740–4747, 2009. [Online]. Available: https://doi.org/10.1021/ef801079u

[53] I. C. Yates and C. N. Satterfield, "Hydrocarbon selectivity from cobalt Fischer-Tropsch catalysts," *Energy & Fuels*, vol. 6, no. 3, pp. 308–314, 1992. [Online]. Available: https://doi.org/10.1021/ef00033a011

[54] D. B. Bukur, L. Nowicki, and X. Lang, "Fischer-Tropsch Synthesis in a Slurry Reactor. Pretreatment Effect Studies," *Energy & Fuels*, vol. 9, no. 4, pp. 620–629, 1995. [Online]. Available: https://doi.org/10.1021/ef00052a008

[55] E. F. G. Herington, "Fischer-Tropsch synthesis considered as a polymerization reaction," *Chem. Ind. (London)*, vol. 45, p. 346, 1946.

[56] B. Todic, T. Olewski, N. Nikacevic, and D. Bukur, "Modeling of Fischer-Tropsch Product Distribution over Fe-based Catalyst," *Chemical Engineering Transactions*, vol. 32, pp. 793–798, 2013. [Online]. Available: https://www.cetjournal.it/index.php/cet/article/view/CET1332133

[57] F. G. Botes, "Proposal of a New Product Characterization Model for the Iron-Based Low-Temperature Fischer-Tropsch Synthesis," *Energy & Fuels*, vol. 21, no. 3, pp. 1379–1389, 2007. [Online]. Available: https://doi.org/10.1021/ef060483d

[58] B. S. Todic, W. Ma, G. Jacobs, B. Davis, and D. Bukur, "CO-insertion mechanism based kinetic model of the Fischer-Tropsch synthesis reaction over Re-promoted Co catalyst," *Catalysis Today*, vol. 228, pp. 32–39, 2014. [Online]. Available: https://doi.org/10.1016/j.cattod.2013.08.008

[59] B. Todic, M. Mandic, N. Nikacevic, and D. B. Bukur, "Effects of process and design parameters on heat management in fixed bed Fischer-Tropsch synthesis reactor," *Korean Journal of Chemical Engineering*, vol. 35, no. 4, pp. 875–889, 2018. [Online]. Available: https://doi.org/10.1007/s11814-017-0335-3

[60] A. Jess, R. Popp, and K. Hedden, "Fischer–Tropsch-synthesis with nitrogen-rich syngas: Fundamentals and reactor design aspects," *Applied Catalysis A: General*, vol. 186, no. 1, pp. 321–342, 1999. [Online]. Available: http://www.sciencedirect.com/science/article/pii/S0926860X99001520

[61] R. Krishna and S. Sie, "Strategies for multiphase reactor selection," *Chemical Engineering Science*, vol. 49, no. 24, Part A, pp. 4029–4065, 1994. [Online]. Available: http://www.sciencedirect.com/science/article/pii/S0009250905800053

[62] B. Todic, T. Bhatelia, G. F. Froment, W. ma, G. Jacobs, B. Davis, and D. B. Bukur, "Kinetic model of fischer–tropsch synthesis in a slurry reactor on co–re/al2o3 catalyst," *Industrial & Engineering Chemistry Research*, vol. 52, no. 2, p. 669–679, 2013. [Online]. Available: https://doi.org/10.1021/ie3028312

[63] G. Froment, K. Bischoff, and J. De Wilde, *Chemical Reactor Analysis and Design, 3rd Edition*, 3rd ed., ser. Wiley series in Chemical Engineering. New York: John Wiley & Sons, Incorporated, 2010. [Online]. Available: https://books.google.nl/books?id=lbQbAAAAQBAJ

[64] C. G. Visconti and M. Mascellaro, "Calculating the product yields and the vapor–liquid equilibrium in the low-temperature Fischer–Tropsch synthesis," *Catalysis Today*, vol. 214, pp. 61–73, 2013. [Online]. Available: http://www.sciencedirect.com/science/article/pii/S0920586112007365

[65] J. D. Swart, R. Krishna, and S. Sie, "Selection, design and scale up of the fischer-tropsch reactor," in *Natural Gas Conversion IV*, ser. Studies in Surface Science and Catalysis, M. de Pontes, R. Espinoza, C. Nicolaides, J. Scholtz, and M. Scurrell, Eds. Elsevier, 1997, vol. 107, pp. 213 – 218. [Online]. Available: http://www.sciencedirect.com/science/article/pii/S0167299197803370

[66] G. F. Froment and K. Bischoff, *Chemical Reactor Analysis and Design, 2nd Edition*, 2nd ed., ser. Wiley series in Chemical Engineering. New York: John Wiley & Sons, Incorporated, 1990. [Online]. Available: https://books.google.nl/books?id=Y9tTAAAAMAAJ

[67] D. W. Green and R. H. Perry, *Perry's Chemical Engineers' Handbook, Eighth Edition*, 8th ed. New York: McGraw-Hill Education, 2008. [Online]. Available: https://www.accessengineeringlibrary.com/content/book/9780071422949

[68] K. Brunner, J. C. Duncan, L. Harrison, K. Pratt, R. Peguin, C. Bartholomew, and W. Hecker, "A Trickle Fixed-Bed Recycle Reactor Model for the Fischer-Tropsch Synthesis," *International Journal of Chemical Reactor Engineering*, vol. 10, no. 1, p. 1542, 2012. [Online]. Available: https://doi.org/10.1515/1542-6580.2840

[69] A. Matsuura, Y. Hitaka, T. Akehata, and T. Shirai, "Effective radial thermal conductivity in packed beds with gas-liquid downflow," *Heat Transfer- Japanese Research*, vol. 8, p. 44–52, 1979.

[70] S. Yagi and D. Kunii, "Studies on effective thermal conductivities in packed beds," *AIChE Journal*, vol. 3, no. 3, pp. 373–381, 1957. [Online]. Available: https://aiche.onlinelibrary.wiley.com/doi/abs/10.1002/aic.690030317

[71] S. Ergun, "Fluid flow through packed columns," *Journal of Chemical Engineering Progress*, vol. 48, no. 2, pp. 89–94, 1952.

[72] C. Knobloch, R. Güttel, and T. Turek, “Holdup and Pressure Drop in Micro Packed-Bed Reactors for Fischer-Tropsch Synthesis,” *Chemie Ingenieur Technik*, vol. 85, no. 4, pp. 455–460, 2013. [Online]. Available: https://onlinelibrary.wiley.com/doi/abs/10.1002/cite.201200202

[73] D.-Y. Peng and D. B. Robinson, “A New Two-Constant Equation of State,” *Industrial & Engineering Chemistry Fundamentals*, vol. 15, no. 1, pp. 59–64, 1976. [Online]. Available: https://doi.org/10.1021/i160057a011

[74] S. Yagi and D. Kunii, “Studies on heat transfer near wall surface in packed beds,” *AIChE Journal*, vol. 6, no. 1, pp. 97–104, 1960. [Online]. Available: https://aiche.onlinelibrary.wiley.com/doi/abs/10.1002/aic.690060119

[75] V. Specchia, G. Baldi, and S. Sicardi, “Heat transfer in packed bed reactors with one phase flow,” *Chemical Engineering Communications*, vol. 4, no. 1-3, pp. 361–380, 1980. [Online]. Available: https://doi.org/10.1080/00986448008935916

[76] J. Wu, H. Zhang, W. Ying, and D. Fang, “Thermal Conductivity of Cobalt-Based Catalyst for Fischer–Tropsch Synthesis,” *International Journal of Thermophysics*, vol. 31, no. 3, pp. 556–571, 2010. [Online]. Available: https://doi.org/10.1007/s10765-010-0740-x

[77] R. E. Hicks, “Pressure Drop in Packed Beds of Spheres,” *Industrial & Engineering Chemistry Fundamentals*, vol. 9, no. 3, pp. 500–502, 1970. [Online]. Available: https://doi.org/10.1021/i160035a032

[78] J. A. Tallmadge, “Packed bed pressure drop- an extension to higher reynolds numbers,” *AIChE Journal*, vol. 16, no. 6, pp. 1092–1093, 1970. [Online]. Available: https://aiche.onlinelibrary.wiley.com/doi/abs/10.1002/aic.690160639

[79] M. Mandić, B. Todić, L. Živanić, N. Nikačević, and D. B. Bukur, “Effects of Catalyst Activity, Particle Size and Shape, and Process Conditions on Catalyst Effectiveness and Methane Selectivity for Fischer–Tropsch Reaction: A Modeling Study,” *Industrial & Engineering Chemistry Research*, vol. 56, no. 10, pp. 2733–2745, 2017. [Online]. Available: https://doi.org/10.1021/acs.iecr.7b00053

[80] C. R. Wilke and P. Chang, “Correlation of diffusion coefficients in dilute solutions,” *AIChE Journal*, vol. 1, no. 2, pp. 264–270, 1955. [Online]. Available: https://aiche.onlinelibrary.wiley.com/doi/abs/10.1002/aic.690010222

[81] N. Tsakoumis, M. Rønning, O. Borg, E. Rytter, and A. Holmen, “Deactivation of cobalt based fischer–tropsch catalysts: A review,” *Catalysis Today*, vol. 154, pp. 162–182, 2010. [Online]. Available: https://doi.org/10.1016/j.cattod.2010.02.077

[82] C. I. Méndez, J. Ancheyta, and F. Trejo, “Modeling of Catalytic Fixed-Bed Reactors for Fuels Production by Fischer–Tropsch Synthesis,” *Energy & Fuels*, vol. 31, no. 12, pp. 13 011–13 042, 2017. [Online]. Available: https://doi.org/10.1021/acs.energyfuels.7b01431

[83] AspenTech, “Aspen properties,” [Accessed 22 April 2019]. [Online]. Available: https://www.aspentech.com/en/products/pages/aspen-properties

[84] MathWorks, “COM Objects,” [Accessed 07 May 2019]. [Online]. Available: https://nl.mathworks.com/help/matlab/using-com-objects-in-matlab.html?s_tid=CRUX_lftnav

[85] M. E. Dry, “Practical and theoretical aspects of the catalytic Fischer-Tropsch process,” *Applied Catalysis A: General*, vol. 138, no. 2, pp. 319–344, 1996, chemical Engineering and Catalysis. [Online]. Available: http://www.sciencedirect.com/science/article/pii/0926860X95003061

[86] A. Hoek and L. Kersten, “The shell middle distillate synthesis process: technology, products and perspective,” in *Natural Gas Conversion VII*, ser. Studies in Surface Science and Catalysis, X. Bao and Y. Xu, Eds. Elsevier, 2004, vol. 147, pp. 25–30. [Online]. Available: http://www.sciencedirect.com/science/article/pii/S0167299104800223

[87] C. Boyer, J. M. Gazarian, V. Lecocq, S. M. Maury, A. M. Forret, J. M. Schweitzer, and V. Souchon, "Development of the Fischer-Tropsch Process: From the Reaction Concept to the Process Book," *Oil & Gas Science and Technology - Revue d'IFP Energies nouvelles*, vol. 71, no. 3, 2016. [Online]. Available: https://hal.archives-ouvertes.fr/hal-01395119

[88] L. Fratalocchi, C. G. Visconti, G. Groppi, L. Lietti, and E. Tronconi, "Intensifying heat transfer in Fischer-Tropsch tubular reactors through the adoption of conductive packed foams," *Chemical Engineering Journal*, vol. 349, pp. 829–837, 2018. [Online]. Available: http://www.sciencedirect.com/science/article/pii/S1385894718309215

[89] A. Jess and C. Kern, "Influence of Particle Size and Single-Tube Diameter on Thermal Behavior of Fischer-Tropsch Reactors. Part I. Particle Size Variation for Constant Tube Size and Vice Versa," *Chemical Engineering & Technology*, vol. 35, no. 2, pp. 369–378, 2012. [Online]. Available: https://onlinelibrary.wiley.com/doi/abs/10.1002/ceat.201100615

[90] A. Jess and C. Kern, "Influence of Particle Size and Single-Tube Diameter on Thermal Behavior of Fischer-Tropsch Reactors. Part II. Eggshell Catalysts and Optimal Reactor Performance," *Chemical Engineering & Technology*, vol. 35, no. 2, pp. 379–386, 2012. [Online]. Available: https://onlinelibrary.wiley.com/doi/abs/10.1002/ceat.201100616

[91] M. E. Dry, T. Shingles, L. J. Boshoff, and C. S. van H. Botha, "Factors influencing the formation of carbon on iron Fischer-Tropsch catalysts: II. The effect of temperature and of gases and vapors present during Fischer-Tropsch synthesis," *Journal of Catalysis*, vol. 17, no. 3, pp. 347–354, 1970. [Online]. Available: http://www.sciencedirect.com/science/article/pii/0021951770901107

[92] M. E. Dry, "The Fischer-Tropsch process - commercial aspects," *Catalysis Today*, vol. 6, no. 3, pp. 183–206, 1990. [Online]. Available: http://www.sciencedirect.com/science/article/pii/0920586190850026

[93] PetroSA, "Operations and Refinery," [Accessed 02 March 2019]. [Online]. Available: http://www.petrosa.co.za/innovation_in_action/Pages/Operations-and-Refinery.aspx

[94] V. van Wechem and M. Senden, "Conversion of Natural Gas to Transportation Fuels Via the Shell Middle Distillate Synthesis Process (SMDS)," in *Natural Gas Conversion II*, ser. Studies in Surface Science and Catalysis, H. E. Curry-Hyde and R. F. Howe, Eds. Elsevier, 1994, vol. 81, pp. 43–71. [Online]. Available: http://www.sciencedirect.com/science/article/pii/S0167299108638483

[95] P. J. A. Tijm, J. M. Marriott, H. Hasenach, M. M. G. Senden, and T. van Herwijnen, "The Markets For Shell Middle Distillate Synthesis Products," in *Alternative Energy Symposium*, ser. Alternate Energy- Council on Alternate Fuels. Vancouver, Canada: The Council, May 1995, pp. 228–242.

[96] Shell, "Shell Middle Distillate Synthesis," [Accessed 02 March 2019]. [Online]. Available: https://www.shell.com.my/business-customers/shell-middle-distillate-synthesis.html

[97] Shell, "Pearl GTL- Overview," [Accessed 02 March 2019]. [Online]. Available: https://www.shell.com/about-us/major-projects/pearl-gtl/pearl-gtl-an-overview.html

Appendices

A. FT Iron Catalysts

Some important aspects of fused iron and precipitated iron catalysts used in FTS are covered in the following sections.

A.1 Fused Iron Catalysts

Fused iron catalysts are usually prepared by adding alkali promoters and structural promoters into the molten bath of magnetite. Former enhances the activity and selectivity of the catalyst, while the latter enhances the surface area of the final catalyst. Fluidised bed reactors require fine catalyst particles, and this is prepared by powdering the solid formed while cooling the molten magnetite. The final metallic catalyst, which is loaded into the FT reactor, is prepared by the reduction of previously obtained magnetite powder with hydrogen [8, 26].

The catalyst particles in the reactor undergo several changes during the synthesis process [8]. The core of larger catalyst particles are susceptible to oxidation and revert back to iron oxide (magnetite). The grain boundaries with promoter rich inclusions are prone to accumulation of free carbon, resulting in swelling and breaking of the catalyst after some time under FT synthesis conditions. Hence, it is required to partially replace used catalyst and reload fresh catalyst continuously in order to maintain the catalyst properties and reactant conversion within the desired ranges [26, 91].

Methane selectivity of the FTS process can be decreased by the addition of alkali promoters in high levels. The methane selectivity cannot be reduced beyond a practical lower limit as it would result in various operational problems in the fluidised bed. This can be attributed to the formation of heavy or long chain hydrocarbons in the liquid phase. The rate of carbon as well as organic acid formation increases with the alkali content and results in the deactivation of catalyst and various corrosion problems in the reactor, respectively [26]. Organic acids may also create some problems in the downstream refining stages. Hence, taking all these factors into consideration, the lowest methane selectivity that could be achieved by a fused iron catalyst is only around 7% of the product hydrocarbons [8].

Fused iron catalyst produces liquid hydrocarbons with high olefin content, making it the most preferred catalyst in the petrochemical industry for olefin production. The primary olefin products, mainly ethylene, may undergo secondary reactions such as hydrogenation or chain growth to give paraffins or longer hydrocarbon products, respectively. In order to suppress these secondary reactions and increase the light olefin content, the use of specific promoters are desirable. It is also possible to introduce other promoters to the catalyst to reduce the formation of unwanted substances such as free carbons or organic acids during FT reactions [26, 91].

A.2 Precipitated Iron Catalysts

The use of liquid phase hydrocarbons in FT slurry reactors results in a decrease in the selectivity towards methane, and the lowest selectivity towards methane, achieved by a precipitated iron catalyst, is around 3% of the hydrocarbon products [8]. Maintaining the liquid phase operation demands a lower temperature than that in the fluidised bed reactor with fused iron catalyst. The reduced temperature in the reactor adversely affects the reaction rate, and to compensate this decrease, it is desirable to have higher catalyst surface areas. However, by increasing the surface area, the catalyst becomes structurally weaker. Thus, the use of structural promoters and special procedures during the preparation of catalyst is necessary to enhance the strength of catalyst [26].

Precipitated iron catalysts are prepared using costly iron metal as raw material, as opposed to cheaper iron oxide in the case of fused iron catalysts. The desired promoters are added into an aqueous acidic solution (such as nitric acid) in which the metal is dissolved. In order to keep the iron in its reduced form, a reduction/conditioning step is also involved in the preparation process, where metals, such as copper, are also added [26].

A precipitate is prepared by adding a basic solution (e.g. sodium carbonate or ammonia) into the acidic solution. The final catalyst is then prepared by filtering, washing, drying and using shaping techniques to obtain the required shape [8]. For use in a fixed bed reactor, the catalyst shape is obtained via extrusion of the dried precipitate, whereas for use in a slurry reactor, drying and powdering take place simultaneously with the help of a spray drier. The mechanical strength of the catalyst is enhanced using various heat treatment methods, and the stability of the final catalyst is achieved in the FT reactor and/or in a separate reduction/conditioning step with the formation of iron carbide [26].

An excess or lack of promoters during the preparation would result in a catalyst with undesirable characteristics and selectivities [8]. Hence, an optimum level of promoters has to be identified and chosen. Catalyst activity and strength, however, are influenced by a large number of variables during the catalyst preparation.

B. Commercial FT Plants

Fischer-Tropsch technology has been successfully implemented in several CTL and GTL plants worldwide for the production of a variety of hydrocarbon products. The most important ones among them include the plants of Sasol and PetroSA in South Africa and that of Shell in Malaysia and Qatar. The technologies used in these plants are briefly discussed in the following sections of this chapter.

B.1 Sasol (Sasolburg and Secunda, South Africa)

Sasol has two large production plants in Sasolburg and Secunda, respectively, in South Africa. Both the plants initially used coal as feedstock for the production of syngas; however, the Sasolburg plant started using natural gas as the feedstock since the establishment of a gas pipeline between Mozambique and South Africa in 2004. Sasol consumes around 40 million tons of low-grade coal every year for the production of syncrude in the Secunda plant [8].

The plant in Sasolburg comprises five multi-tubular fixed bed reactors and one high capacity slurry phase reactor, all utilising the low-temperature Fischer-Tropsch (LTFT) technology. The process conditions in these reactors have been optimised for maximising the production of linear alkanes/alkenes, and all the oxygenates and alkenes formed are hydroprocessed to produce alkanes, making Sasol one of the largest producers of linear paraffinic waxes. The FT tail gas also contains some valuable products, such as LPG (C_3 and C_4 fractions) and hydrogen, which are substantially recovered in the further steps. The remaining tail gas, also called fuel gas, is sold in the market [8]. Figure B.1 shows the simplified block diagram of the Sasolburg plant.

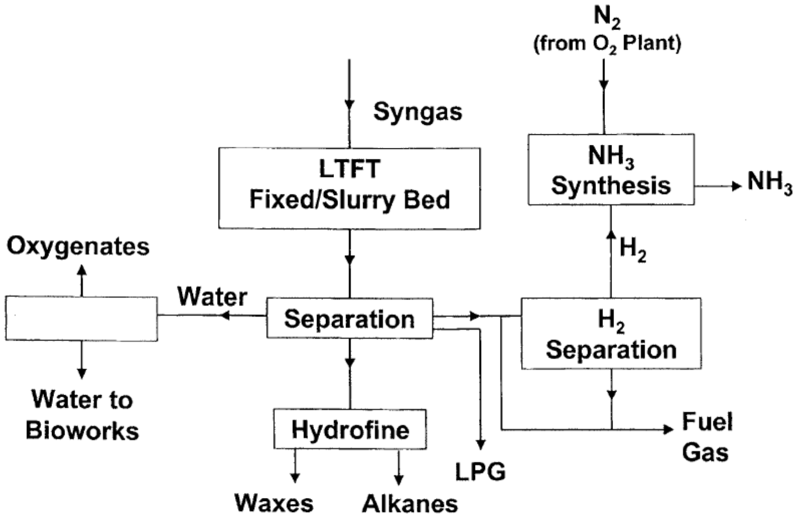

Figure B.1: Simplified block diagram of the Sasol plant in Sasolburg [8].

The Sasol plant in Secunda utilises high temperature Fischer Tropsch (HTFT) technology in fluidised bed reactors. The reactors use iron-based catalyst, and the process conditions have been optimised to maximise the production of 1-olefins and gasoline. The separation and refining of FT products in this plant is quite complicated due to the production of a wide range of hydrocarbons, i.e., methane to heavy oils, in the FT reactors. The products are condensed and separated into a gas, oil and an aqueous phase as soon as it leaves the reactor, for further processing. The aqueous phase, which generally contains dissolved acids, aldehydes and ketones, is distilled to recover the non-acid components and the remaining oxygenates are hydroprocessed. The acetaldehydes are used for the production of N-Crotonaldehyde and n-butanol. The acids are separated using liquid-liquid extraction in a packed tower, and the effluent water is used as make-up cooling water after removing the residual organic components from it using a biological treatment [8].

The FT tail gas, obtained after condensing out the oil and aqueous phases, is subjected to a cryogenic separation process in order to extract a hydrogen-rich, methane-rich and three light hydrocarbon streams. The H_2 obtained by the pressure swing absorption (PSA) of the hydrogen-rich stream is mainly utilised for hydroprocessing and the rest is recycled to the FT reactors. The light hydrocarbon streams are fractionated and separated to obtain high value 1-olefins. The methane-rich stream is mainly used for the production of syngas in autothermal catalytic reformers, which is recycled back to the FT reactors, and the rest of the methane-rich stream is sold in the market as fuel gas [8].

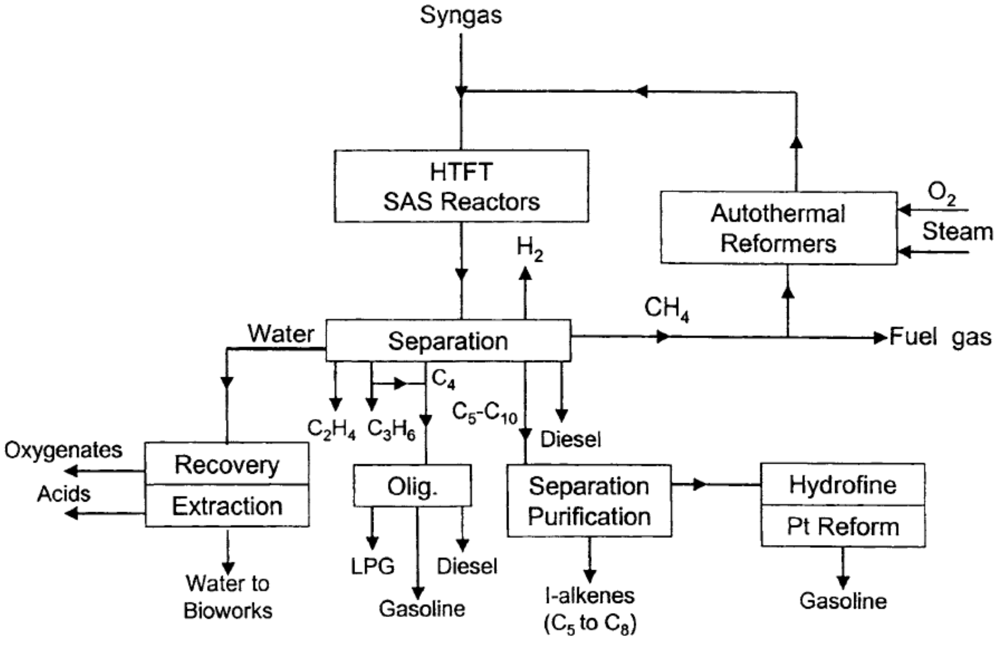

Figure B.2: Simplified block diagram of the Sasol plant in Secunda [8].

The olefin products obtained from the process find a variety of industrial applications. Ethylene is a raw material for the polyethylene production units in Sasolburg and propene finds use in polypropylene and acrylonitrile plants. LPG, gasoline and diesel fuel are obtained by the oligomerisation of C_3 and C_4 cuts, and the higher olefins upto C_8 are processed to find applications as co-monomers in the polyethylene industry. Around 120,000 tons of detergent alcohols are produced annually by the hydroformulation of the long chain linear alkenes. Gasoline with desired octane number is also produced by the hydrotreatment and catalytic reforming of the light FT naphtha. All the diesel cuts are also linearised using hydrotreatment methods. Figure B.2 shows the simplified block diagram of the Secunda plant [8]. At present, Sasol produces more than 7.5 MMTPA (million metric tons per annum), catering to over 30% of the liquid fuel demands of South Africa.

B.2 PetroSA/Mossgas (Mossel Bay, South Africa)

The PetroSA plant in Mossel Bay (Figure B.3) utilises off-shore natural gas to produce syngas, and the FT process is optimised for the production of gasoline and diesel fuel as the main products [92]. The methane from natural gas is first filtered and then reformed in catalytical reformers, followed by autothermal reformers to produce syngas [8]. The FT process occurs in circulating fluidised bed (CFB) reactors based on fused iron catalyst, at high temperatures (HTFT). The FT products are condensed and separated into aqueous, oil and gaseous phases and are further processed to obtain the desired products. The aqueous phase, containing dissolved aldehydes, ketones and alcohols, is extracted and hydrogenated to convert the aldehydes and ketones to alcohols. The FT tail gas is initially subjected to refrigeration in order to recover the C_3 and higher hydrocarbon products, and the rest of the tail gas, containing mainly methane and higher alkenes, is recycled to the secondary reformers. High octane gasoline is produced by alkylating isobutane (formed by the isomerisation of natural gas butane) with C_3 and C_4 alkenes extracted from the FT tail gas. The rest of the C_{3+} alkenes from tail gas is oligomerised to produce gasoline and diesel fuel. High octane gasoline is also produced from the hydrotreatment of all gasoline cuts, isomerisation of C_5/C_6 paraffins, and catalytic (Pt) reforming of C_{7+} paraffins. Hydrotreatment is also performed on all FT diesel cuts to linearise the products. Currently, the Mossel Bay GTL plant produces around 2.24 MMTPA fuels [93].

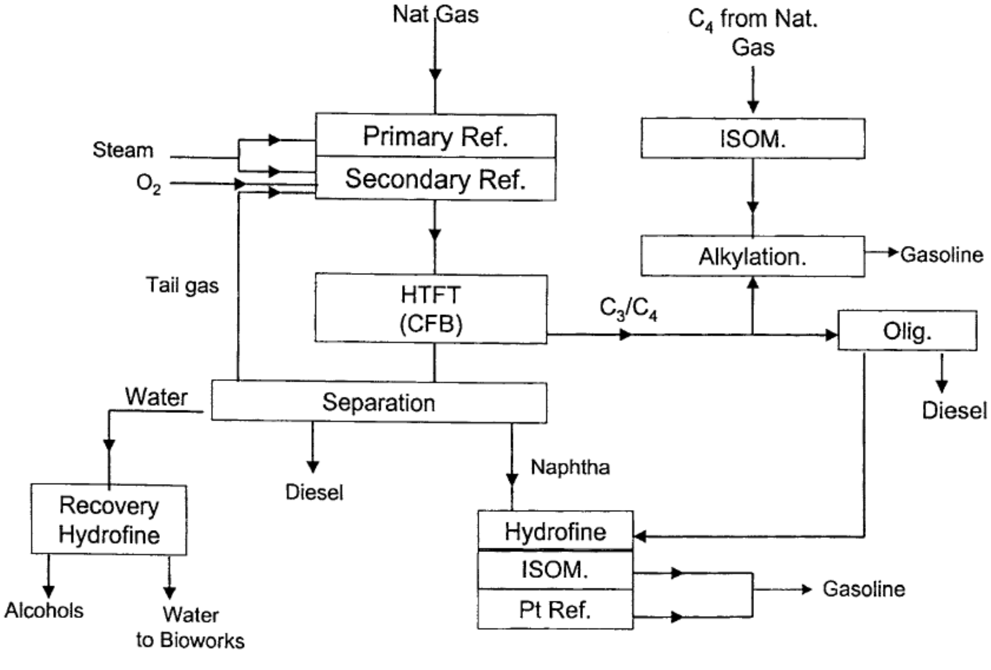

Figure B.3: Simplified block diagram of the PetroSA plant in Mossel Bay [8].

B.3 Shell (Bintulu, Malaysia and Ras Laffan, Qatar)

The Shell plant in Bintulu is based on the SMDS (Shell Middle Distillate Synthesis) technology and utilises off-shore natural gas for the production of syngas feed. The natural gas is subjected to a non-catalytic partial oxidation (POX) process at high pressure and around 1673K (1400°C) [94, 95] to obtain syngas. The carbon efficiency of the reformer is higher than 95% and methane loss is only around 1%. The FT process occurs at around 473-493K (200-230°C) and 3 MPa in multi-tubular fixed bed reactors using cobalt-based catalyst. The desired syngas H_2/CO usage ratio for cobalt catalyst is around 2.1, but since the syngas produced in the reformer only has a usage ratio of 1.7, additional H_2-rich gas is provided by the catalytic steam reforming of the FT tail gas. Although H_2 production via tail gas reforming is a low efficient and high cost operation, it also supplies H_2 for the hydroprocessing operations in the product refining section. The process conditions have been optimised for maximising the production of waxes, and the conversion levels and C_{5+} selectivities in the reactor are claimed to be around 80% and 85%, respectively [95]. The FT products are condensed and separated into aqueous, oil and wax phases, and the FT tail gas is fed to the catalytic steam reformer to convert the C_1 - C_4 and the slight amounts of C_{5+} present into syngas. The wax products are processed in two modes in the plant. The first mode involves the elimination of alkenes and oxygenated compounds in waxes using the hydrofining process, followed by the fractionation of the waxes into various grades. The other mode involves the hydroisomerisation/hydrocracking of waxes to produce high quality diesel and kerosene fuels. Figure B.4 shows the simplified block diagram of the SMDS plant in Bintulu [8], and at present, this plant produces around 0.5 MMTPA of solid and liquid hydrocarbons [96].

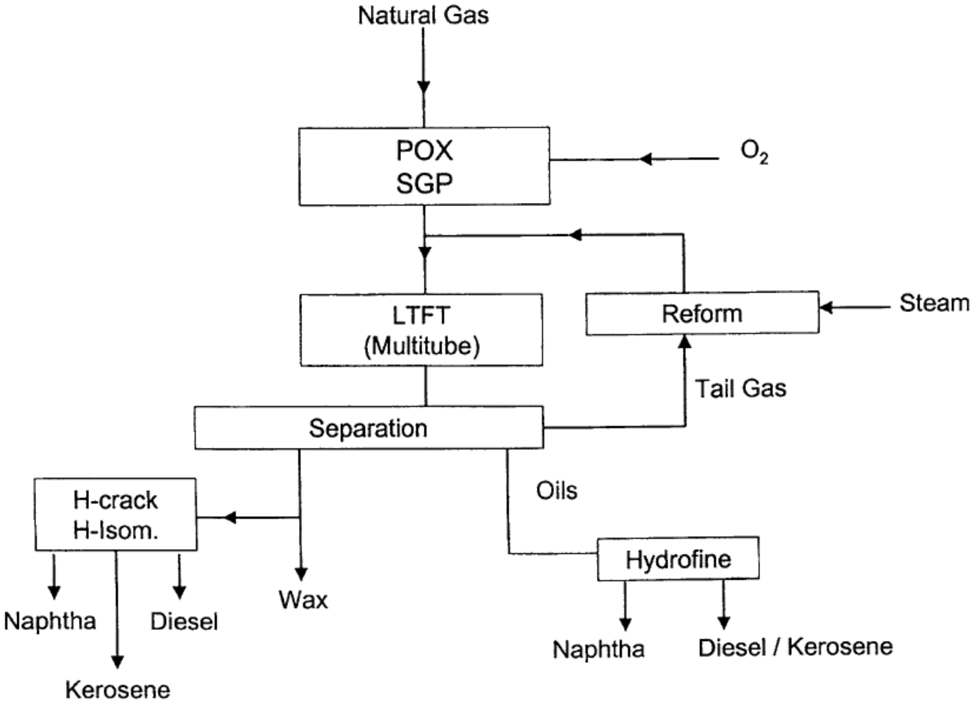

Figure B.4: Simplified block diagram of the Shell SMDS plant in Bintulu [8].

The Pearl GTL plant of Shell in Ras Laffan Industrial City, Qatar, is an integrated gas and gas-to-liquids project and is claimed to be one of the most complex and challenging energy projects ever commissioned. This plant also utilises the Shell SMDS technology for the conversion of natural gas to liquid products. The plant achieved its maximum capacity by the end of 2012, producing around 7 MMTPA of GTL products and around 6 MMTPA of natural gas liquids and methane, making it the largest GTL plant in the world [97].

C. Heat Transfer through Wall

Consider a reactor tube wall element as shown in Figure C.1, where T_w is the temperature of the inner reactor wall that is assumed to be constant throughout the reactor length, T_{cw} is the temperature of the outer reactor wall that is in contact with the coolant, T_c is the temperature of the coolant, d_w is the thickness of the reactor wall, dA is the heat transfer area of the wall element, dQ_w is the heat transferred through the wall from the inside to the outside of the reactor, and dQ_{cw} is the heat transferred from the outside of the wall to the coolant. The flow rate of coolant is assumed to be sufficiently high so that the temperature of the coolant remains constant irrespective of the amount of heat absorbed by the coolant (see Section 3.4).

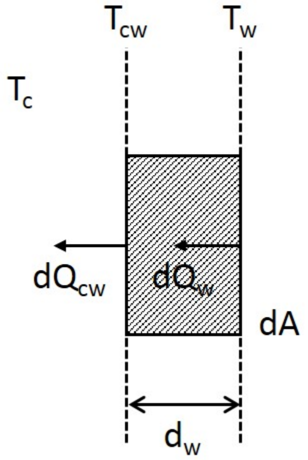

Figure C.1: Reactor tube wall element considered for the heat balance.

Now, the heat transferred through the reactor wall dQ_w can be calculated as:

$$dQ_w = k_w \cdot dA \cdot \frac{(T_w - T_{cw})}{d_w} \tag{C.1}$$

where k_w is the thermal conductivity of the reactor wall. On rearranging and translating the equation in terms of the heat transfer resistance offered by the wall element:

$$(T_w - T_{cw}) = dQ_w \cdot \frac{d_w}{k_w \cdot dA} \tag{C.2}$$

$$(T_w - T_{cw}) = dQ_w \cdot R_w \tag{C.3}$$

where R_w is the heat transfer resistance offered by the wall element. Similarly, the heat transferred from the outer wall to the coolant can be calculated as:

$$dQ_{cw} = h_{cw} \cdot dA \cdot (T_{cw} - T_c) \tag{C.4}$$

where h_{cw} is the heat transfer coefficient between the outer wall and the coolant. On rearranging and translating the equation in terms of the heat transfer resistance between the outer wall and the coolant:

$$(T_{cw} - T_c) = \frac{dQ_{cw}}{h_w \cdot dA} \tag{C.5}$$

$$(T_{cw} - T_c) = dQ_{cw} \cdot R_{cw} \tag{C.6}$$

Now, as discussed in Section 3.4, the heat transfer resistances between the wall and the coolant, and through the wall are assumed to be negligible. Thus the RHS of Equations C.3 and C.6 become 0, i.e.,

$$(T_w - T_{cw}) = 0 \tag{C.7}$$

$$(T_{cw} - T_c) = 0 \tag{C.8}$$

From the above equations, it can be inferred that $T_w = T_{cw}$ and $T_{cw} = T_c$. Therefore, the temperature of the inner wall is equal to the temperature of the coolant, i.e., $T_w = T_c$.

D. Thermodynamic Properties

The thermodynamic and transport properties of the system components used in the basic MTFBR model are given in Table D.1. All the properties in the basic MTFBR model are estimated assuming that the components follow ideal gas behaviour.

Table D.1: Thermodynamic and transport properties of the system components assuming ideal gas behaviour [1, 67].

Component	Property	Formula used for prediction
CO	c_p (J/mol/K)	(6.60+0.00120*T)*4.184
	μ (Pa·s)	1.1127e-6*T^0.5338/(1+94.7/T)
	λ (W/m/K)	0.00059882*T^0.6963/(1+57.13/T+501.92/T^2)
H_2	c_p (J/mol/K)	(6.62+0.000810*T)*4.184
	μ (Pa·s)	1.797e-7*T^0.685/(1-0.59/T+140/T^2)
	λ (W/m/K)	0.002653*T^0.7452/(1+12/T)
H_2O	c_p (J/mol/K)	(8.22+0.00015*T)*4.184
	μ (Pa·s)	1.7096e-8*T^1.1146
	λ (W/m/K)	6.2041e-6*T^1.3973
CH_4	c_p (J/mol/K)	(5.34+0.0115*T)*4.184
	μ (Pa·s)	5.2546e-7*T^0.59006/(1+105.67/T)
	λ (W/m/K)	8.3983e-6*T^1.4268/(1-49.654/T)
C_2	c_p (J/mol/K)	(0.4033e5+1.3422e5*(1.6555e3/T/sinh(1.6555e3/T))^2 +0.7322e5*(752.87/T/sinh(752.87/T))^2)/1e3
	μ (Pa·s)	4.9054e-8*T^0.90125
	λ (W/m/K)	-1.12*T^0.10973/(1-9834.6/T-7535.8/T^2)
C_3	c_p (J/mol/K)	(0.5195e5+1.9245e5*(1.6265e3/T/sinh(1.6265e3/T))^2 +1.1680e5*(723.6/T/sinh(723.6/T))^2)/1e3
	μ (Pa·s)	4.9054e-8*T^0.90125
	λ (W/m/K)	-1.12*T^0.10973/(1-9834.6/T-7535.8/T^2)
C_4	c_p (J/mol/K)	(0.7134e5+2.4300e5*(1.6300e3/T/sinh(1.6300e3/T))^2 +1.5033e5*(730.42/T/sinh(730.42/T))^2)/1e3
	μ (Pa·s)	4.9054e-8*T^0.90125
	λ (W/m/K)	-1.12*T^0.10973/(1-9834.6/T-7535.8/T^2)
C_{5+}	c_p (J/mol/K)	(1.3554e5+4.43e5*(1.6356e3/T/sinh(1.6356e3/T))^2 +3.0540e5*(746.4/T/sinh(746.4/T))^2)/1e3
	μ (Pa·s)	3.1191e-8*T^0.92925/(1+55.092/T)
	λ (W/m/K)	-1.12*T^0.10973/(1-9834.6/T-7535.8/T^2)

E. Miscellaneous Parameters

The bulk density of the packed-bed is calculated as:

$$\rho_b = \rho_c(1 - \varepsilon_b) \tag{E.1}$$

where ρ_c is the density of catalyst (typical value for Co-based catalyst is 1200 kg/m^3) and ε_b is the porosity of the packed-bed. The dimensionless groups are calculated as:

$$Re_g = \frac{\rho_g u_{s,g} d_p}{\mu_g} \tag{E.2}$$

$$Pr_g = \frac{c_{p,g}\mu_g}{\rho_g} \tag{E.3}$$

$$Re_l = \frac{\rho_l u_{s,l} d_p}{\mu_l} \tag{E.4}$$

$$Pr_l = \frac{c_{p,l}\mu_l}{\rho_l} \tag{E.5}$$

where Re and Pr are Reynolds number and Prandtl number, respectively. The superficial velocities of gas and liquid phases are calculated as:

$$u_{s,g} = \frac{F_g M_g}{\rho_g A_{cs}} \tag{E.6}$$

$$u_{s,l} = \frac{F_l M_l}{\rho_l A_{cs}} \tag{E.7}$$

where M is the average molar mass of gas/liquid, and F is the molar flow rate of gas/liquid, calculated as:

$$F_g = Y \cdot F_{tot} \tag{E.8}$$

$$F_l = (1 - Y) \cdot F_{tot} \tag{E.9}$$

where Y is the vapour fraction and F_{tot} is the total flow rate of gas and liquid in the reactor. The partial pressures of components are calculated as:

$$P_i = y_i \cdot P_{tot} \tag{E.10}$$

where y_i is the vapour composition of component i and P_{tot} is the total pressure in the reactor.

F. Modified Heat Balance Equation

Consider a reactor element as shown in Figure F.1, where the inlet to the element is at temperature T_{in} and outlet is at T_{out}, the length of the element is dl and the diameter of the reactor element is d_t. The enthalpy of the inlet stream is H_{in} and that of the outlet stream is H_{out}, and the heat removed from the reactor element is denoted by dQ.

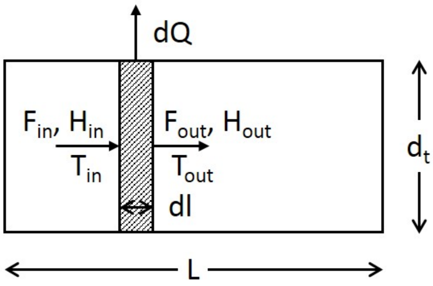

Figure F.1: Reactor element considered for the heat balance.

By performing a steady-state heat balance over the element and rearranging the terms:

$$H_{in} - H_{out} - dQ = 0 \tag{F.1}$$

$$H^{\circ}_{in} + \dot{m}_{in} c_{p,in}(T_{in} - T^{\circ}) - H^{\circ}_{out} - \dot{m}_{out} c_{p,out}(T_{out} - T^{\circ}) - dQ = 0 \tag{F.2}$$

where $\dot{m}$ is the mass flow rate of the stream, c_p is the heat capacity of the stream and T° is the reference state temperature. Now, considering the reference state to be at the inlet conditions, T° can be considered equal to T_{in}, and further rearranging the terms:

$$H^{\circ}_{in} - H^{\circ}_{out} - \dot{m}_{out} c_{p,out}(T_{out} - T_{in}) - dQ = 0 \tag{F.3}$$

$$\dot{m}_{out} c_{p,out}\ dT = (H^{\circ}_{in} - H^{\circ}_{out}) - dQ \tag{F.4}$$

$$\dot{m}_{out} c_{p,out}\ dT = dH_{tot} - U\ dA(T - T_w) \tag{F.5}$$

where dT is the temperature difference across the reactor element, dA is the heat transfer area of the element, T_w is the wall temperature of the reactor and dH_{tot} is the total heat released during the reaction at reference conditions (here, inlet conditions), calculated using Equation 4.36. Assuming the reactor element to be a CSTR, the outlet temperature (T_{out}) will be same as the temperature of the element ($T_{element}$). With further substitution:

$$\dot{m}_{out} c_{p,out}\ dT = dH_{tot} - U\pi d_t dl(T - T_w) \tag{F.6}$$

Now, dimensionless length of the reactor, $z = l/L$. Differentiating the equation on both sides gives, $dz = dl/L$. Replacing dl in the above equation with dz and further rearranging:

$$\dot{m}_{out} c_{p,out}\ dT = dH_{tot} - U\pi d_t dz(T - T_w)L \tag{F.7}$$

$$\dot{m}_{out} c_{p,out} \frac{dT}{dz} = \frac{dH_{tot}}{dz} - U\pi d_t(T - T_w)L \tag{F.8}$$

Now, the $\dot{m}_{out} c_{p,out}$ values can be expressed as a contribution of gas and liquid phases, neglecting the effect of mixing, as:

$$(\dot{m}^{out}_{g} c^{out}_{p,g} + \dot{m}^{out}_{l} c^{out}_{p,l}) \frac{dT}{dz} = \frac{dH_{tot}}{dz} - U\pi d_t(T - T_w)L \tag{F.9}$$

Equation (F.9) is the modified heat balance equation, which is used in Section 4.3.1.4.

G. Kinetic Model Validation Results

The results for the second and third validation cases of the FTS kinetic model are shown in Figures G.1 and G.2, respectively.

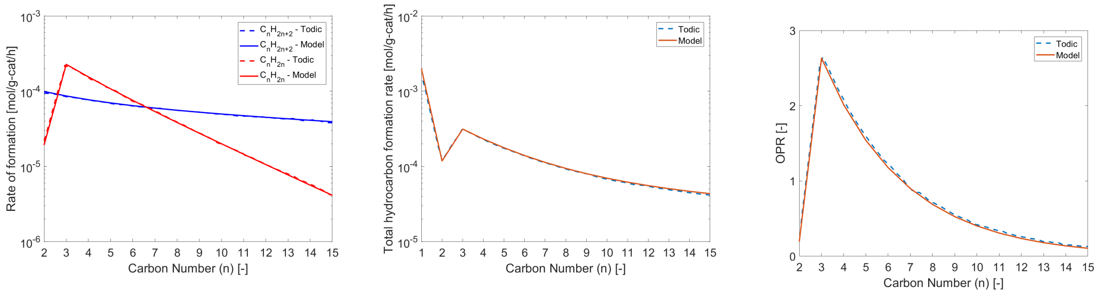

(a) Formation rates of n-paraffins and 1-olefins

(b) Total hydrocarbon formation rate

(c) Olefin-to-Paraffin ratio (OPR)

Figure G.1: Validation of kinetic model with results of Todic et al. (Process conditions: T = 493K, P = 1.5 MPa, H_2/CO = 1.4, WHSV = 5.6 NL/gcat/h, X_{CO} = 34%) [58].

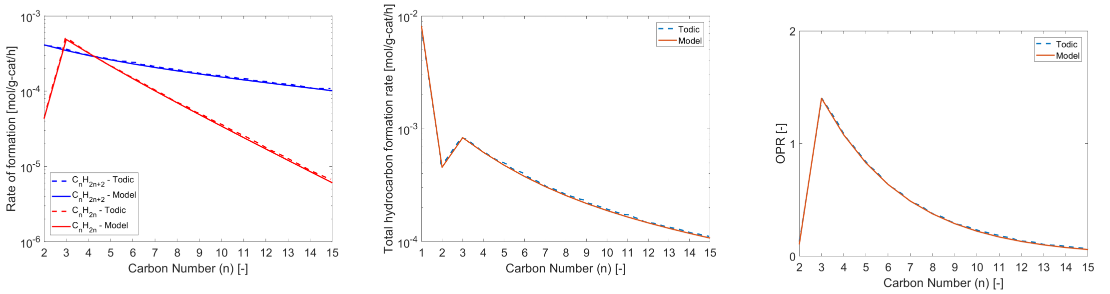

(a) Formation rates of n-paraffins and 1-olefins

(b) Total hydrocarbon formation rate

(c) Olefin-to-Paraffin ratio (OPR)

Figure G.2: Validation of kinetic model with results of Todic et al. (Process conditions: T = 503K, P = 1.5 MPa, H_2/CO = 2.1, WHSV = 11.3 NL/gcat/h, X_{CO} = 42%) [58].